Fabrication of Cu_2ZnSnS_4 Semiconductor Thin Films using A Spray Pyrolysis Method for Photovoltaic Applications

Nguyen Thi Hiep

March 2018

Fabrication of Cu_2ZnSnS_4 Semiconductor Thin Films using A Spray Pyrolysis Method for Photovoltaic Applications

A dissertation submitted to

The Graduate School of Engineering Science

Osaka University

In partial fulfillment of the requirements for the degree of

Doctor of Philosophy in Engineering

By

Nguyen Thi Hiep

March 2018

Abstract

The demand for utilization of solar energy has motivated many researchers to develop novel photovoltaic (PV) systems having high conversion efficiencies and applicability for low-cost fabrication processes. In thin film PV technologies, several compound semiconductor thin films have been developed as absorber layers. Among them, the kesterite Cu_2ZnSnS_4 (CZTS) compound has been studied extensively because it has optimum band gap energy of 1.4 *eV* for sunlight absorption and a high absorption coefficient of more than 10^4 cm^{-1}. Less-toxic and earth-abundant features of all of the constituent elements in the compound are also advantageous for its practical applications. The current highest power conversion efficiency of CZTS-based thin film solar cells has reached 9.2 % by vacuum sputtering method. However, non-vacuum process used less energy consumption is more environmentally friendly. Among various techniques, spray pyrolysis is an attractive technique because of its simplicity and easiness to deposit the thin film in a large scale, it also does not require vacuum at any stage during the deposition. There have been only a few reports on fabrication of CZTS-based solar cells prepared by the spray pyrolysis method and only very low conversion efficiencies (~1%) were achieved. Therefore, in this study, structural and electrical controls of the CZTS thin films prepared by a facile spray pyrolysis deposition method were investigated to obtain a film optimal for high efficiency solar cells.

Firstly, an attempt was made to fabricate the CZTS thin film on an Mo-coated glass substrate using a spray pyrolysis deposition of a precursor film from an aqueous solution containing $Cu(NO_3)_2$, $Zn(NO_3)_2$, $Sn(CH_3SO_3)_2$ and thiourea. In order to obtain a stable

solution for the spray pyrolysis without formation of a SnO_2 precipitate, the mixing order of source materials was found to be important. Annealing of the thus-obtained precursor film in sulfur vapor at temperatures ranging from 580 °*C* to 600 °*C* resulted in successful formation of homogeneous CZTS films. Based on structural analyses of CZTS films having different Sn contents, an Sn-rich composition compared to its stoichiometric amount was found to be essential for efficient grain growth of the resulting CZTS films. A solar cell based on the Sn-rich CZTS film obtained by an optimum annealing condition exhibited maximum conversion efficiency of 5.8%.

In the second, effects of precursor compositions on structural and photovoltaic properties of spray-deposited CZTS thin films were investigated. When a precursor solution containing a stoichiometric composition of Cu, Zn, and Sn was used, the resulting CZTS thin film contained a $Cu_{2-x}S$ impurity phase due to the evaporation of Sn components during the annealing process. Removal of the $Cu_{2-x}S$ impurity in the CZTS thin film was succeeded by reduction in the concentration of Cu in the precursor solution: this results in improvement of structural features (grain sizes and compactness) as well as electric properties. A solar cell based on the CZTS film with an empirically optimal composition showed conversion efficiency of 8.1%.

For further improvement of film quality, a silver (Ag)-incorporated CZTS (Ag-CZTS) thin film was fabricated. From the results of morphological investigations, Ag-CZTS films had larger crystal grains than those of the CZTS film. The sample with a relatively low Ag content (Ag/(Ag+Cu) of ca. 0.02) had a compact morphology without appreciable voids and pinholes. However, an increase in the Ag content in the CZTS film (Ag/(Ag+Cu) ca. 0.10) induced formation of a large number of pinholes. As can be expected from these morphological properties, the best sunlight conversion efficiency was obtained by the solar

cell based on the film with Ag/(Ag+Cu) of ca. 0.02. Electrostructural analyses of the devices suggested that the Ag-CZTS film in the device achieved reduction in the amounts of unfavorable copper on zinc antisite defects in comparison with those in the bare CZTS film. Moreover, the use of an Ag-CZTS film improved band alignment at the p-n junction. These alterations should also contribute to enhancement of device properties.

Finally, effects of In incorporation on structural and photovoltaic properties of CZTS thin films were investigated. The crystallographic analyses of thus-obtained films indicated successful formation of In-incorporated CZTS (In-CZTS) films without any impurity components when the In/(Zn+Sn) ratio was lower than 0.2. From the morphological studies, In incorporation into the CZTS lattice was found to suppress the grain growth, especially for the film with high indium contents. Despite of the detrimental effect, the solar cell based on the In-CZTS film with very low In content (In/(Zn+Sn)=0.01) showed better conversion efficiency than that of the cell base on the bare CZTS film: the maximum conversion efficiency of 6.0% was achieved.

Contents

Chapter I

General Introduction

I.1. Photovoltaic as A Renewable Energy Source

Energy is one of the most important topics in the word since energy consumption has increased with the development of the world in recent decades. In 2015, global energy consumption was reported about 17.4 *TW* with 32.94% from oil, 29.20% from coal, 23.85% from natural gas, 4.44% from nuclear and only 9.57% from all renewable energies as showed in Figure I.1 [1, 2]. Although the amount of renewable energies is increasing in recent years, it is still low compared to the non-renewable energies. Consequently, the consumed energies are mainly from fossil fuels. However, these fossil fuels are gradually becoming exhausted, leading to increases in their prices. Moreover, using these energy sources induce high emissions of CO_2 and other pollutants resulting in severe problems of global warming and environmental pollutions. Therefore, the future energies in the world should be based on renewable energies such as hydroelectric, wind, geothermal, biomass and solar energies.

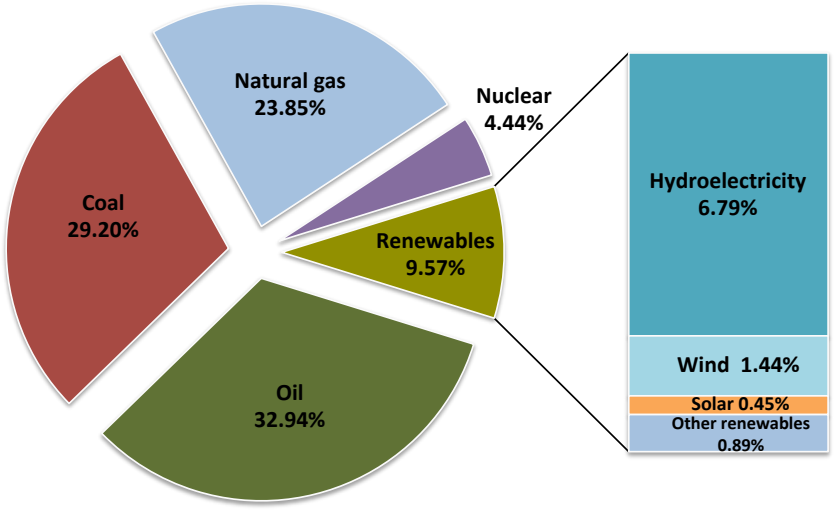

Figure I.1. Comparison of primary world energy consumptions in 2015 and inset shows share of energy consumption from renewable energies. Adapted from Ref. 2.

Among renewable energies, solar energy is the most abundant energy. Every second, more than 100000 *TW* of solar power reaches the earth. This is a huge energy compared to the energy from the fossil fuels [3]: the amount of sunlight energy reached at the earth's surface in one hour is more than the total energy consumption in the world in one year. Moreover, solar energy is renewable, sustainable and environmentally friendly. Therefore, solar energy is a promising solution to the world's energy problem.

Various possible strategies for harvesting solar energy have been studied. Among them, photovoltaic is an attracted candidate. This is a process of converting sunlight directly into electricity using complete devices called solar cells. The first observation of photovoltaic effect was discovered by a French scientist Alexandre Edmond Becquerel in 1839. While doing experiments with electrodes in a conducting solution, he found electricity generation when exposed to light [4]. In 1883, New York inventor Charles Fritts developed the first solar cell. His device was made by coating selenium with an extremely thin layer of gold; the conversion efficiency of thus-obtained device was 1-2% [5]. In 1940s, physicists at Bell Laboratories (John Bardeen, Walter Houser Brattain and William Schockley) found that silicon is more efficiency than selenium; silicon solar cells were first developed and produced commercially with conversion efficiency about 6% [6]. At present, silicon solar cells dominate photovoltaic market and they share more than 80% installed solar cells in the world with the best conversion efficiency of crystalline silicon solar cell of more than 26% was reported recently [7]. However, since silicon solar cells are made from thick layer of silicon, they require a high quantity material with high purity level. Moreover, the production of these solar cells needs many steps with high consumption energy, leading to high production costs. In order to make solar powder a primary source of energy, it is necessary to reduce production costs of solar cells by improving their conversion efficiencies

and/or reducing material and manufacturing costs. Regarding the cost reduction, thin film solar cells were developed to solve this problem. To overcome the limitation of crystalline silicon, thin films made from cheaper semiconductor materials that have high light absorption coefficients are used to reduce prices and quantities of materials required. Moreover, device structures and fabrication process are versatile with wide choice of substrates and deposition techniques, leading to low manufacturing cost.

Figure I.2 shows some typical types of solar cells, which are classified to three generations based on the material used. Beside the first generation of silicon solar cells and the second generation of thin film solar cells, the third generation of organic solar cells was developed with the main target to push conversion efficiency close to the thermodynamic limits. At current, the highest conversion efficiency of these solar cells has reached 22.1% [8]. However, the third generation solar cells are still under demonstration and have not commercialized yet due to their short lifetime and low stability.

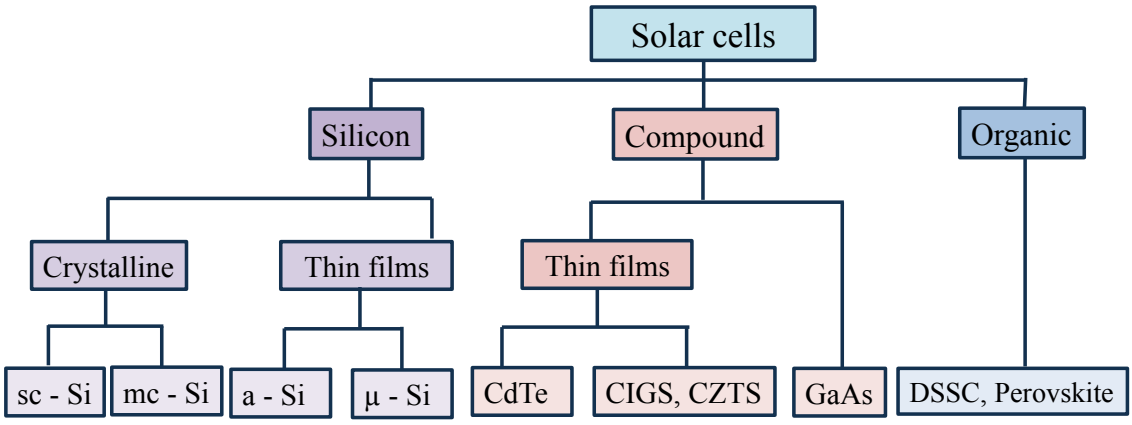

Figure I.2. Typical types of solar cells.

I. 2. Thin Film Solar Cells

Thin film solar cells belong to the second generation solar cells after the first generation

of crystalline silicon solar cells. They were developed from the 1970s with the original aim to reduce production costs by using cheaper materials and lower manufacturing costs. Thin film technologies based on direct band gap semiconductors, which have high light absorption coefficients, this leads to the use of a thin film to collect the sun light radiation, leading to reducing of material usages. Indeed, thicknesses of the absorber films used in current thin film solar cells (i.e., CdTe, CIGS, and CZTS) are only some micrometers (~ 2 μm), much thinner than the first generation of crystalline silicon solar cell that uses wafer of up to 200 μm. Therefore, thin film cells are lightweight and flexible to deposit on many kinds of substrates such as glass, stainless steel and plastic, suitable for solar buildings and space applications.

In addition, there are various possible materials used for thin film solar cells. Required purities are not as high as those of crystalline silicon solar cells. Two important points required for these materials are high absorption coefficients and suitable band gap energies. An advantage for thin film materials is the possibility to adjust the band gap energy by controlling elemental composition. According to the Schokley-Quisser limit for theoretical efficiency of a solar cell, the band gap energy of semiconductor materials used for thin film solar cells should be in the range of 1-1.5 eV [9] to reach high efficiencies.

Currently, the main commercial thin film solar cells are from amorphous silicon (a-Si), cadmium telluride (CdTe), copper indium selenium ($CuInSe_2$ or CIS), copper indium gallium selenium ($Cu(In,Ga)Se_2$ or CIGS). Among them CdTe hold around 50% of the market share for thin film solar cells with the world record efficiency of 22.1% [10]. However, CdTe contain a toxic cadmium element, a harmful factor needs to give a consideration. For a-Si solar cell, the highest efficiency of 9.1 % [11] reported is still low and it is used for small load requirements: these efficiency and scale problems are a

hindrance for a-Si. Compared to CdTe and a-Si, CIGS is a relatively new technology and promising in terms of conversion efficiency. The highest efficiency has reached 22.6 % for laboratory CIGS solar cell by ZSW [12], which is one of the highest efficiencies reached by using thin film solar cells. Despite the good performance of the CIGS solar cell, it uses rare elements of In and Ga resulting in limitation of its production capacity because of material shortages. Therefore, it is necessary to find a substitutional compound, in which all components are not only non-toxic but also earth abundant. For this reason, kesterite Cu_2ZnSnS_4 (CZTS) was emerged as one of the most promising candidates for low cost and high efficiency thin film solar cells. From the isoelectronic substitution, CZTS in quaternary group I_2-II-IV-VI_4 was obtained by replacing indium and gallium of group III by zinc of group II and tin of group IV in CIGS (Figure I.3). As a result, CZTS has similar properties to CIGS but requires raw material cost of 0.0049 *¢/W*, which is 4 times cheaper than that of CIGS (0.023 *¢/W*) [13].

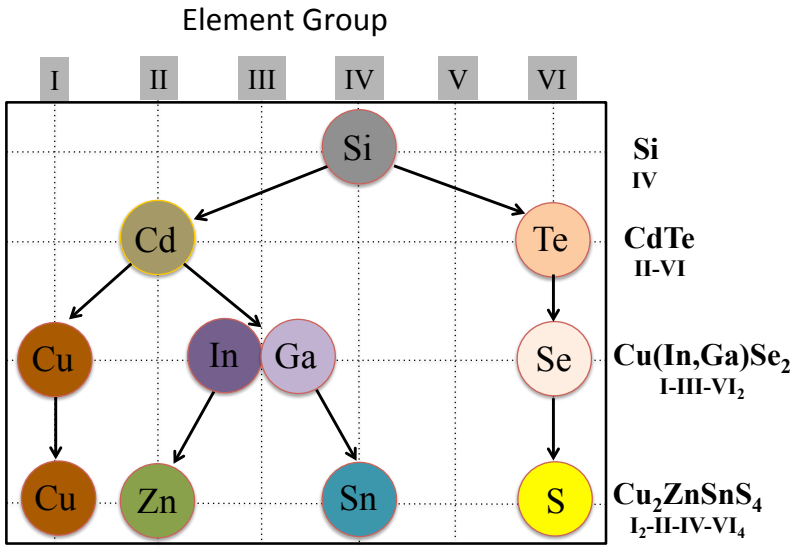

Figure I.3. Schematic illustration to form quaternary Cu_2ZnSnS_4 compound obtained by gradual substitution of elements.

I.3. Cu_2ZnSnS_4 Thin Film Solar Cells

The potential of the CZTS compound for the use of solar cells was firstly reported by Ito and Nakazawa in 1988. They prepared CZTS thin films by atom beam sputtering and made a device with cadmium tin oxide transparent conductive layer: the thus-obtained device showed an open circuit voltage V_{OC} of 165 mV under AM 1.5G illumination [14]. After their findings, many efforts were made to develop thin film solar cells using CZTS as an absorber layer. In 1996, Katagiri et al. reported successful fabrication of CZTS thin films by sulfurization of electron beam (E-B) evaporated precursor. They constructed a solar cell with structure of Al/ZnO/CdS/CZTS/Mo/SLG, and achieved an appreciable conversion efficiency of 0.66% for the first time [15]. In 1997, Friedlmeier et al. fabricated CTZS thin films using thermal evaporation of the elements and binary chalcogenides in high vacuum, then these layer used to make a solar cell with structure of CZTS/CdS/ZnO structure: the thus-obtained solar cell exhibited 2.3% of conversion efficiency [16]. This was record conversion efficiency at that time, but it was soon broken by Katagiri et al. in 1999. They produced CZTS solar cell with 2.63% of conversion efficiency using CZTS thin films, which fabricated by sulfurization of Cu/Sn/ZnS precursor layer using E-B evaporation and then sulfidized in an environment containing H_2S and N_2 gases [17]. This group also improved conversion efficiency of solar cell to 5.45% in 2003 and then to 6.7% in 2008 by optimizations of the sulfurization process [18]. Then a rapid improvement was demonstrated in 2010 by Todorov et al. They reported 9.6% of conversion efficiency solar cells by using a sulfoselenide $Cu_2ZnSn(S,Se)_4$ absorber layers deposited by spin coating a hydrazine-based precursor solution containing metal binary chalcogenides followed by sulfurization or selenization [19]. The conversion efficiency was then improved to be 11.1% in 2013 [20]. The current record conversion efficiency of CZTSSe thin film solar cells has reached 12.6 %

as reported by joint research from technology development companies IBM and Tokyo Ohka Kogyo [21]. The progress of power conversion efficiency of CZTSSe-based solar cells was shown in Figure I.4 [22].

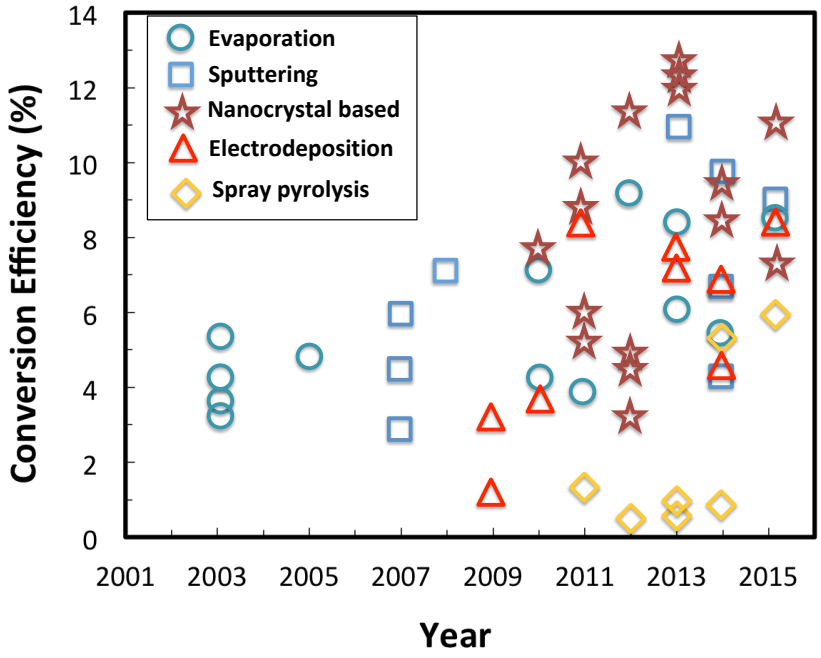

Figure I.4. Progress of power conversion efficiency of CZTSSe-based solar cell. Adapted with permission from Ref. 22.

I.3.1 Material Properties

In recent years, $Cu_2ZnSn(S,Se)_4$ compound semiconductors have attracted much attention not only from scientific society but also from industry because of their promising properties in solar conversion efficiency and low cost materials. These compounds are known as pure-sulfide Cu_2ZnSnS_4 (CZTS), sulfoselenide $Cu_2ZnSn(S,Se)_4$ (CZTSSe) and selenide $Cu_2ZnSnSe_4$. They are p-type semiconductors with band gap energies ranging from ca. 1.0 *eV* (for selenide) to ca. 1.5 *eV* (for pure sulfide) [23-26]. From theoretical calculation, CZTS and CZTSe can exhibit maximum efficiencies of 32.4 % and 31.0 %, respectively

(Figure I.5) [27]. Moreover, these compounds have high optical absorption coefficients of more than 10^4 cm^{-1} in the visible range, corresponding to 90% of incident light being absorbed within 100 *nm* of the surface [28-31].

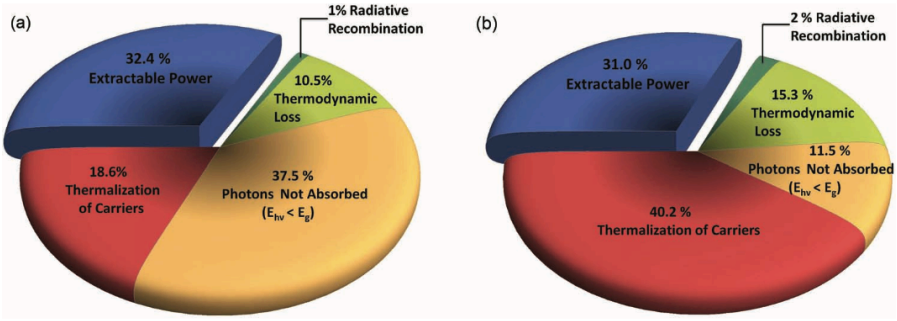

Figure I.5. Detailed balance calculations showing the magnitude of the fundamental loss processes with (a) CZTS and (b) CZTSe. Quoted with permission from Ref. 27.

In general, CZTSSe has two principal structures known as kesterite type and stannite type (Figure I.6) [32]. Both of them are tetragonal structures, consist of a cubic close packing array of sulfur anions and one half of the tetrahedral voids of cations. These two structures are similar except for the difference on the arrangements of Cu and Zn atoms. Kesterite with space group *I*-4 was ordered by Cu and Sn atoms alternate on the z = 0 and z = ½ planes and Cu and Zn atoms alternate on the z = ¼ and z = ¾ planes. Whereas the stannite belongs to space group *I*-42*m*: Zn and Sn atoms alternate on the z = 0 and z = ½ planes and Cu atoms are order on z = ¼ and z = ¾ planes. The lattice constant a and c are similar for both structures (a = 5.46 *Å* and c = 10.93 *Å*) [33-35]. However, CZTS and CZTSSe usually appear in kesterite phase because kesterite is thermodynamically more stable than stannite. That is the reason why these compounds often called “kesterite”, and in this study “kesterite” will be used for these compounds.

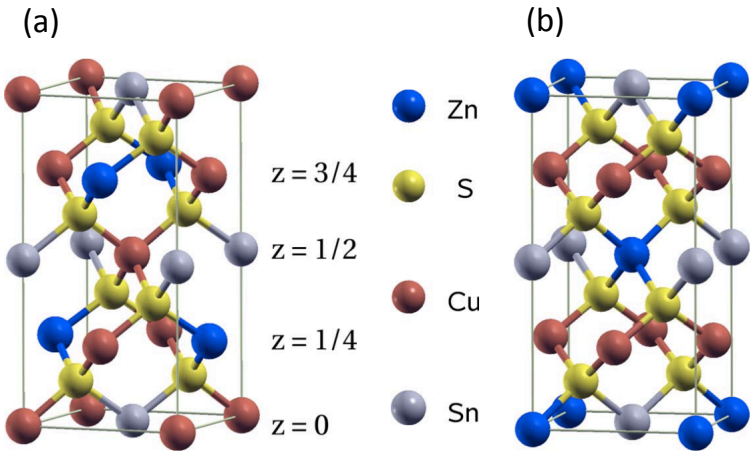

Figure I.6. (a) Kesterite and (b) stannite structures of CZTS material. Adapted with permission from Ref. 32.

Secondary Phases and Lattice Defects in CZTS Material

Although Cu_2ZnSnS_4 compound semiconductor has many advantages, there is some problems need to be solved to improve the properties of this material for photovoltaic applications. Since CZTS is a quaternary compound, it has more possible secondary phases and lattice defects than those in binary or ternary compounds. These structural failures caused recombination of electron-hole pairs in the bulk and the interface between absorber and buffer layers, leading to affecting the performance of photovoltaic device.

In CZTS, several secondary phases, such as CuS, Cu_2S, SnS, SnS_2, ZnS and Cu_2SnS_3 are expected to be formed depending on synthesis conditions. Figure I.7 shows a Cu_2S-ZnS-SnS_2 pseudoternary phase diagram [36]. CZTS single phase is present only within a small region at the center of the diagram. In other regions, there are presences of secondary phases alongside CZTS. Cu_2S and ZnS often appear in Cu-rich and Sn-poor compositions, whereas Sn_2S and Cu_2SnS_3 appear in Sn-rich and Zn-poor compositions. Among these secondary phases, CuS, Cu_2S, SnS, SnS_2 have different crystal structures from CZTS: they

are detectable from X-ray diffraction (XRD). However, ZnS and Cu_2SnS_3 have the same zincblende framework as CZTS. Therefore, it is quite difficult to detect the presence of these secondary phases in CZTS thin films by using XRD. There are some experimental studies on the formation of secondary phases in CZTS films; it is found that controlling elemental compositions could reduce formation of these secondary phases, leading the improvement in solar cell performance. Compared to the stoichiometric ratio of Cu, Zn, Sn and S elements of 2:1:1:4 with Cu/(Zn + Sn) = 1 and Zn/Sn = 1, most reported high efficiency CZTS solar cells have Cu/(Zn + Sn) and Zn/Sn ratios of ca. 0.8 and 1.2, respectively [37-42].

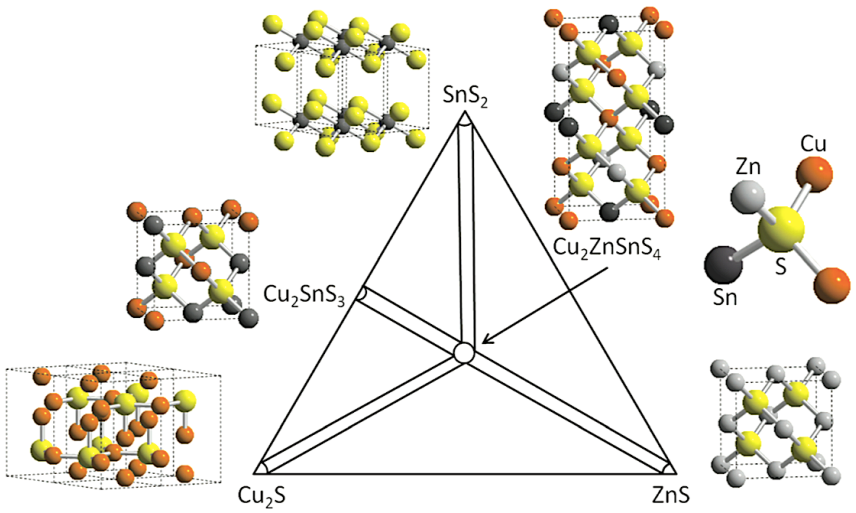

Figure I.7. A Cu_2S-ZnS-SnS_2 pseudoternary phase diagram. Quoted with permission from Ref.35.

Another structural feature of CZTS is presences of lattice defects such as vacancies (V_{Cu}, V_{Zn}, V_{Sn} and V_S) and antisites (Cu_{Zn}, Zn_{Cu}, Cu_{Sn}, Sn_{Cu}, Zn_{Sn} and Sn_{Zn}) as shown in Figure I.8 [43]. Among them, Cu_{Zn} is the dominant defect because it has lower formation energy than other defects [44]. This Cu_{Zn} might form defect complexes with other defects such as Cu_{Sn} and Sn_{Zn}, which have deep levels inside the band gap and act as recombination centers [45].

Therefore, it is necessary to reduce formation of these antisite defects in CZTS structure to improve open circuit voltage and solar cell efficiency. To solve this problem, one possible option can be attempted is doping with other elements for substitution. There have been some reports on improvement of quality of CZTS film by doping with other elements such as Ag, Ge, Cd and In [46-51].

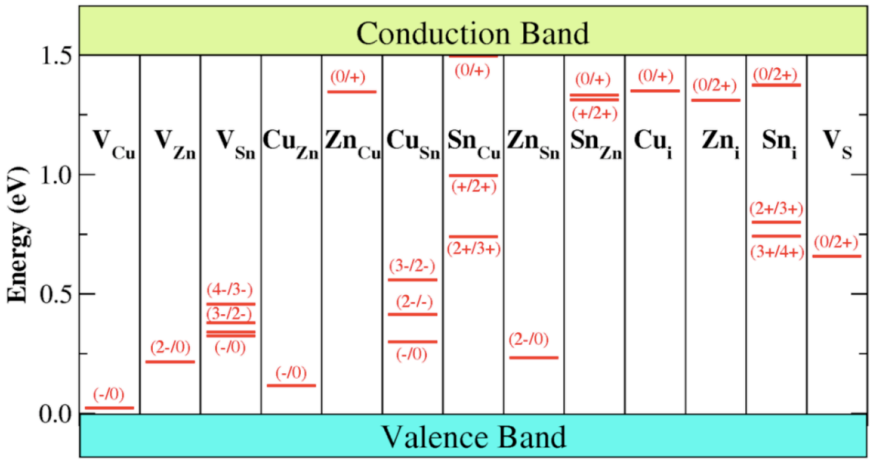

Figure I.8. The various point defects in the band gap of Cu_2ZnSn_4. Quoted with permission from Ref. 43.

I.3.2. Deposition Techniques of CZTS Thin Films

Various physical and chemical deposition techniques are used to fabricate CZTS thin films. These techniques can be classified into two general categories: vacuum and non-vacuum based techniques. Vacuum based deposition techniques are advantageous due to their possible fabrication of high quality thin films with good reproducibility. They include several techniques such as sputtering, evaporation, and pulsed laser deposition.

Sputtering deposition technique is a physical vapor deposition. This has been widely used for fabrication of CZTS thin films including various technologies such as argon beam,

ion beam, DC, RF, hybrid and reactive magnetron sputtering. CZTS films were fabricated by deposition of metallic precursors Cu-Zn-Sn/Cu-Zn-Sn-Cu or Cu-ZnS-SnS on the substrate then continue with or without a sulfurization [52-54].

Evaporation techniques such as electron beam, co-evaporation and thermal evaporation are often chosen to deposit thin films. CZTS thin films can be fabricated by two different approaches: a single-step deposition of all precursors at once followed by sulfurization or a two-step with sequential deposition of metallic precursors Cu-Zn-Sn/Cu-Zn-Sn-Cu or Cu-ZnS-SnS followed by a sulfurization/annealing [55-57].

Pulsed laser deposition is suitable for fabrication thin films with complex compositions. A high-power pulsed laser beam is focused inside a vacuum chamber to strike a target of the material to make this material vaporized from the target to a substrate. For this technique, the variation of pulsed laser density and the temperature of substrate can affect strongly to the properties of thus-obtained CZTS films [58,59].

The vacuum based deposition techniques use high cost equipment and consume very high energy. Therefore, in view of cost effectiveness, non-vacuum deposition techniques are more preferable. These techniques include spray pyrolysis deposition, electrodeposition, sol-gel deposition, etc.

Spray pyrolysis deposition is a technique widely used for fabricating thin films due to its simplicity and ease handling in fabrication process. This technique does not require vacuum at any stage during the deposition and can deposit thin film in a large scale: they are great advantages for industrial application. Thin films are deposited by spraying a precursor solution on heated substrates, where the constituents react to form the required chemical compound. Composition of the films could be controlled effectively by varying the concentration of constituents in the spray solution [60-62].

Electrodeposition or electrochemical deposition is also a common technique used for fabrication low cost thin films. This technique is a process that uses electrical current to reduce the cations of a desired material from an electrolyte and coat them as a thin film on a conductive substrate surface. CZTS films can be fabricated using two approaches: sequential electroplating of precursors and single step electrodeposition of precursors, followed by annealing for sulfurization or selenization at different atmosphere [63-65].

Sol-gel deposition is a chemical solution deposition using spin coating or deep coating. Thin films are prepared by two steps: preparation of sol-gel solution of precursor and coating of precursor solution onto the substrate [66-68].

Due to the main target for low production cost, spray pyrolysis is an attractive deposition technique among these non-vacuum techniques because of its versatility, simplicity and ease handling in fabrication process. Moreover, this technique can realize a fast deposition rate and the equipment for large–scale production is similar to that used for conventional spray coating used in various industrial processes. Therefore, in this study, spray pyrolysis technique was used to fabricate CZTS absorber layers for thin film solar cells.

I.3.2.1. Evolution of CZTS Thin Film Solar Cells processed by Spray Pyrolysis Deposition

Many research groups have been attempted to fabricate CZTS and CZTSSe thin films using spray pyrolysis techniques. The first successful fabrication of spray deposited CZTS films was reported by Nakayama and Ito in 1996. They fabricated CZTS films by spraying a precursor solution composed of CuCl, $ZnCl_2$ and $(CH_3NH)_2CS$ (thiourea) dissolved in a mixed solution of water and ethanol on glass substrates heated to 280-360 $^{\circ}C$ followed by

sulfurization at 550 $^{\circ}$C in an H_2S flow condition. The fabricated CZTS films exhibited p-type conduction showed a resistivity of 2×10^2 Ωcm [69]. K. Kumar et al. studied effects of substrate temperatures during the spray deposition on properties of thus-obtained CZTS films. Under optimized conditions, the direct optical band gap of CZTS films is found to lie between 1.40 and 1.45 eV with an average optical absorption coefficient of more than 10^4 cm^{-1} [70]. M. Valdes et al. prepared high quality CZTS films from aqueous solutions containing $CuCl_2$, $ZnCl_2$, $SnCl_2$ and CH_4N_2S. They applied a sulfurization treatment using sulfur vapor to avoid the use of toxic H_2S. They found that the sulfurization treatment had no significant effect on elemental compositions and band gap energies of fabricated films, whereas there was appreciable dependence on their grain sizes [71].

Although there are some reports on successful fabrications of the CZTS thin films, just only few groups reported on fabrication of complete CZTS solar cell devices using the films fabricated by spray pyrolysis technique in the literature. O. Vigil-Galan et al. studied effect of substrate temperature and annealing condition on properties of spayed films. CZTS films were obtained by spraying a precursor solution consisting of $(CH_3COO)_2Zn$, $CuCl_2$, $SnCl_4$ and thiourea dissolved in deionized water on Mo coated soda lime glass substrates, followed by heating at various temperatures. The post-annealing temperatures were changed from 550 $^{\circ}C$ to 580 $^{\circ}C$ in S and Sn atmosphere. The solar cell based on thus-obtained films with structure glass/Mo/CZTS/CdS/ZnO/ZnO:Al showed the best solar cell properties of an open circuit voltage of 361 mV, a short circuit current density of 7.5 mA/cm^2, a fill factor of 0.37 and an efficiency of 1% under irradiation of AM 1.5G (100 mW/cm^2) [72]. M. Patel *et al*. studied the structural, optical and electrical properties of spray deposited CZTS thin films under a non-equilibrium growth condition. They showed that growth condition would produce different magnitudes of microstrains in the fabricated films. The microstrains are

largely developed due to presence of secondary phases such as ZnS, Cu_xS and SnS_2, co-existing with the primary phases. CZTS solar cell with conversion efficiency of 0.154 % was reported [73]. Influences of concentrations of precursor solutions and annealing conditions on properties of the CZTS films was investigated by M. Espindola-Rodriguez et al.. They showed that Cu-poor and Zn-rich composition minimized formation of secondary phases without any detrimental effects on electrical properties of the films. CZTS solar cells with a device structure of SLG/MoCZTS/CdS/i-ZnO/ZnO:Al exhibited efficiencies between 0.45 to 0.5 % [74]. S. M. Bhosale *et al*. fabricated highly crystalline photoactive CZTS thin films without sulfurization treatment. They investigated the influence of substrate temperatures on properties and photoelectrochemical (PEC) performances of CZTS films and found that the significant improvement in the PEC properties was observed with increase in the growth temperature. The best solar cell device showed conversion efficiency of 0.86% [75]. Above studies reported results on pure sulfide CZTS solar cells, which had very low conversion efficiency (less than 1%). X. Zeng *et al*. prepared a sulfoselenide CZTSSe absorber thin film from an aqueous precursor solution containing $CuCl_2$, $ZnCl_2$, $SnCl_2$, and thiourea followed by annealing under selenium vapor at 520 $^{\circ}C$ for 12 min. They overcame the problem of instability of the spray solution by controlling pH of the precursor solution, leading to successful formation of a uniform CZTSSe thin film. The solar cell based on this absorber showed 5.1 % efficiency with open circuit voltage of 370 mV, short circuit current density of 27.3 mA/cm^2 and fill factor of 50.6% [76]. D. B. Khadka et al. reported fabrication of pure selenide CZTSe thin film solar cell with conversion efficiency of 5.74% [77]. The CZTSe thin film was deposited on Mo coated soda lime glass substrate by spraying an aqueous solution containing $CuCl_2$, $ZnCl_2$, $SnCl_4$ and thiourea in an alcohol-deionized water solvent followed by selenization at 500-520 $^{\circ}C$. This fabricated film

was used to make a complete solar cell with structure SLG/Mo/$MoSe_2$/CZTSe/In_2S_3/ZnO/ITO. They found that the increased efficiency is due to the improved quality of the interface between the CZTSe absorber layer and the In_2S_3 buffer layer. At present, most of high performance kesterite-based solar cells reported in the literature employed selenium containing kesterites, i.e., CZTSS and CZTSe. However, it should be more beneficial to use the pure sulfide form (CZTS) without including the highly toxic and less abundant selenium component.

I.3.2.2. Spray Pyrolysis Deposition Technique

A home-made spray pyrolysis system was used in the present study. The system consists of a spraying chamber, an atomizer with a spray nozzle, a reserve of precursor solution, a compressor for N_2 carrier gas, a heater and a temperature controller (Figure I.9). The main part is the atomizer having two supply routes and valves for spray solution and N_2 carrier gas, for controlling the spray rate by adjusting the N_2 flow rate. The substrate was put on the heater; the temperature of this heater was controlled by the temperature controller. The distance from the spray nozzle to the substrate was fixed at 20 *cm*. The fabrication of CZTS precursor thin films by using the apparatus can be divided in three steps: Spraying of the precursor solution, transportation of the droplets to the substrate and pyrolysis of the droplets.

There are some key parameters of the spray pyrolysis technique: the most important thing is preparation of the precursor solution used having sufficient solubility of source materials and stability without formation of any precipitate during the spray deposition. Other parameters such as substrate temperature, spray rate and annealing condition should also affect homogeneity, smoothness, grain size and crystallinity of the fabricated films.

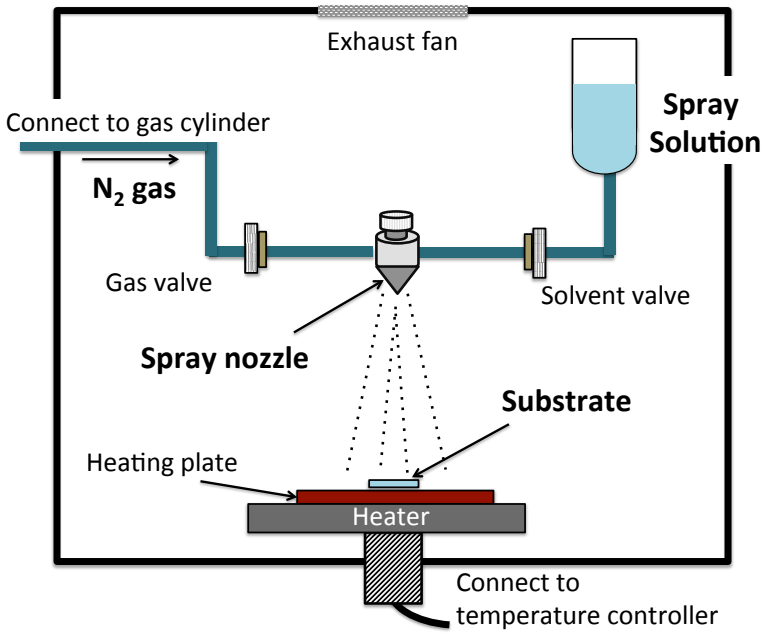

Figure I.9. The Schematic diagram of spray pyrolysis system.

I.3.3. Device Structure

In order to obtain a high performance solar cell, it is necessary to care not only qualities of absorber layers but also improvements of solar cell architectures. The structure of our typical CZTS thin film solar cell devices is illustrated in Figure I.10. The most common used substrate for CZTS solar cell is molybdenum coated glass substrate. A thin molybdenum layer was deposited on the glass substrate by DC magnetron sputtering technique with thickness of 1 μm; this is a back contact with good conductivity and high stability. On the top of the back contact, an absorber layer, a p-type semiconductor CZTS thin film with the thickness of 1 μm, was deposited. This absorber produces excited electron-hole pairs by absorption of sunlight radiations. The p-n junction was formed by coating on the top of the absorber layer with a thin n-type semiconductor buffer layer. Typical material used as buffer layer is CdS because it was found to give the best performance devices for CIGS, CZTS and CZTSSe solar cells. This layer also has roles to improve the lattice matching and to adapt the

band gaps between the absorber and the window layers. CdS with thickness of 70 *nm* is deposited by chemical bath deposition from $CdSO_4$, NH_3, and thiourea solution at 60 $^{\circ}C$ in 7 *min*. Then a 50 *nm*-thick i-ZnO and 350 *nm* thick ITO bilayer was deposited on the top of the CdS layer by radio frequency (RF) magnetron sputtering. This bilayer is a transparent conducting oxide with wide band gap to admit maximum amount of light to the absorber, so it is called window layer. Finally, Al grid as a top contact with thickness of 500 *nm* was deposited by thermal evaporation with a mask protection to complete the device structure of Al/ITO/ZnO/CdS/CZTS/Mo/Glass.

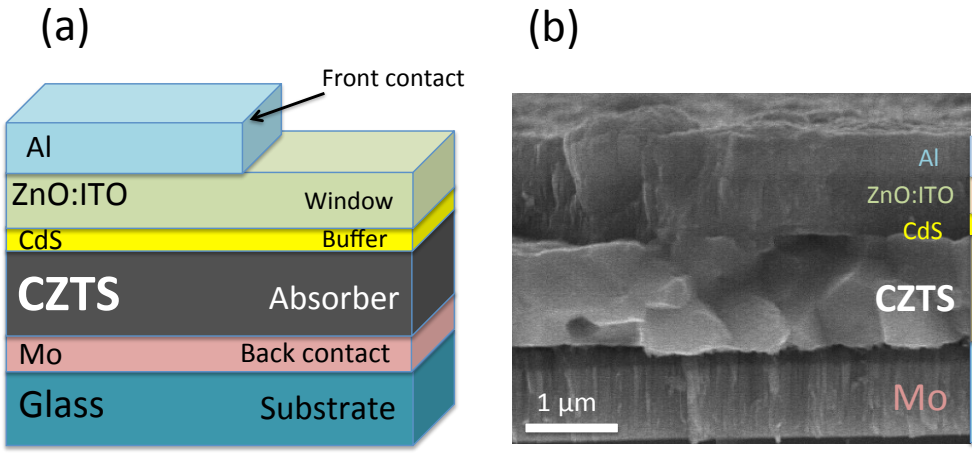

Figure I.10. Typical structure (a) and cross-sectional SEM image (b) of a complete CZTS solar cell device.

I.4. Operation of Solar Cells

Solar cells are electrical devices, which are built to convert directly the energy of sunlight into electricity by photovoltaic effect. The operation of a solar cell based on the absorption of the sunlight energy to generate charge carriers, the separation and the extraction of these carriers to an external circuit. The incident photon has energy greater than that of band gap energy of the absorber used can generate electron-hole pairs. The electrons

and holes will exist for a length of time equal to the minority carrier lifetime. In order to complete the photovoltaic conversion process, these charge carriers need to be extracted and collected before the carrier recombination occurs. These charge carries are separated by the action of an electric field existing at the p-n junction. Then they are driven towards one or another metal contact layer to establish photovoltage at open circuit and a photocurrent at short circuit; electric power will be generated by connected this system to an external circuit. Therefore, in order to increase efficiency of solar cells, the absorber layer needs to create more electron-hole pairs by absorbing more incident photon; the separation of charge carries by p-n junction extract as currents and photovoltage need to occur without including appreciable losses.

I.4.1. P-n Junctions

In a typical photovoltaic cell, p-n junction is formed by joining n-type and p-type semiconductor materials in a close contact. If these p-type and n-type semiconductors are the same material, they will form a homojunction. Otherwise, a heterojunction is formed by using two different semiconductor materials. In p-type semiconductors, holes are majority carriers and electrons are minority carriers; whereas holes are minority carriers and electrons are majority carriers in p-type semiconductors. When a p-type and n-type semiconductors are interconnected, electrons from the n-type side and holes from p-type side near the interface diffuse in the other side of the junction leaving the donor and acceptor atoms behind. This diffusion process makes the region close to the junction becomes depleted of mobile charge carriers, which called “depletion region” or “space charge region”. This region causes internal electric field between the positive ions in n-type material and negative ions in the p-type material; which drives electrons towards the n side and holes towards the p

side. This is drift process, which drift carrier in an opposite direction of diffusion process. An equilibrium condition is reached when the drift and diffusion currents are equal, and the net electron current through the junction becomes zero. At that time, the Fermi level of the p-type and n-type layers is equal in the band diagram. Under illumination, minority carriers are generated in both p-type and n-type semiconductors, electrons and holes are transferred to n-type and p-type sides, respectively as shown in Figure I.11.

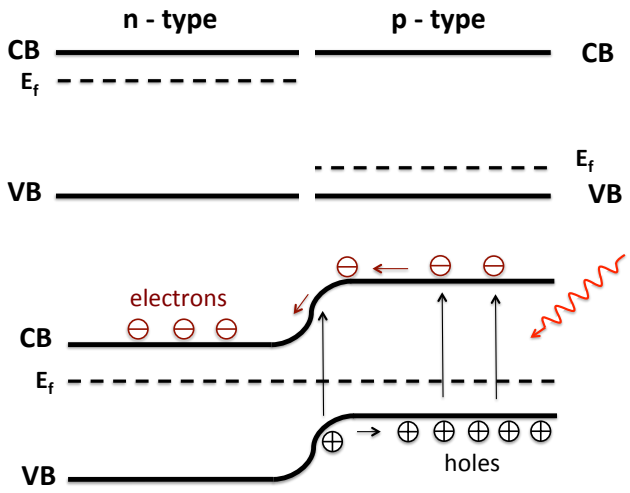

Figure I.11. Working principle of p-n junction under illumination.

CZTS thin film solar cells are based on the p-n heterojunction formed by the p-type semiconductor absorber layer of CZTS and an n-type semiconductor layer such as CdS, In_2S_3 and ZnS [78-83]. An important parameter in a heterojunction is the band offset of alignment of valence and conduction bands of contacted layers because it has influence to the transportation of carriers. Spike-like type alignment is formed when the conduction band minimum of the buffer layer higher and the buffer valence band maximum lower than the corresponding bands of the absorber (Figure I.12a). The opposite alignment called cliff-like type is formed when the conduction band minimum and the valence band minimum of the buffer layer lower than that of the absorber layer (Figure I.12b). The optimal band alignment

of the absorber/buffer interface is spike-like type alignment because it supports for transportation of charge carries and reduces recombination at absorber/buffer interface that causes loss in open circuit voltage V_{OC}.

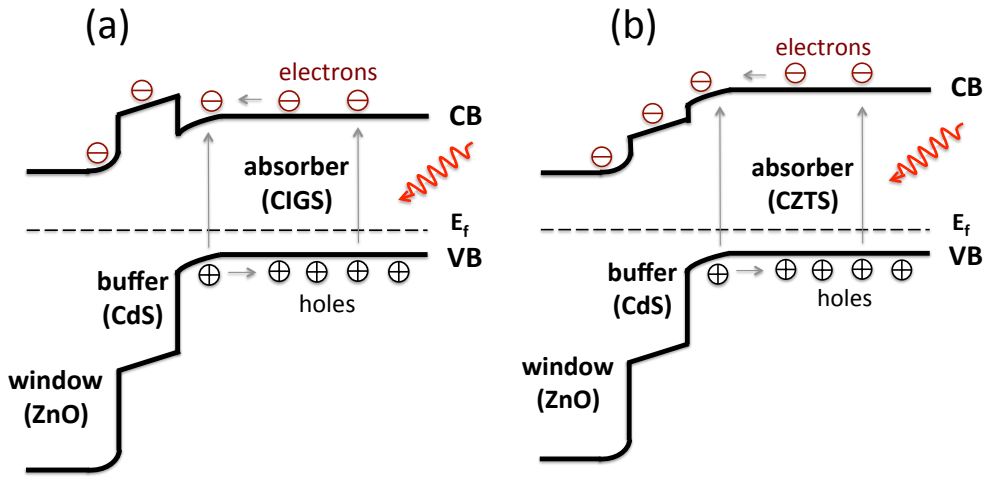

Figure I.12. Spike-like type (a) and cliff-like type (b) band alignments of CIGS and CZTS thin film solar cells, respectively.

I.4.2. Current Density – Voltage Characteristics of Solar Cells

Current density – voltage measurements in the dark and under illumination are often used to characterize solar cell as shown in Figure I.13. Primary parameters expressed the performance of a device are open circuit voltage (V_{OC}), short circuit current density (J_{SC}), fill factor (FF) and power conversion efficiency (η).

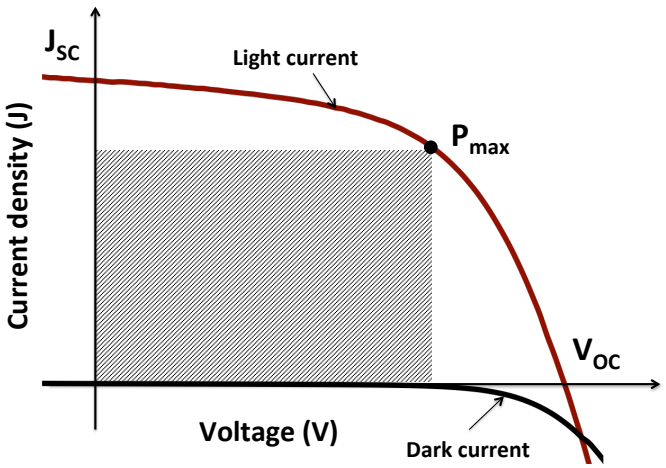

Figure I.13. Typical J-V characteristic of a solar cell.

Open circuit voltage (V_{OC}) is a maximum voltage, which appears when the terminals are not connected. At voltages between 0 and V_{OC}, the cell will generate electric power. V_{OC} depends on light intensity as well as band gap of material; V_{OC} is always less than the value of band gap energy.

Short circuit current density (J_{SC}) is the maximum photocurrent density of a solar cell observed when terminals are connected. It depends on the number of incident photons, the collection probability and strongly depends on the band gap of the absorber material. A material with a small band gap will absorb more photons, so J_{SC} increases with the decrease of band gap energy.

Fill factor (FF) also determines the maximum power of a solar cell. For ideal solar cell, the value of FF is close to one. It describes the "squareness" of the J-V curve. FF is defined as the ratio of the values of product of the current density and voltage of the cells at its maximum power point to the product of open circuit voltage and short circuit current density.

$$FF = \frac{J_m V_m}{J_{SC} V_{OC}} \tag{1.1}$$

Efficiency (η) is the most important parameter that is commonly used for expressing the performance of solar cells. It is defined by a ratio of the maximum power density output by the cell to the power density input of incident light source.

$$\eta = \frac{J_m V_m}{P_{Input}} = \frac{J_{SC} V_{OC} FF}{P_{Input}} \tag{1.2}$$

The efficiency of solar cell depends on the spectrum as well as the intensity of the incident light and the temperature of the solar cell. Current density – voltage measurement for terrestrial solar cell often performs at room temperature 25 $^{\circ}C$ under AM1.5 G spectrum, this is a standard spectrum at the Earth's surface.

I.5. Motivation and Research Objectives

The purpose of this thesis is to study on fabrication of CZTS thin films using spray pyrolysis technique for low cost, high efficiency and environmental friendly solar cells. In this work, developments of fabrication procedures to obtain a CZTS film having a sufficient quality applicable to an absorber layer of solar cells, and electrostructural modifications of the CZTS film by controlling chemical composition and introduction of dopants for improvements of its solar cell properties were discussed. Details of the objectives presented in this study are:

(1) Investigation of the fabrication procedure of CZTS thin films using spray pyrolysis followed by sulfurization with different annealing conditions to obtain a homogeneous and compact CZTS film with large grain size.

(2) Evaluation of the optimal composition of Cu_2ZnSnS_4 thin films and its effects to solar cell performance.

(3) Investigation for reduction of antisite defects of CZST film by doping Ag to precursor solution and studies on structural, morphological and electrical properties of Ag-containing CZTS thin films and their solar cell performance.

(4) Investigations of the effects of indium incorporation on structural and photovoltaic properties of CZTS thin films.

I.6. Outline of Thesis

This thesis consists of 6 chapters. The outline of each chapter is as follows:

Chapter 1

This chapter described historical backgrounds of photovoltaics specifically focused on physicochemical/optical properties of CZTS material, device structures of thin film photovoltaics, their fabrication techniques, and progresses in record efficiencies reported by the other groups. The motivation and research objectives of this study were also given in the chapter.

Chapter 2

Fabrication conditions of the CZTS absorber layer by controlling several parameters and procedures of spray pyrolysis to obtain a smooth and homogeneous film with large grain size were investigated. CZTS film was fabricated on an Mo-coated glass substrate by using a facile spray pyrolysis deposition of a precursor film from an aqueous solution containing $Cu(NO_3)_2$, $Zn(NO_3)_2$, $Sn(CH_3SO_3)_2$ and thiourea. Effects of annealing temperature and

annealing duration on crystalline structures and morphologies of the films were examined. A solar cell with a structure of glass/Mo/CZTS/CdS/*i*-ZnO/indium tin oxide (ITO)/Al was fabricated using Sn-rich CTZS film at an optimal annealing condition, exhibited maximum conversion efficiency of 5.8%.

Chapter 3

Impact of precursor compositions on the structural and photovoltaic properties of spray-deposited Cu_2ZnSnS_4 thin films was studied. Cu, Zn and Sn compositions in CZTS films were adjusted by controlling the concentrations of the corresponding metallic ions in the precursor solutions. Effects of metallic composition on grain sizes, morphologies, acceptor densities, the nature of the acceptor defects and carrier lifetime were discussed in detail. A solar cell based on the CZTS film with an empirically optimal composition showed conversion efficiency of 8.1%.

Chapter 4

We attempted to reduce antisite defects in the CZTS film by a partial replacement of Cu to Ag to obtain $(Cu_{1-x}Ag_x)_2ZnSnS_4$ (ACZTS) film. The precursor films with different amount of Ag were fabricated by varying the molar ration of Ag/(Cu + Zn + Sn) in aqueous precursor solutions. We found that incorporation of Ag to CZTS film enhanced grain growth and reduced amounts of unfavorable copper on zinc antisite defects in comparison with those in the bare CZTS film. The Ag incorporation also improved the band alignment at the p-n junction with CdS buffer layer. The best PCE achieved was 7.1% using a device based on the ACZTS film with Ag/(Ag + Cu) ratio of 0.02.

Chapter 5

In this chapter, effects of indium (In) incorporation on structural and photovoltaic

properties of CZTS thin films were investigated. Different In amounts of the In precursor ($In(NO_3)_3$) were added to precursor solution, which used to fabricate In-incorporated CZTS films by using spray pyrolysis technique. The structural and morphological analyses showed significant effects of In incorporation on properties of CZTS films. As a result, the addition of In to the CZTS film with low doping ratio In/(Zn + Sn) = 0.01 had beneficial for improvement of solar cell performance.

Chapter 6

General conclusions with the results obtained from this work, remarks, and perspectives for the future were given in this chapter.

References

[1] B. Seger, *Global Energy Consumption*, 2016.

[2] World Energy Resources 2016, *World Energy Council*, 2017.

[3] Kevin P. Musselman and Lukas Schmidt-Mende, *Green*, 2011, 1, 7-27.

[4] E. Becquerel, *Comptes Rendus*, 1839, 9, 561-567.

[5] C. Fritts, *Van Nostrands Engineering Magazine*, 1885, 32, 388-395.

[6] APS News, American Physical Society, 2009, 18.

[7] K. Yoshikawa, W. Toshida, T. Irie, H. Kawasaki, K. Konishi, H. Ishibashi, T. Asatani, D. Adachi, M. Kanematsu, H. Uzu and K. Yamamoto, Solar Energy Materials and Solar Cells, 2017, 173, 37-42.

[8] W. Shockley and H. J. Queisser, Journal of Applied Physics, 1961, 32, 510-519.

[9] W. S. Yang, B. W. Park, E. H. Jung, N. J. Jeon, Y. C. Kim, D. U. Lee, S. S. Shin, J. Seo,

E. K. Kim, J. H. Noh and S. I. Seok, Science, 2017, 356, 1376.

[10] E. Wesoff, Search Greentech Media, 2016.

[11] E. L. Salabas, A. Salabas, B. Mereu, O. Caglar, M. Kupich, J. S. Cashmore and I. Sinicco, Progress in Photovoltaics: Research and Applications, 2016, 24, 1068-1074.

[12] P. Jackson, R. Wuerz, D. Hariskos, E. Lotter, W. Witte and M. Powalla, Phys. Status Solidi RRl, 2016, 10, 538-586.

[13] C. Wadia, A. P. Alivisatos and D. M. Kammen, Environ. Sci. Technol, 2009, 43, 2072-2077.

[14] K. Ito and T. Nakazawa, Japanese Journal of Applied Physics, 1988, 27, 2094-2097.

[15] H. Katagiri, M. Nishimura, T. Onozawa, S. Maruyama, M. Fujita, T. Sega and T. Watanabe, Proceeding of the Power Conversion Conference, 1997, 2, 1003-1006.

[16] M. Friedlmeier, N. Wieser, T. Walter., 14th Eur PVSEC Exhib, Barcelona, Spain, 1997, 10–13

[17] H. Katagiri, K. Jimbo, W.S. Maw, K. Oishi, M. Yamazaki, H. Araki, A. Takeuchi, 2009, 517, 2455-2460.

[18] H. Katagiri, K. Jimbo, S. Yamada, T. Kamimura, W.S. Maw, T. Fukano, T. Ito, T. Motohiro, Applied Physics Express, 2008, 1, 041201.

[19] Teodor K. Todorov, Kathleen B. Reuter, and David B. Mitzi, Adv. Mater., 2010, 22, E156-E159.

[20] Teodor K. Todorov, Jiang Tang, Santanu Bag, Oki Gunawan, Tayfun Gokmen, Yu Zhu and David B. Mitzi, Adv. Energy. Mater. 2013, 3, 34-38.

[21] Wei Wang, Mark T. Winkler, Oki Gunawan, Tayfun Gokmen, Teodor K. Todorov, Yu Zhu and David B. Mitzi, Adv. Energy Mater. 2014, 4, 1301465.

[22] S. A. Vanalakar, G. L. Agawane, S. W. Shin, M. P. Suryawanshi, K. V. Gurav, K. S. Jeon, P. S. Patil, C. W. Jeong, J. Y. Kim, J. H. Kim, Journal of Alloys and Compounds, 2015, 619, 109-121.

[23] H. Yoo and J. Kim, Thin Solid Films, 2010, 518, 6567-6572.

[24] K. Fu, P. Liu, C. Liu, F. Yang, Y. Chen, J. Lu and S. Yang, Mater. Electron. Eng., 2014, 1, 7.

[25] K. V. Gurav, S. M. Pawar, S. W. Shin, M. P. Suryawanshi, G. L. Agawane, P. S. Patil, J. H. Moon, J. H. Yun and J. H. Kim, Applied Surface Science, 2013, 283, 74-80.

[26] S. Tajima, R. Asahi, D. Isheim, D. N. Seidman, T. Itoh, M. Hasegawa and K. Ohishi, Applied Physics Letter, 2014, 105, 093901.

[27] Wooseok Ki and Hugh W. Hillhouse, Adv. Energy Mater. 2011, 1, 732-735.

[28] S. Khoshmashrab, M. J. Turnbull, D. Vaccarello, Y. Nie, S. Martin, D. A. Love, P. K. Lau, X. Sun and Z. Ding, Electrichimica Acta, 2015, 162, 176-184.

[29] R. Schurr, A. Holzing, S. Jost, R. Hock, T. Vob, J. Schulze, A. Kirbs, A. Ennaoui, M. Lux-Steiner, A. Weber, I. Kotschau and H. W. Schock, Thin Solid Films, 2009, 517, 2465-2468.

[30] M. Cao, L. Li, B. L. Zhang, J. Huang, L. J. Wang, Y. Shen, Y. Sun, J. C. Jiang and G. J. Hu, Solar Energy Materials & Solar Cells, 2013, 117, 81-86.

[31] S. K. Saha, A. Guchhait and A. J. Pal, Phys. Chem. Chem. Phys., 2012, 14, 8090-8096.

[32] J. Paier, R. Asahi, A. Nagoya and G. Kresse, Phys. Rev. B, 2009, 79, 115126.

[33] S. Delbos, EPJ Photovoltaics, 2012, 3, 35004.

[34] X. Song, X. Ji,, M. Li, W. Lin, X. Luo and H. Zhang, International Journal of Photoenergy, 2014, 2014, 1-11.

[35] S. Ji and C. Ye, Reviews in Advanced Sciences and Engineering, 2012, 1, 42-58. [35] Y. P. Lin, Y. F. Chi, T. E. Hsieh, Y. C. Chen, K. P. Huang, Journal of Alloys and Compounds, 2016, 654, 498-508.

[36] H. Du, F. Yan, M. Young, B. To, C. S. Jiang, P. Dippo, D. Kuciauskas, Z. Chi, E. A. Lund, C. Hancock, W. M. H. OO, M. A. Scarpulla and G. Teeter, J. Appl. Phys., 2014, 115, 173502.

[37] V. Tunuguntla, W. C. Chen, P. H. Shih, I. Shown, Y. R. Lin, J. S. Hwang, C. H. Lee, L. C. Chen and K. H. Chen, J. Mater. Chem. A, 2015, 3, 15324.

[38] A. Emrani, P. Vasekar and C. R. Westgate, Solar Energy, 2013, 98, 335-340.

[39] S. Kahraman, S. Cetinkaya, M. Podlogar, S. Bernik, H. A. Cetinkara and H. S. Guder, Ceramics International, 2013, 39, 9285-9292.

[40] J. J. Scragg, P. J. Dale and L. M. Peter, Electrochemistry Communications, 2008, 10, 639-642.

[41] T. J. Huang, X. Yin, C. Tang, G. Qi and H. Gong, J. Mater. Chem. *A*, 2015, 3, 17788.

[42] J. Tao, J. Liu, L. Chen, H. Cao, X. Meng, Y. Zhang, C. Zhang, L. Sun, P. Yang and J. Chu, Green Chem., 2016, 18, 550.

[43] S. Chen, X. G. Gong, A. Walsh and S. H. Wei, MRS Online Proceeding Library Archive, 2011, 1370, 1-12.

[44] S. Chen, A. Walsh, X. G. Gong and S. H. Wei, Adv. Mater., 2013, 25, 1522-1539.

[45] A. Polizzotti, I. L. Repins, R. Noufi, S. H. Wei and D. B. Mitzi, Energy Environ. Sci., 2013, 6,, 3171.

[46] S. Giraldo, C. M. Ruiz, M. E. Rodriguez, Y. Sanchez, M. Placidi, D. Cozza, D. Barakel, L. Escoubas, A. P. Rodriguez and E. Saucedo, Solar Energy Materials & Solar Cells,

2016, 151, 44-51.

[47] D. H. Kuo and M. Tsega, Jpn. J. Appl. Phys., 2014, 53, 035801.

[48] C. J. Hages, M. J. Koeper and R. Agrawal, Solar Energy Materials & Solar Cells, 2016, 145, 342-348.

[49] M. Neuschitzer, J. Marquez, S. Giraldo, M. Dimitrievska, M. Placidi, I. Forbes, V. I. Roca, A. P. Rodriguez and E. Saucedo, J. Phys. Chem. C, 2016, 120, 9661-9670.

[50] A. Guchhait, Z. Su, Y. F. Tay, S. Shukla, W. Li, S. W. Leow, J. M. R. Tan, S. Lie, O. Gunawan, L. H. Wong, *ACS Energy Lett.* **2016**, *1*, 1256-1261.

[51] J. Ge, J. Chu, J. Jiang, Y. Yan and R. Yang, ACS. Appl. Mater. Interfaces, 2014, 6, 21118 – 21130.

[52] S. Zhou, R. Tan, Z. Jiang, X. Shen, W. Zu and W. Song, J Mater Sci: Mater Electron, 2013, 24, 4958–4963.

[53] T. P. Dhakal, C. Y. Peng, R. R. Tobias, R. Dasharathy, C. R. Westgate, Solar Energy, 2014, 100, 23-30.

[54] B. T. Jheng, P. T. Liu, M. C. Wu, Solar Energy Materials & Solar Cells, 2014, 128, 275-282.

[55] F. Biccari, R. Chierchia, M. Valentini, P. Mangiapane, E. Salza, C. Malerba, C. L. A. Ricardo, L. Mannarino, P. Scardi, A. Mittiga, Energy Procedia, 2011, 10, 187-191.

[56] J. Zhang, B. Long, S. Cheng and W. Zhang, International Journal of Photoenergy, 2013, 2013, 1-6.

[57] U. Chalapathi, S. Uthanna and V. S. Raja, Journal of Renewable and Sustainable, 2013, 5, 031610.

[58] A. V. Moholkar, S. S. Shinde, A. R. Babar, K. U. Sim, Y. B. Kwon, K. Y. Rajpure, P. S.

Patil, C. H. Bhosale, J. H. Kim, Solar Energy, 2011, 85, 1354-1363.

[59] Y. Watanabe, H. Miura, Y. G. Shim, K. Wakita, Physica status solidi (c), 2015, 12, 733-736.

[60] K. Moriya, K. Tanaka and H. Uchiki, Japanese Journal of Applied Physics, 2007, 46, 5780.

[61] K. Diwate, K. Mohite, M. Shinde, S. Rondiya, A. Pawbake, A. Date, H. Pathan, S. Jadkar, Energy Procedia, 2017, 110, 180-187.

[62] Z. Seboui, Y. Cuminal and N. K. Turki, Journal of Renewable and Sustainable Energy, 2013, 5, 023113.

[63] M. I. Khalil, R. Bernasconi, L. Magagnin, Electrochimia Acta, 2014, 145, 154-158.

[64] D. Colombara, A. Crossay, L. Vauche, S. Jaime, M. Arasimowicz, P. J. Dale, Physica Status Solidi (a), 2015, 212, 88-102.

[65] M. Jeon, T. Shimizu, S. Shingubara, Materials Letters, 2011, 65, 2364-2367.

[66] H. Park, Y. H. Hwang, B. S. Bae, Journal of Sol-Gel Science and Technology, 2013, 65, 23-27.

[67] L. Dong, S. Cheng, Y. Lai, H. Zhang, H. Jia, Thin Solid Films, 2017, 626, 168-172.

[68] X. Yu, A. Ren, F. Wang, C. Wang, J. Zhang, W. Wang, L. Wu, W. Li, G. Zeng and L. Feng, International of Journal of Photoenergy, 2014, 2014, 1-6.

[69] N. Nakayama and K. Ito, Applied Surface Science, 1996, 92, 171-175.

[70] Y. B. Kishore Kumar, G. Suresh Babu, P. Uday Bhaskar and V. Sundara Raja, Solar Energy Materials & Solar Cells, 2009, 93, 1230-1237.

[71] M. Valdes, G. Santoro and M. Vazquez, Journal of Alloys and Compounds, 2014, 585, 776-782.

[72] O. Vigil-Galan, Maykel Courel, M. Espindola-Rodriguez, V. Izquierdo-Roca, E. Saucedo and A. Fairbrother, Journal of Renewable and Sustainable Energy 2013, 5, 053137.

[73] M. Patel, I. Mukhopadhyay and A. Ray, J. Phys. D: Appl. Phys., 2012, 45, 445103.

[74] M. Espindola-Rodriguez, M. Placidi, O. Vigil Galan, V. Izquierdo Roca, Z. Fontane, A. Fairbrother, D. Sylla, E. Saucedo and A. Perez-Rodriguez, Thin Solid Films, 2013, 535, 67-72.

[75] S. M. Bhosale, M. P. Suryawanshi, M. A. Gaikwad, P. N. Bhosale, J. H. Kim and A. V. Moholkar, Materials Letters, 2014, 129, 153-155.

[76] X. Zeng, K. F. Tai, T. Zhang, C. W. J. Ho, X. Chen, A. Huan, T. C. Sum and L. H. Wong, Solar Energ Materials & Solar Cells, 2014, 124, 55-60.

[77] Dhruba B. Khadka, SeongYeon Kim and JunHo Kim, J. Phys. Chem. C, 2015, 119, 12226-12235.

[78] N. S. Das, P. K. Ghosh, M. K. Mitra, K. K. Chattopadhyay, Physca E: Low-dimensional Systems and Nanostructures, 2010, 42, 2097-2102.

[79] A. I. Oliva, O. S. Canto, R. C. Rodriguez, P. Quintana, Thin Solid Films, 2001, 391, 28-35.

[80] N. E. Fard, R. Fazaeli, R. Ghiasi, Chemical Engineering & Technology, 2016, 39, 149-157.

[81] N. Kamarulzaman, M. F. Kasim and R. Rusdi, Nanoscale Res Lett., 2015, 10, 346.

[82] V. Srikant and D. R. Clarke, Journal of Applied Physics, 1988, 83, 5447.

[83] M. H. M. Zaid, K. A. Matori, S. H. A. Aziz, A. Zakaria and M. S. M. Ghazali, Int. J. Mol. Sci., 2012, 13, 7550-7558.

Chapter II

Fabrication of Cu_2ZnSnS_4 Thin Film Solar Cells by A Facile Spray Pyrolysis Technique

II.1. Introduction

Various techniques have been used to synthesize CZTSSe thin films for application in solar cells [1-6]. In view of environmental effects, it should be advantageous to apply non-vacuum technology for fabrication of the thin films such as electrodeposition [7-9], spin coating [6, 10-12], and spray pyrolysis [13-19]. Among them, spray pyrolysis is an attractive non-vacuum technique because of its versatility and easiness to deposit the film in a large area [20]. $Cu(In,Ga)(S,Se)_2$ solar cells with conversion efficiencies of over 10% have been obtained by this method, and the capability of this method for fabricating high quality thin film photoabsorbers has been proven [21, 22]. Some groups have reported successful fabrication of CZT(S,Se)-based thin film solar cells using the spray pyrolysis technique [13,19].

Most of the CZTSSe-based solar cells reported in the literature employed CZTSSe films with selenium-rich compositions. In view of the toxicity issue, the use of pure sulfide (i.e., CZTS) would be preferable. However, there have been only a few reported examples of fabrication of CZTS-based solar cells by the spray pyrolysis method; reported PECs were quite low (less than 1%) [23, 24], despite several examples of successful fabrication of pure sulfide CZTS-based solar cells with high PCEs using other vacuum [25] and non-vacuum [26] techniques. These facts motivated us to prepare a highly efficient CZTS-based solar cell using the spray pyrolysis technique.

In this chapter, several conditions for fabricating a smooth and homogeneous CZTS film with large grain size appreciable for the absorber layer were investigated. Achievement of 5.8% PCE was demonstrated for the first time using a spray-deposited pure sulfide CZTS absorber.

II.2. Experimental

II.2.1. Fabrication of CZTS Thin Film Solar Cells

An aqueous solution containing 0.019 M copper nitrate ($Cu(NO_3)_2$), 0.009 *M* zinc nitrate ($Zn(NO_3)_2$), 0.0125 *M* tin methanesulfonate ($Sn(CH_3SO_3)_2$) and 0.06 *M* thiourea ($SC(NH_2)_2$) with pH adjusted to 1.5 by adding a few drops of conc. HCl was used as a precursor solution. Eight *ml* of the solution was sprayed on a Mo-coated glass substrate (Mo/glass) that was heated at 380 °*C* using a hotplate. The as-deposited film was placed in an evacuated borosilicate glass ampoule together with 20 *mg* sulfur powder; the ampoule was annealed at 580–600 °*C* for 10–50 *min*. On the thus-obtained CZTS absorber film, a CdS buffer layer was deposited by chemical bath deposition (CBD) [27]. An ITO/ZnO bilayer was then deposited on the top of the CdS layer by radio frequency (RF) magnetron sputtering to form a device with a structure of ITO/ZnO/CdS/CZTS/Mo/glass. In this study, active area of all the devises was fixed at 0.03 cm^2.

II.2.2. Characterizations

Crystalline structures of the films were analyzed by X-ray diffraction (XRD) using a Rigaku MiniFlex X-ray diffractometer (Cu Ka, Ni filter). Raman spectra were analyzed by a Jasco NRC 3100 Laser Raman Spectrophotometer with excitation laser of wavelength of 532 *nm*. Morphologies of the films were examined using a Hitachi S-5000 FEG field emission scanning electron microscope (SEM) at an acceleration voltage of 20 *kV*. Atomic compositions of the precursor solution, as-deposited films and finally obtained CZTS films were determined by inductively coupled plasma (ICP) analysis on a Perkin-Elmer OPTIMA 3000-XL ICP emission spectrometer. For this measurement, the film samples were immersed in aqua regia overnight to dissolve all of the components. The thus-obtained clear solution was then diluted to an appropriate concentration before analysis. Current density–

voltage (J–V) characteristics of solar cell devices under simulated AM1.5G irradiation (100 $mW\ cm^{-2}$) were determined with a Bunkoh-Keiki CEP-015 photovoltaic measurement system.

II.3. Results and Discussion

In order to prepare an aqueous solution for spray pyrolysis, tetravalent Sn^{4+} salts such as $SnCl_4$ are unfavorable because they easily undergo hydrolysis to be precipitated even in a strongly acidic solution. Moreover, in view of its availability as a source material, the use of a divalent copper salt is better than the use of a monovalent salt, for which there is the possibility of occurrence of disproportionation or oxidation that results in loss of its chemical purity. In this work, therefore, we employed Sn^{2+} and Cu^{2+} salts as precursor materials as in the work reported by Zeng et al [13]. It should also be noted that care was needed in the mixing order, and appropriate content of thiourea and control of pH were indispensable to prevent precipitation induced by the oxidation of Sn^{2+} with Cu^{2+} to form an insoluble Sn^{4+} hydroxide (oxide). Indeed, when we attempted to prepare the spray solution by a mixed solution of Cu^{2+}, Sn^{2+}, and Zn^{2+} salts without addition of thiourea at uncontrolled pH as the starting solution, a white precipitate was gradually formed within a few hours, as shown in Figure I.1a. The corresponding X-ray diffraction (XRD) pattern of the precipitate indicated formation of SnO_2 (Figure I.1c). In order to overcome the problem of precipitation, therefore, it is necessary to mix Cu^{2+} and thiourea initially with a Cu^{2+}/thiourea ratio of less than 0.3. Since the divalent Cu^{2+} ion is known to be reduced by thiourea into the monovalent Cu^{+} and the thus-formed Cu induces complexation with one or two thiourea molecules [28], oxidation of Sn^{2+} is inhibited. The thus-obtained precursor solution maintained its transparency even after exposure to open air for more than 5 *h*, as shown in Figure II.1b.

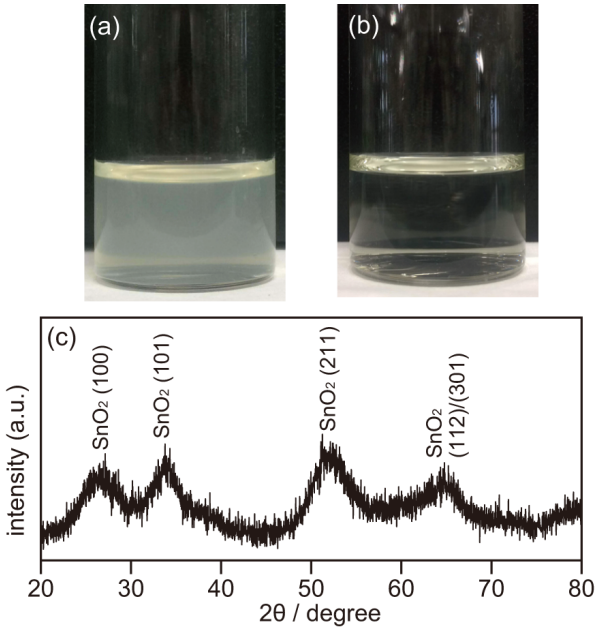

Figure II.1. Photographs of (a) an aqueous solution containing Cu^{2+}, Sn^{2+}, and Zn^{2+} salts after leaving for 4 *h* in an ambient condition and (b) the spray solution used in this study after exposure to an open air for 8 *h*. (c) An XRD pattern of the white precipitate collected from the solution containing Cu^{2+}, Sn^{2+}, and Zn^{2+} salts. Quoted from original manuscript: *T. H. Nguyen et al*., RSC Advances, 5 (95) (2015) 77565-77571.

Figure II.2 shows XRD patterns and Raman spectra of as-deposited films obtained by spray pyrolysis using the above stable precursor solution and those annealed at 580 °*C* and 600 °*C* in an evacuated glass ampoule containing sulfur powder for 10 min. As shown in Figure II.2a, the XRD pattern of the precursor film exhibited almost no diffraction peak except for peaks due to the Mo substrate, indicating that the film did not have a good crystalline nature. On the other hand, when the precursor film was annealed, the resulting film showed typical diffraction peaks corresponding to reflections derived from the kesterite CZTS [29, 30]. Relatively intense and sharp peaks were observed for the film annealed at

600 °*C* compared to those of the film annealed at 580 °*C*. Indeed, full width at half maximum (FWHM) value of the most intense (112) reflections of the 600 °*C* annealed film (0.157) was smaller than that of the 580 °*C* annealed film (0.165), suggesting the achievement of a high degree of crystallinity induced by the increment of annealing temperature. It should also be noted that there are weak reflections of MoS_2 in XRD patterns of the films after annealing due to the partial sulfurization of the bottom Mo substrate (see below). Raman spectra of as-deposited film showed a significantly broad peak centered at 330 cm^{-1}, whereas the annealed films gave three separated bands at 286 cm^{-1}, 336 cm^{-1}, and 369 cm^{-1} assignable to the kesterite CZTS [31, 32] without providing other signals (Figure II.2b). Hence, the annealed films obtained in this study were confirmed to form a CZTS crystal. On the other hand, since the main peak of the tetragonal Cu–Sn–S ternary compound of Cu_2SnS_3 (CTS) is present at 336 cm^{-1} and since zinc blend ZnS has a main Raman band at 351 cm^{-1} [33, 34] the observed broad Raman band of the as-deposited film was likely to indicate inclusions of several less-crystalline sulfide compounds.

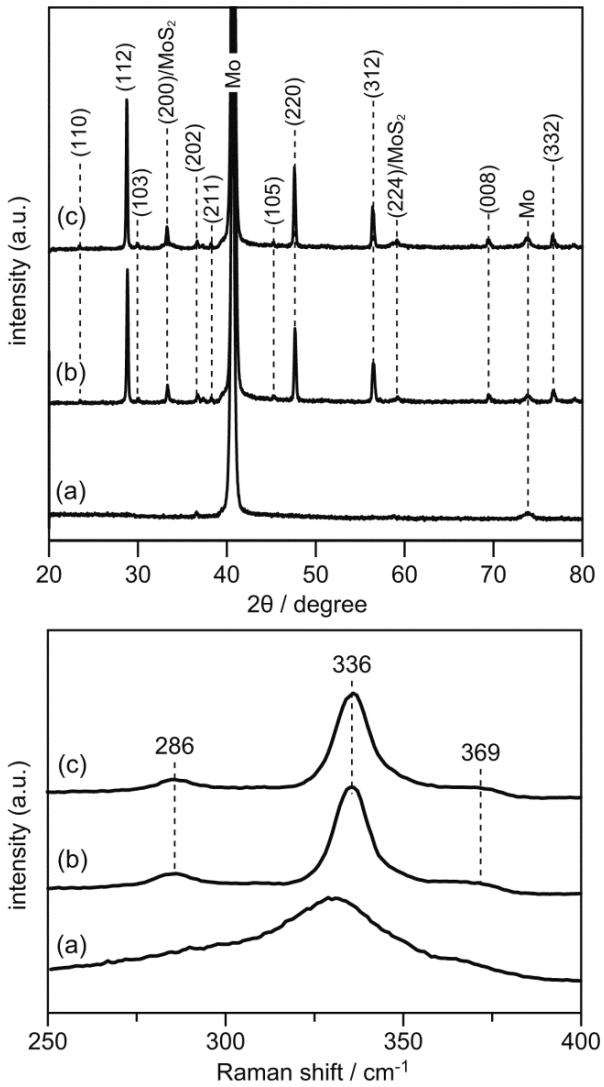

Figure II.2. (Upper) XRD patterns and (lower) Raman spectra of (a) the as-deposited film and the film annealed (b) at 580 °*C* for 10 *min* and (c) at 600 °*C* for 10 *min*. Quoted from original manuscript: *T. H. Nguyen et al*., RSC Advances, 5 (95) (2015) 77565-77571.

Figure II.3 shows cross-sectional and surface SEM images of an as-deposited film and CZTS films obtained at different annealing temperatures and durations. The as-deposited film was composed of densely packed small granule particles with a thickness of more than 1 μm, indicating successful deposition of a homogeneous film (Figure II.3a). The annealing treatment induced appreciable grain growth without alteration of thicknesses when compared

to that of the as-deposited film. As expected from the above XRD results, the film annealed at 600 °*C* showed larger grain sizes than those of the film annealed at 580 °*C* (Figure II.3b and c). Another point worth noting is that dark regions on the upper part of the Mo substrate are attributed to formation of MoS_2, as confirmed by the above XRD analyses. Although formation of well-grown CZTS grains seemed to be achieved by the annealing at 600 °*C*, the corresponding surface SEM image shown in Figure II.3c and d indicated incomplete grain growth and thereby a more severe annealing condition would be required. Due to the limitation of the thermal stability of the glass substrate, annealing temperature could not be increased to a temperature over 600 °*C*. Therefore, the annealing duration was extended for 30 *min* and 50 *min* to accelerate the grain growth of CZTS. Figure II.3e–h show cross-sectional and surface SEM images of thus-obtained CZTS films. As we expected, clear micron-sized grains were observed in their surface images. XRD analyses of those films (Figure II.4) showed narrower FWHMs (0.151 and 0.143 for 30 *min* and 50 *min* annealed films, respectively) than that of the 10 *min* annealed film (see above) in agreement with the SEM results. Dense morphologies of these films were seemed to be favorable for photovoltaic application. Corresponding cross-sections also showed densely packed large grains: however, sulfurization of the Mo layer advanced compared to that of the film annealed at the short duration (10 *min*, as shown in Figure II.3c). Specifically for the film obtained by 50 *min* annealing, most parts of the Mo substrate had sulfurized into MoS_2. The thick MoS_2 should affect the device performance because of induction of an increase in series resistance, as discussed below.

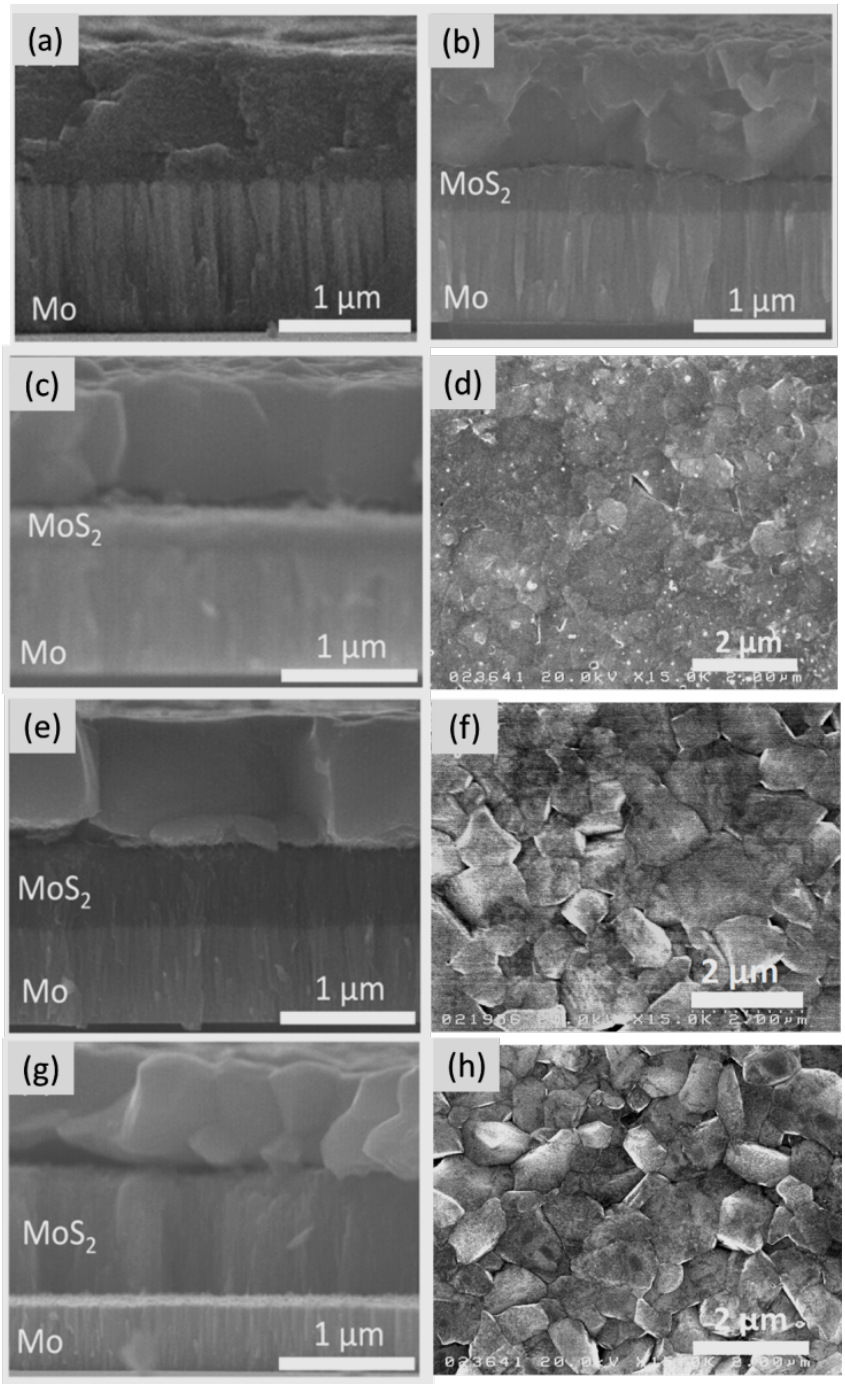

Figure II.3. Cross-sectional and surface SEM images of (a) as-deposited film and CZTS films obtained by annealing the as-deposited film (b) at 580 °*C* for 10 *min*, (c, d) at 600 °*C* for 10 *min*, (e, f) at 600 °*C* for 30 *min*, and (g, h) at 600 °*C* for 50 *min*. Quoted from original manuscript: *T. H. Nguyen et al*., RSC Advances, 5 (95) (2015) 77565-77571.

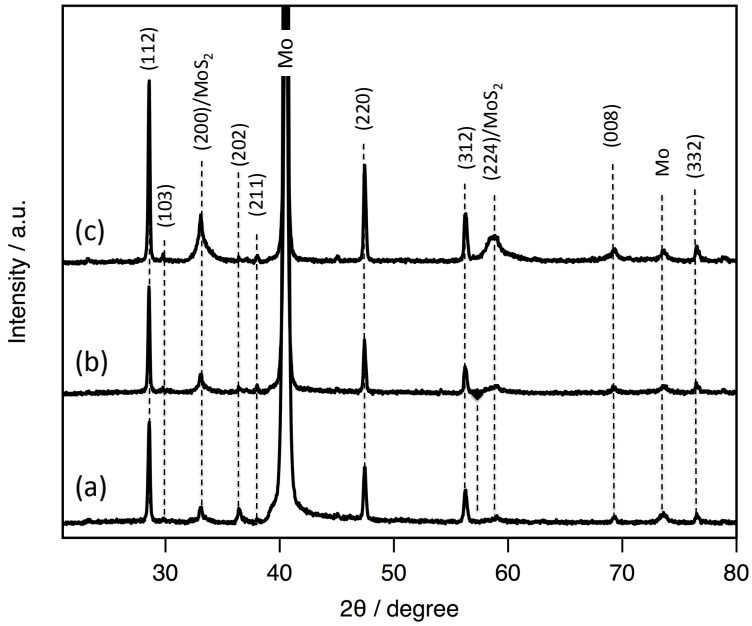

Figure II.4. XRD patterns of the film annealed at 600 °*C* (a) for 10 *min* (b) for 30 *min* and (c) for 50 *min*. Quoted from original manuscript: *T. H. Nguyen et al*., RSC Advances, 5 (95) (2015) 77565-77571.

ICP measurements were performed to determine metallic compositions of the as-deposited film and the film annealed at 600 °*C* for 30 *min*. Because of the deliquescent nature of the copper source ($Cu(NO_3)_2$) used, accurate composition of the precursor solution was also determined by ICP analysis. Table II.1 summarizes the results. When compared to the stoichiometric composition, the precursor solution used contained excess amounts of the Sn component, whereas both Cu and Zn components were close to their stoichiometry. A notable feature is that the Sn content was reduced significantly in the as-deposited film, while the film annealed at 600 °*C* still had an Sn-rich composition. The loss of Sn indicated the occurrence of evaporation during the spray pyrolysis deposition even at ambient pressure. One of the possible explanations is formation of tin monosulfide (SnS) because of its low

vapor pressure [35-37]. Since the as-deposited film did not form CZTS crystallite and other sulfides containing a smaller amount of Sn (CTS) and without Sn (ZnS), a highly Sn-rich composition is likely to be indispensable to compensate for a shortage induced by evaporation. Regarding the composition of the final CZTS film obtained by annealing at 600 °*C* for 30 *min*, the Sn content was slightly reduced but still Sn-rich compared to its stoichiometry. The annealing was performed in an evacuated glass ampoule containing sulfur vapor (see Experimental). Thus, loss of the Sn component was suppressed even though the temperature was elevated to a temperature higher than that of spray deposition.

Table II.1. Metallic compositions of the precursor solution, as-deposited film on an Mo/glass, and the film annealed at 600 °C for 30 min in an evacuated glass ampoule containing sulfur powder. Quoted from original manuscript: *T. H. Nguyen et al*., RSC Advances, 5 (95) (2015) 77565-77571.

Sample	Metal content ratio			Cu/Sn ratio	Cu/Zn ratio
	Cu	Sn	Zn		
Precursor[a]	0.34	0.49	0.17	0.7	2.0
As-deposited[b]	0.49	0.27	0.23	1.8	2.1
Annealed[c]	0.49	0.26	0.25	1.9	2.0
(stoichiometry)[d]	0.50	0.25	0.25	2.0	2.0

[a] Precursor solution. [b] As-deposited film obtained by the spray pyrolysis deposition. [c] The CZTS film obtained by annealing the as-deposited film at 600 °*C* for 30 *min*. [d] Ideal composition of metallic components in the stoichiometric CZTS compound.

The literature work indicated that both Cu-poor and Zn-rich compositions from the stoichiometric composition were indispensable to obtain an efficient absorber for photovoltaic applications [38]. Although the CZTS film obtained in this study was not such an empirical optimum, use of the composition, at least the Sn-rich composition, was found to

be advantageous for grain growth. In fact, when precursor solutions containing relatively small amounts of Sn (i.e., close to its stoichiometry and Sn-poor relative to Cu and Zn) were used, final CZTS films obtained by annealing at 600 °*C* were composed of small grains with less compact morphologies, as shown in Figure II.5. Based on the fact that appreciable grain growth could be achieved by using SnS vapor during a high temperature (550 °*C*) annealing process as reported by Toyama et al. [39], the excess Sn component in the as-deposited film would have a similar function in the present annealing performed in the evacuated glass ampoule.

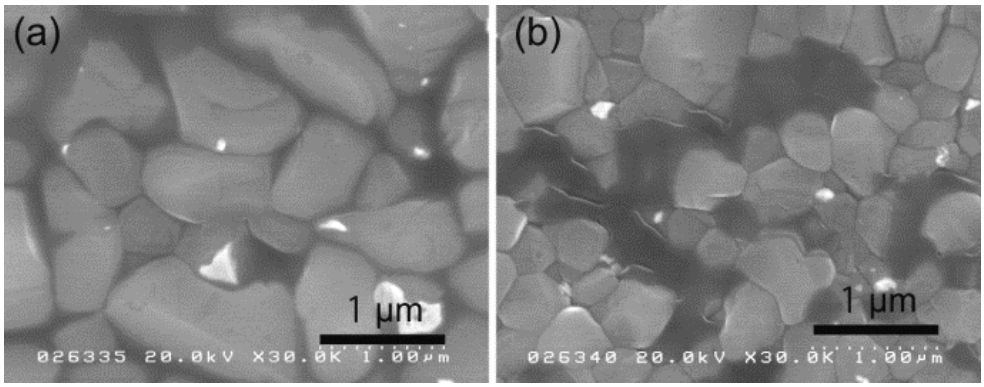

Figure II.5. Surface SEM images of CZTS films obtained by annealing the as-deposited film at 600 °*C* for 30 *min*. (a) The film was derived from a precursor solution containing almost stoichiometric amounts of Sn^{2+} salt. (b) The film was obtained by using a precursor solution having a slightly Sn-poor composition relative to the stoichiometry of metallic components in CZTS. Quoted from original manuscript: *T. H. Nguyen et al*., RSC Advances, 5 (95) (2015) 77565-77571.

Solar cells with a device structure of ITO/ZnO/CdS/CZTS/Mo/ glass (without an antiflection coating) were prepared by deposition of CdS, ZnO, and ITO layers on CTZS films obtained by annealing at 600 °*C* for 10 *min*, 30 *min*, and 50 *min*. From the measurements of device properties for the three samples, all of the devices exhibited solar

cell performance with good productivity. Figure II.6 shows the best J–V curves of these devices based on the CZTS films obtained by annealing at 600 °*C* for different durations under irradiation of simulated sunlight (AM1.5G) together with their corresponding semi-logarithmic dark J–V characteristics. Short-circuit current density (J_{SC}), open circuit voltage (V_{OC}), fill factor (FF) and PCE of these cells were determined from the illuminated J–V curves. These cell parameters are summarized in Table II.2. The best performance with PCE of 5.8% was achieved by the device made from the 30 *min* annealed CZTS (DEV30), whereas appreciable drops in all of the solar cell parameters were observed for the device based on the 10 *min* annealed CZTS (DEV10); further reduction of solar cell parameters, especially J_{SC}, appeared in the device composed of the 50 *min* annealed CZTS film (DEV50). Compared to the J–V characteristic of the best device of DEV30, the best device of DEV10 showed poor electrical rectification with a significantly low FF value, as shown in Figure II.6a. The relatively gentle slope of the J–V curve of DEV10 at the X-intersect compared to that of DEV30 suggests a large series resistance (R_S) of the DEV10 device. As discussed above SEM results of CZTS films employed for these devices, the large R_S of DEV10 is likely to be derived from incomplete crystallization of CZTS grains.

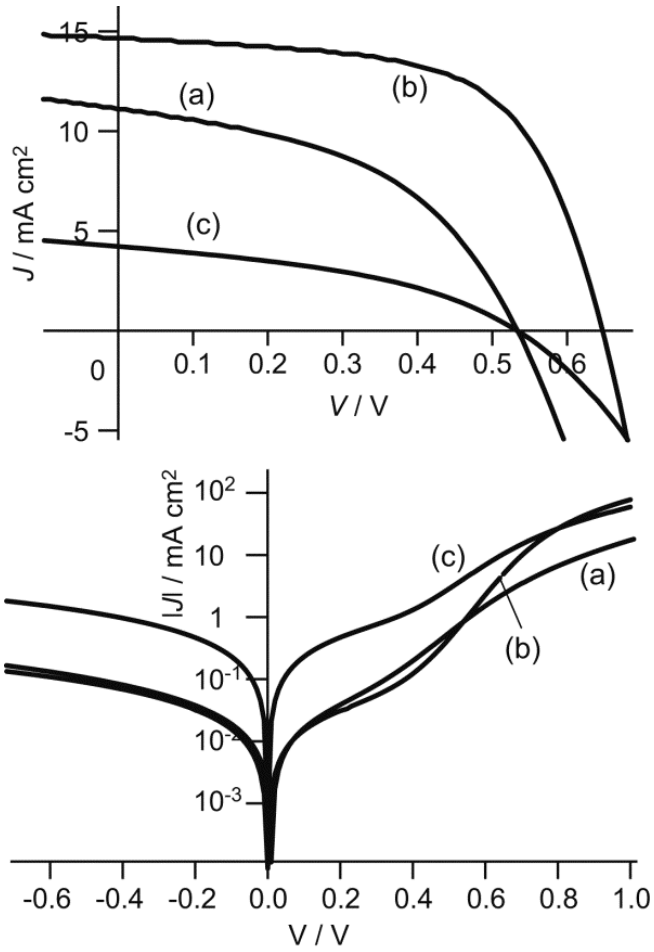

Figure II.6. *J-V* characteristics of ITO/ZnO/CdS/CZTS/Mo/glass solar cells. These devices were made from CZTS films obtained by annealing the as-deposited film at 600 °*C* for (a) 10 *min*, (b) 30 *min*, and (c) 50 *min*. Upper: under simulated AM1.5G irradiation; lower: in the dark (on a semi-logarithmic scale). Quoted from original manuscript: *T. H. Nguyen et al*., RSC Advances, 5 (95) (2015) 77565-77571.

Table II.2. Solar cell parameters of solar cells made from CZTS films obtained by annealing of the as-deposited film at 600 °*C* for different durations. Quoted from original manuscript: *T. H. Nguyen et al*., RSC Advances, 5 (95) (2015) 77565-77571.

Annealing duration[a] / *min*	J_{SC} /*mA cm*$^{-2}$	V_{OC}/*mV*	FF	PCE (%)
10	11.1	534	0.44	2.8
30	14.6	647	0.61	5.8
50	4.2	531	0.40	0.9

[a] Duration of annealing of the as-deposited film at 600 °*C*.

Regarding dark J–V curves of DEV10 and DEV30 devices shown in Figure II.6b, appreciable differences were also observed in both negative and positive bias regions. In the former negative bias region, a relatively strong current was observed for DEV10 compared to that for DEV30, indicating the presence of appreciable shunts in the DEV10 device. In the latter positive bias region (at ca. 0.2–0.6 *V*), DEV10 also showed an appreciably large dark current relative to that of DEV30. The result suggests presences of appreciable recombination currents in addition to diffusion currents in the device due probably to the poor quality of the p–n junction (i.e., presences of appreciable amounts of defects at the CZTS-CdS interface). Therefore, these poor device properties of DEV10 are attributable to incomplete crystallization of the CZTS grains as well as significant amounts of defects at the CZTS-CdS junction. On the other hand, the dark J–V curve of DEV50 showed a different characteristic, i.e., it showed a weak current flow at the highly positive bias region (>ca. 0.6 *V*) even though it gave better rectification than that of DEV10. Considering the above cross-sectional SEM results for the 50 *min* annealed film (see Figure II.3g), the observed weak currents were derived from the presence of a thick MoS_2 layer, leading to a large series

resistance of the device. Due to less structural failures of the DEV30 device, it gave the best efficiency in the present study.

Figure II.7 shows the external quantum efficiency (EQE) spectrum of the best device (DEV30) in wavelengths ranging from 300 *nm* to 1000 *nm*. It can be seen that the spectrum increases gradually from ca. 370 *nm* to ca. 500 *nm* and rapidly increases to ca. 540 *nm*; and then gradually degreases from ca. 700 *nm* to the onset wavelength of ca. 900 *nm*. The loss in the spectrum in the short wavelength was attributed to absorption losses in the buffer CdS layers. Meanwhile, the loss in the long wave- length region indicated loss of deeply absorbed photons due to poor minority carrier diffusion length and/or insufficient penetration of depletion width into the absorber. Such structural failures led to insufficient solar cell parameters (specifically J_{SC}) when compared to the efficient CZTS-based solar cells reported in the literature [25, 26]. The optimization of the deposition condition of the CdS buffer layer to reduce its thickness or the use of an alternative buffer layer should reduce the loss in the short wavelength region. Moreover, as mentioned above, successful fabrication of a CZTS film having an empirical optimum composition would be one of the most significant key structures to be achieved in order to obtain a high quality CZTS film without a significant loss in the long wavelength region.

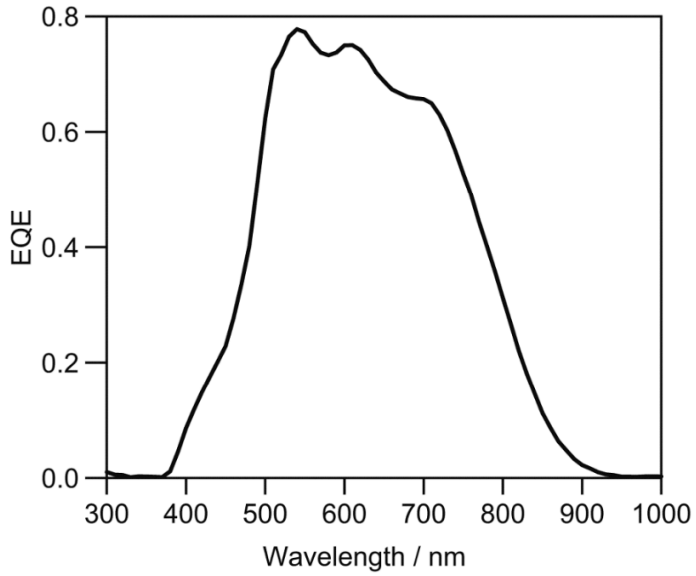

Figure II.7. An EQE spectrum of the device made from CZTS film obtained by annealing the as-deposited film at 600 °*C* for 30 *min*. Quoted from original manuscript: *T. H. Nguyen et al*., RSC Advances, 5 (95) (2015) 77565-77571.

II.4. Conclusion

In this study, we fabricated a CZTS thin film-based solar cell by using a facile spray pyrolysis technique. Successful grain growth of the CZTS absorber was achieved by employing an Sn-rich composition of the precursor solution with application of adequate post annealing at a high temperature (600 °*C*) for a sufficient duration (30 *min*). The solar cell based on the thus-obtained CZTS absorber reached PCE of 5.8%. To the best of our knowledge, this value is the best value so far reported for a pure-sulfide CZTS-based device obtained through spray deposition of the CZTS film. Concerning the chemical composition of the CZTS film, the performance of the present solar cell can be improved by its optimization to achieve a Cu-poor and Zn-rich composition as reported in the literature. Moreover, since the present spray technique enables easy control of the chemical composition by just changing the concentration of the precursor solution, it is also possible

to add other beneficial components such as sodium and potassium [40-42]. Hence, we can expect further improvement of PEC after optimizations of such compositional properties of the CZTS film as well as various modifications of device structures.

References

[1] H. Katagiri, *Thin Solids Films*, 2005*,* **480-482**, 426-432.

[2] A. H. Reshak, K. Nouneh, I. V. Kityk, J. Bila, S. Auluck, H. Kamarudin and Z. Sekkat, *Int. J. Electrochem. Sci*., 2014, **9**, 955-974.

[3] X. Lin, J. Kavalakkatt, K. kornhuber, S. Levcenko, M. C. L. Steiner and A. Ennaoui, *Thin Solid Films*, 2013, **535**, 10-13.

[4] J. Krustok, R. Josepson, T. Raadik and M. Danilson, *Physica B*, 2010, **405**, 3186-3189.

[5] G. Larramona, S. Bourdais, A. Jacob, C. Chone, T. Muto, Y. Cuccaro, B. Delatouche, C. Moisan, D. Pere and G. Dennler, *J. Phys. Chem. Lett*., 2014, **5**, 3763-3767.

[6] W. Wang, M. T. Winkler, O. Gunawan, T. Gokmen, T. K. Todorov, Y. Zhu and D. B. Mitzi, *Adv. Energy Mater*., 2014, **4**, 1301465.

[7] H. Chen, Q. Ye, X. He, J. Ding, Y. Zhang, J. Han, J. Liu, C. Liao, J. Mei and W. Lau, *Green Chem*., 2014, **16**, 3841-3845.

[8] J. O. Jeon, K. D. Lee, L. S. Oh, S. W. Seo, D. K. Lee, H. Kim, J. H. Jeong, M. J. Ko, B. S. Kim, H. J. Son and J. Y. Kim, *ChemSusChem*, 2014, **7**, 1073-1077.

[9] M. I. Khalil, R. Bernasconi and L. Magagnin, *Electrochimica Acta*, 2014, **145**, 154-158.

[10] K. D. Zhang, Z. R. Tian, J. B. Wang, B. Li, X. L. Zhong, D. Y. Guo and S. M. He, *J. Sol-Gel Sci. Technol.*, 2015, **73**, 452-459.

[11] J. Wang, P. Zhang, X. Song and L. Gao, *RSC Adv.*, 2014, **4**, 21318-21324.

[12] S. K. Swami, A. Kumar and V. Dutta, *Energy Procedia*, 2013, **33**, 198-202.

13] X. Zeng, K. F. Tai, T. Zhang, C. W. J. Ho, X. Chen, A. Huan, T. C. Sum and L. H. Wong, *Sol. Energy Mater. Sol. Cells*, 2014, **124**, 55-60.

[14] M. Valdes, G. Santoro and M. Vazquez, *J. Alloys and Compd.*, 2014, **585**, 776-782.

[15] N. M. Shinde, R. J. Deokate and C. D. Lokhande, *J. Anal. Appl. Pyrolysis*, 2013, **100**, 12-16.

[16] Y. B. K. Kumar. P. U. Bhaskar, G. S. Babu, S. Raja, *phys. stat. solidi A*, 2010, **207**, 149-156.

[17] M. Patel, I. Mukhopadhyay and A. Ray, *J. Phys. D: Appl. Phys.*, 2012, **45**, 445103.

[18] Y. B. K. Kumar, G. S. Babu, P. U, Bhaskar and V. S, Raja, *Sol. Energy Mater. Sol. Cells*, 2009, **93**, 1230-1237.

[19] D. B. Khadka, S. Y. Kim and J. H. Kim*, J. Phys. Chem. C*, 2015, **119**, 12226-12235.

[20] S. Ikeda, M. Nonogaki, W. Septina, G. Gunawan, T. Harada and M. Matsumura, *Catal. Sci. Technol.*, 2013, **3**, 1849-1854.

[21] W. Septina, M. Kurihara, S. Ikeda, Y. Nakajima, T. Hirano, Y. Kawasaki, T. Harada and M. Matsumura, *ACS Appl. Mater. Interfaces*, 2015, **7**, 6472-6479.

[22] M. A. Hossain, Z. Tianliang, L. K. Keat, L. Xianglin, R. R. Prabhakar, S. K. Batabyal, S. G. Mhaisalkar and L. H. Wong, *J. Mater. Chem. A*, 2015, **3**, 4147-4154.

[23] O. V. Galan, M. Courel, M. E. Rodriguez, V. I. Roca, E. Saucedo, A. Fairbrother, *J. Renewable Sustainable Energy,* 2013, **5**, 053137.

[24] M. E. Rodriguez, M. Placidi, O. V. Galan, V. I. Roca, X. Fontane, A. Fairbrother, D. Sylla, E. Saucedo and A. P. Rodriguez, *Thin Solid Films*, 2013, **535**, 67-72.

[25] B. Shin, O. Gunawan, Y. Zhu, N. A. Bojarczuk, S. J. Chey and S. Guha, *Prog. Photovolt: Res. Appl.,* 2013, **21**, 72-76.

[26] F. Jiang, S. Ikeda, T. Harada and M. Matsumura, *Adv. Energy Mater.*, 2014, **4**, 1301381.

[27] S. Ikeda, R. Kamai, T. Yagi and Michio Matsumura, *Journal of The Electrochemical Society*, 2010, **157**, B99-B103.

[28] G. A. Bowmaker, J. V. Hanna, C. Pakawatchai, B. W. Skelton, Y. Thanyasirikul and A. H. White, *Inorg. Chem*., 2009, **48**, 350-368.

[29] J. W. Cho, A. Ismail, S. J. Park, W. Kim, S. Yoon and B. K. Min, *Appl. Mater. Interfaces*, 2013, **5**, 4162-4165.

[30] Z. Su, K. Sun, Z. Han, H. Cui, F. Liu, Y. Lai, J. Li, X. Hao, Y. Liu and M. A. Green, *J. Mater. Chem. A*, 2014, **2**, 500-509.

[31] S. K. Swami, N. Chaturvedi, A. Kumar, N. Chander, V. Dutta, D. K. Kumar, A. Ivaturi, S. Senthilarasu and H. M. Upadhyaya, *Phys. Chem. Chem. Phys.*, 2014, **16**, 23993-23999.

[32] Z. Li, J. C. W. Ho, K. K. Lee, X. Zeng, T. Zhang, L. H. Wong and Y. M. Lam, *RSC Adv.*, 2014, **4**, 26888-26894.

[33] P. A. Fernandes, P. M. P. Salomé and A. F. da Cunha, *phys. stat. solidi c*, 2010, 7, 901-904.

[34] Y. C. Cheng, C. Q. Jin, F. Gao, X. L. Wu, W. Zhong, S. H. Li and P. K. Chu, *J. Appl. Phys.*, 2009, **106**, 123505.

[35] C. P. Bjorkman, J. Scragg, H. Flammersberger, T. Kubart and M. Edoff, *Sol. Energy Mater. Sol. Cells*, 2012, **98**, 110-117.

[36] M. Cao, L. Li, B. L. Zhang, J. Huang, L. J. Wang, Y. Shen, Y. Sun and J. C. Jiang, *Sol. Energy Mater. Sol. Cells*, 2013, **117**, 81-86.

[37] A. Weber, R. Mainz and H. W. Schock, *J. Appl. Phys.*, 2010, **107**, 013516.

[38] S. Exarhos, K. N. Bozhilov and L. Mangolini, *Chem. Commun.*, 2014, **50**, 11366-11369.

[39] T. Toyama, T. Konishi, Y. Seo, R. Tsuji, K. Terai, Y. Nakashima, H. Okamoto and Y. Tsutsumi, *Appl. Phys. Express,* 2013, **6**, 075503.

[40] J. V. Li, D. Kuciauskas, M. R. Young and I. L. Repins, *Appl. Phys. Lett.*, 2013, **102**, 163905.

[41] M. Johnson, S. V. Baryshev, E. Thimsen, M. Manno, X. Zhang, I. V. Veryovkin, C. Leighton and E. S. Aydil, *Energy Environ. Sci*., 2014, **7**, 1931-1938.

[42] P. Salome, V. Fjallstrom, A. Hultqvist and M. Edoff, *IEEE Journal of Photovoltaics*, 2013, **3**, 509-513.

Chapter III

Impact of Precursor Compositions on Structural and Photovoltaic Properties of Spray-Deposited Cu_2ZnSnS_4 Thin Films

III. 1. Introduction

In chapter II, we reported the successful fabrication of solar cells with a maximum conversion efficiency of 5.8% based on a Cu_2ZnSnS_4 film deposited by a facile spray pyrolysis technique using stable aqueous precursor solutions. The use of an Sn-rich composition of the precursor solution as well as the use of adequate post annealing at a high temperature (600 $°C$) for a sufficient duration (30 *min*) led to efficient grain growth, which is the main reason that high conversion efficiency values were achieved. However, from ICP results, an optimal chemical composition was not achieved for the CZTS films used in our previous study.

Figure III.1 shows efficiency map of CZTSSe thin film solar cells on the ternary phase diagram [1]. The most common compositional ranges suitable for high efficiency devices are Cu-poor and Zn-rich as proposed in many reports [2-27]. Therefore, in this chapter, an attempt was made to adjust the Cu, Zn, and Sn compositions in the CZTS film by controlling the concentrations of the corresponding metallic ions in the precursor solutions. The structural, optical, and electrical properties of the CZTS films related to the photovoltaic properties of the CZTS-based devices are also discussed and a best power conversion efficiency of 8.1 % is achieved.

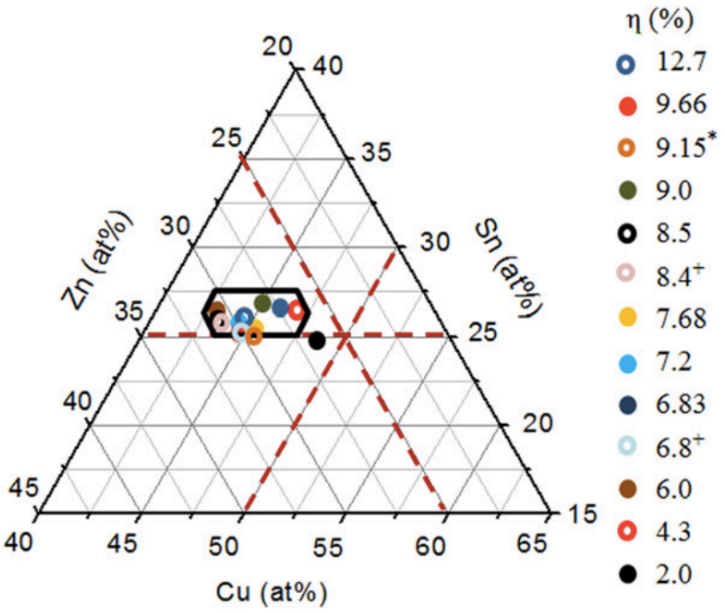

Figure III.1. Efficiency map of CZTSSe thin film solar cells on the ternary phase diagram. Quoted with permission from Ref. 1.

II.2. Experimental

III.2.1. Fabrication of CZTS Thin Film Solar Cells

Aqueous solutions of copper nitrate [$Cu(NO_3)_2$], zinc nitrate [$Zn(NO_3)_2$], and tin methanesulfonate [$Sn(CH_3SO_3)_2$] were added to an aqueous solution containing thiourea [$SC(NH_2)_2$]. The concentrations of $SC(NH_2)_2$, $Zn(NO_3)_2$, and $Sn(CH_3SO_3)_2$ were fixed at 50, 11.5, and 11.5 *mmol* dm^{-3}, respectively, whereas the concentration of $Cu(NO_3)_2$ was changed from 13 to 23 *mmol* dm^{-3} {i.e., the Cu/Zn/Sn compositional ratio was changed from extremely Cu-poor [Cu/ Zn/Sn = 1.13/1/1, for 13 *mmol* dm^{-3} $Cu(NO_3)_2$] to stoichiometric [Cu/Zn/Sn = 2/1/1, for 23 *mmol* dm^{-3} $Cu(NO_3)_2$]}. Excess $SC(NH_2)_2$ compared to the stoichiometric amount was used to prevent the loss of the S component during the spray process and precipitation of a Cu component in the solution. After adjusting the pH to 1.5 by adding a few drops of concd nitric acid, each of the aqueous precursor solutions was sprayed

onto an Mo-coated soda-lime glass substrate (Mo/glass) that was preheated at 380 *°C* using a hot plate. Finally, the films were annealed in an evacuated borosilicate glass ampoule together with 20 *mg* S powder at 600 *°C* for 30 *min* to facilitate grain growth.

For the fabrication of Cu_2ZnSnS_4 solar cells, the obtained Cu_2ZnSnS_4 films were processed to form a device with a structure of Al/ITO/ZnO/CdS/Cu_2ZnSnS_4/Mo/glass. The CdS buffer layer was deposited by chemical bath deposition (CBD) after treatment of Cu_2ZnSnS_4 films with aqueous HCl and KCN solutions. An ITO/ZnO bilayer was then deposited on top of the CdS layer by radio frequency (RF) magnetron sputtering. Finally, an Al top contact was deposited by thermal evaporation.

III.2.3. Characterizations

The crystalline structures of the films were analyzed by Raman spectroscopy using a JASCO NRC 3100 laser Raman spectrophotometer (excitation laser with a wavelength of 532 *nm*). X-ray diffraction (XRD) analyses using a Rigaku Mini Flex X-ray diffractometer (CuK_a, Ni filter) were also performed for structural analyses of the films. The morphologies of the films were examined by using a Hitachi S-5000 FEG field emission scanning electron microscope (SEM) at an acceleration voltage of 20 *kV*. The metallic compositions of the fabricated Cu_2ZnSnS_4 films were determined by inductively coupled plasma (ICP) analysis on a PerkinElmer OPTIMA 3000-XL ICP emission spectrometer. For this measurement, the film samples were immersed in aqua regia overnight to dissolve all of the components. The obtained clear solution was diluted to an appropriate concentration before the ICP analysis. Time-resolved photoluminescence (TRPL) spectra of these films were obtained by using a Hamamatsu C12132 Compact NIR fluorescence lifetime spectroscopy system with laser power and wavelength of 2.08 *mW* and 532 *nm*, respectively.

Current density–voltage (J–V) characteristics and external quantum efficiency (EQE) spectra of solar cell devices under simulated AM1.5G irradiation (100 $mW\ cm^{-2}$) were determined with a Bunkoh-Keiki CEP-015 photovoltaic measurement system. The acceptor density (N_A) values of Cu_2ZnSnS_4 components in these devices were determined from their capacitance–voltage (C–V) characteristics measured by using an HP-HEWLETT PACKED 4284A apparatus.

III.3. Results and discussion

Figure III.2 shows the Raman spectra and XRD patterns of the Cu_2ZnSnS_4 films fabricated from aqueous precursor solutions with various concentrations of Cu ions. In the Raman spectra, all of the films showed main peaks at 286, 336, and 369 cm^{-1} corresponding to the kesterite Cu_2ZnSnS_4 crystal [29-34]. XRD patterns of the films also showed diffraction peaks that could be assigned to Cu_2ZnSnS_4 in addition to peaks derived from the Mo substrate and its sulfurized form (MoS_2). If a precursor solution containing stoichiometric amounts of Cu, Zn, and Sn ions (i.e., a Cu concentration of 23 $mmol\ dm^{-3}$) was used, signals derived from the $Cu_{2-x}S$ phase appeared in both the Raman spectrum and the XRD pattern (Figure III.2a), implying the deposition of a Cu-excess film even though the precursor solution used contained stoichiometric amounts of the metallic components. Therefore, to reduce the Cu component in the final Cu_2ZnSnS_4 film, the content of Cu ions in the precursor solution was reduced. As a result, a slight reduction of Cu ion content (corresponding to the Cu_2ZnSnS_4 film derived from the precursor solution with Cu concentration of 21 $mmol\ dm^{-3}$) resulted in the disappearance of the $Cu_{2-x}S$ phase in the film, as shown in Figure III.2b. Similar Raman spectra and XRD patterns, in which all of the signals were assigned to the kesterite Cu_2ZnSnS_4 crystal, were also obtained if the Cu

content was reduced further (Figures III.2c,d). When the Cu concentration in the precursor solution was decreased to less than 65% of the stoichiometric content, an SnS_2 secondary phase was observed owing to the shortage of Cu, as shown in Figures III.2 e,f.

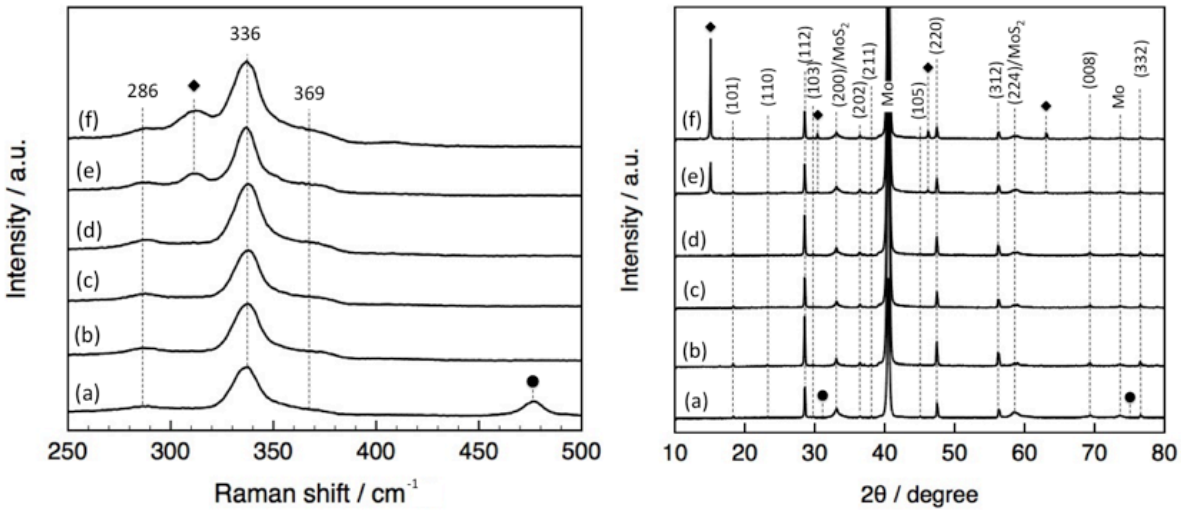

Figure III.2. (Left) Raman spectra and (right) XRD patterns of Cu_2ZnSnS_4 films obtained from precursor solutions with different Cu concentrations: (a) 23 *mmol* dm^{-3}, (b) 21 *mmol* dm^{-3}, (c) 19 *mmol* dm^{-3}, (d) 17 *mmol* dm^{-3}, (e) 15 *mmol* dm^{-3}, and (f) 13 *mmol* dm^{-3}. Circles and diamonds denote derived from $Cu_{2-x}S$ and SnS_2 phases, respectively. Quoted from original manuscript: *T. H. Nguyen et al*., ChemSusChem, 9 (17) (2016) 2414-2420.

To study the compositional alterations of the obtained Cu_2ZnSnS_4 films quantitatively, the metallic compositions of the Cu_2ZnSnS_4 films were determined by inductively coupled plasma (ICP) measurements. The atomic percentages of Cu, Sn, and Zn elements, as well as the calculated atomic ratios of Cu/(Zn+Sn) and Zn/Sn, are summarized in Table III.1. As expected from the results of the Raman and XRD analyses, the Cu_2ZnSnS_4 film obtained from the precursor solution containing stoichiometric amounts of Cu, Zn, and Sn ions (Cu concentration of 23 *mmol* dm^{-3}) was slightly Cu-rich. Based on the fact that the content of

the Sn in the film was lower than that of the stoichiometric composition, the observed compositional deviation was caused by a reduction of the Sn component induced by evaporation during the annealing process, as discussed in previous chapter. Compared to the Cu-rich/Sn- poor Cu_2ZnSnS_4 film, a gradual decrease in the Cu content was observed when we used precursor solutions with Cu concentrations lower than the stoichiometric composition, whereas the Sn and Zn content (or Zn/Sn ratio) were almost constant irrespective of the change in Cu concentration. Because the Cu_2ZnSnS_4 films obtained from precursor solutions containing moderate amounts of Cu ions (17–21 $mmol\ dm^{-3}$) did not contain $Cu_{2-x}S$ and SnS_2 phases, these films should have empirically optimal Cu-poor/Zn-rich compositions reported in the literature [19-27]. In addition, the fact that there was no alteration of the Zn content in the Cu_2ZnSnS_4 films indicates the presence of appreciable amounts of a Zn compound(s) in Cu_2ZnSnS_4 films obtained from precursor solutions with low Cu ion contents (13–15 $mmol\ dm^{-3}$).

Under the present deposition and annealing conditions, the excess Zn would be present as its sulfide (ZnS). The presence of the ZnS phase in these compositional ranges is also predicted by the ternary phase diagram of the Cu_2S–ZnS–SnS_2 system [35-36]. However, as the laser source excitation (at 532 *nm*) used for the Raman measurements in this study did not enable detection of the ZnS phase and the main diffraction peaks of ZnS completely overlap with those of Cu_2ZnSnS_4 in the XRD patterns, we could not observe the ZnS phase.

Table III.1. Metallic compositions of Cu_2ZnSnS_4 films fabricated from precursor solutions with different Cu concentrations. Quoted from original manuscript: *T. H. Nguyen et al*., ChemSusChem, 9 (17) (2016) 2414-2420.

Cu[a]/ *mmol dm*$^{-3}$	Metal content[b] / %			Cu/(Zn+Sn)[c]	Zn/ Sn[d]
	Cu	Sn	Zn		
13	36.6	30.1	33.3	0.58	1.11
15	39.0	28.9	32.1	0.64	1.11
17	43.4	27.6	29.0	0.77	1.05
19	45.0	27.0	28.0	0.82	1.04
21	47.1	26.0	26.9	0.89	1.04
23	51.1	24.0	24.9	1.04	1.04
(Stoichiometry)	50.0	25.0	25.0	1.00	1.00

[a] Concentrations of Cu ions in precursor solutions

[b] Percentage of metal components in Cu_2ZnSnS_4 films

[c] The Cu/(Zn+Sn) ratio in Cu_2ZnSnS_4 films

[d] The Zn/Sn ratio in Cu_2ZnSnS_4 films

Figure III.3 shows cross-sectional SEM images of the fabricated Cu_2ZnSnS_4 films. The corresponding top-view images are also shown in Figure III.4. All of the films showed a flat layer with a thickness of approximately 1 μm on the Mo substrate. The darker part of the upper Mo layer with a thickness of several hundred nm indicated the occurrence of sulfurization to form MoS_2 layers during the high-temperature annealing, as confirmed by the above XRD results (Figure III.2). The $Cu_{2-x}S$-containing Cu_2ZnSnS_4 thin film obtained

from the precursor solution containing stoichiometric amounts of Cu, Zn, and Sn ions was composed of relatively small grains that had significant voids (Figure III.3a). Significant voids were also observed on the top-view SEM image of the film (Figure III.4a). Several studies on the fabrication of the Cu_2ZnSnS_4 thin film have reported the effectiveness of the excess $Cu_{2-x}S$ compound for the grain growth because of the flux effect of the $Cu_{2-x}S$ liquid phase during the high-temperature annealing (sulfurization) [37,38], similar to the selenide ($Cu_{2-x}Se$)-based grain growth mechanism of the $Cu(In,Ga)Se_2$ chalcopyrite thin film [39,40]. The present annealing conditions, probably owing to the short annealing duration, were insufficient to induce the liquid-flux growth of Cu_2ZnSnS_4 grains; the presences of $Cu_{2-x}S$ impurities at the boundaries of Cu_2ZnSnS_4 grains were very influential at suppressing grain growth. Therefore, we would expect larger Cu_2ZnSnS_4 grains to be formed if the annealing duration is extended. However, this would induce the formation of a thicker MoS_2 layer, which is harmful for photovoltaic applications because of increase in the series resistance. The film morphologies became compact and the sizes of the grains became larger in Cu_2ZnSnS_4 films if the content of Cu ions in the precursor solutions was reduced up to 17 $mmol\ dm^{-3}$ (corresponding to a 26 % reduction of Cu from the stoichiometric composition), as shown in Figures III.3 b–d. The dense morphologies and large grain sizes of these films would be promising for obtaining good photovoltaic performance (see below). However, further reduction of the Cu ion content in the precursor solution was detrimental for the growth of Cu_2ZnSnS_4 grains (Figures III.3 e,f). As discussed above, these films contained SnS_2 and ZnS compounds. The corresponding top-view SEM images indicated the presence of sub- micrometer-sized small particles different from the Cu_2ZnSnS_4 grains attributed to SnS_2 or ZnS compounds (Figures III.4e and 4f). Therefore, SnS_2 and/or ZnS compounds were likely to suppress the grain growth of Cu_2ZnSnS_4 [41-45].

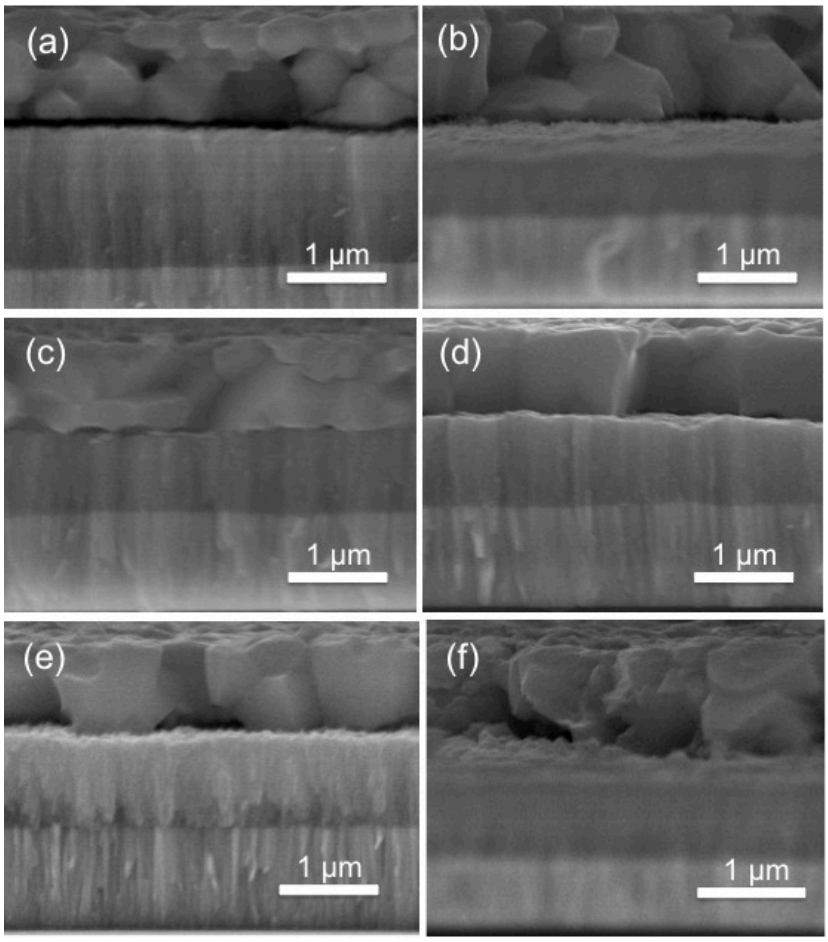

Figure III.3. Cross-sectional SEM images of fabricated Cu_2ZnSnS_4 films obtained from precursor solutions with different Cu concentrations: (a) 23 *mmol* dm^{-3}, (b) 21 *mmol* dm^{-3}, (c) 19 *mmol* dm^{-3}, (d) 17 *mmol* dm^{-3}, (e) 15 *mmol* dm^{-3}, and (f) 13 *mmol* dm^{-3}. Quoted from original manuscript: *T. H. Nguyen et al*., ChemSusChem, 9 (17) (2016) 2414-2420.

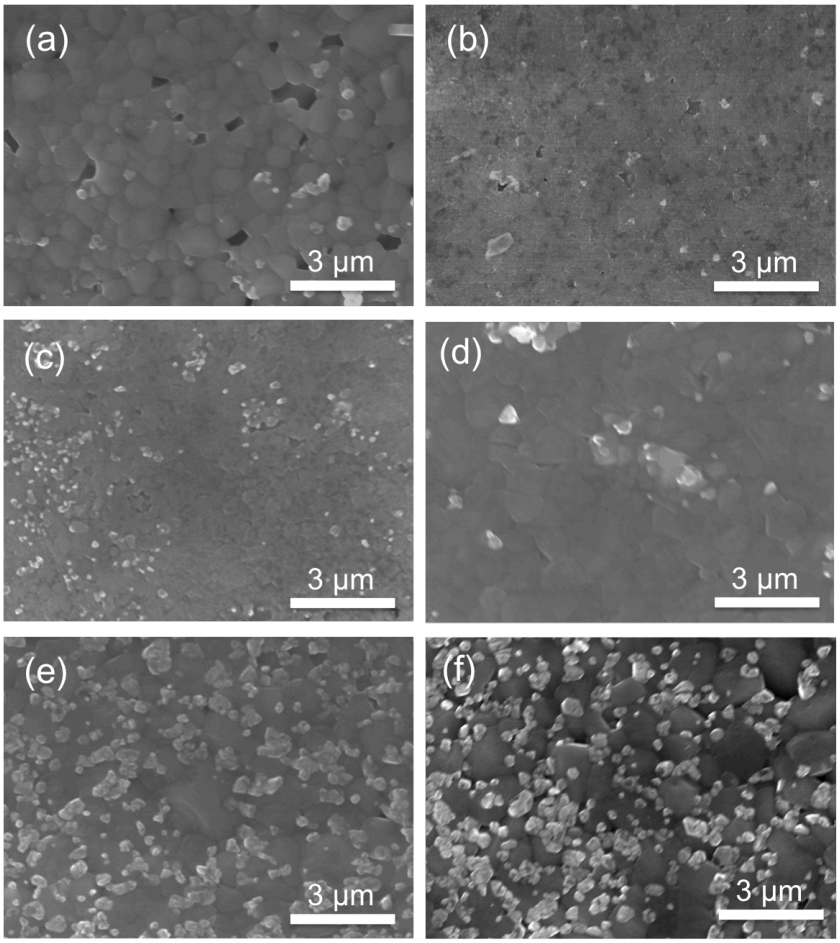

Figure III.4. Top-view SEM images of fabricated Cu_2ZnSnS_4 films obtained from precursor solutions with different Cu concentrations: (a) 23 *mmol* dm^{-3}, (b) 21 *mmol* dm^{-3}, (c) 19 *mmol* dm^{-3}, (d) 17 *mmol* dm^{-3}, (e) 15 *mmol* dm^{-3}, and (f) 13 *mmol* dm^{-3}. Quoted from original manuscript: *T. H. Nguyen et al*., ChemSusChem, 9 (17) (2016) 2414-2420.

Solar cells with a device structure of Al/indium tin oxide (ITO)/ZnO/CdS/ Cu_2ZnSnS_4/Mo/glass (without an antireflection coating) were prepared by deposition of CdS, ZnO, and ITO layers and an Al top contact onto Cu_2ZnSnS_4 films obtained from precursor solutions with various Cu concentrations; The J_{SC}, V_{OC}, fill factor (FF), and η values of these cells were determined from illuminated J–V curves. Typical results of the device parameters were plotted as a function of the Cu con- centration of the precursor solution (Figure III.5). The device based on the Cu_2ZnSnS_4 film derived from the stoichiometric mixture of the precursor solution (Cu concentration of 23 *mmol* dm^{-3}) showed no photovoltaic function. As discussed above for the structural analyses, the presence of significant voids, as well as the relatively conductive $Cu_{2-x}S$ phase in the Cu_2ZnSnS_4 film, would induce appreciable shunts. Conversely, other devices consisting of Cu_2ZnSnS_4 films with Cu content lower than their stoichiometric composition showed good solar cell properties; the highest conversion efficiency of 8.1 % was achieved by the device based on the Cu_2ZnSnS_4 film derived from the precursor solution containing 17 *mmol* dm^{-3} of Cu. To the best of our knowledge, this is the best performance of a solar cell based on a pure sulfide Cu_2ZnSnS_4 film deposited by spray pyrolysis. Another point worth noting is that good solar cell properties were also obtained even with devices based on the Cu_2ZnSnS_4 film containing SnS_2 and ZnS phases (the film prepared from the precursor solution with Cu concentration of 15 *mmol* dm^{-3}), although the device properties became significantly worse if the Cu content in the Cu_2ZnSnS_4 film was reduced further (13 *mmol* dm^{-3}).

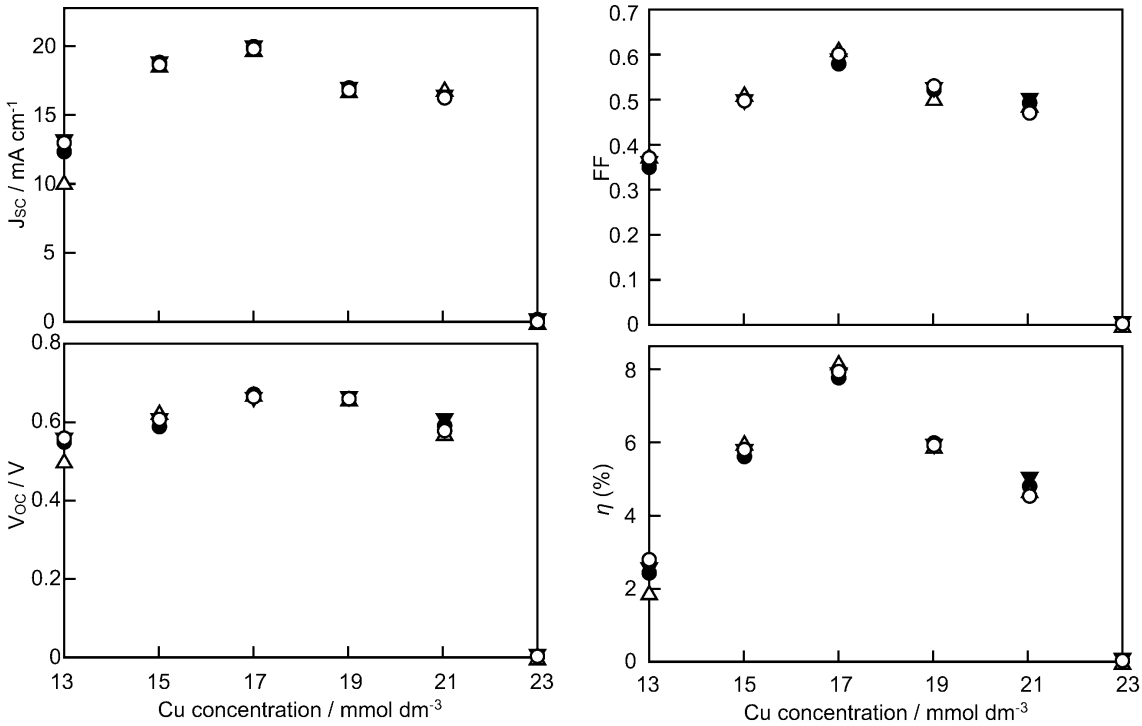

Figure III.5. Solar cell parameters of several devices made from Cu_2ZnSnS_4 films fabricated from precursor solutions with different Cu concentrations. Quoted from original manuscript: *T. H. Nguyen et al*., ChemSusChem, 9 (17) (2016) 2414-2420.

For further evaluation of device properties related to the film characteristics, the acceptor density (N_A) values of Cu_2ZnSnS_4 films were determined by capacitance–voltage (C– V) measurements of the corresponding devices (Figure III.6). The plots of N_A as a function of the Cu concentration of the precursor solutions are shown in Figure III.7. The N_A values for the Cu_2ZnSnS_4 films obtained from precursor solutions with Cu concentrations of 13 and 23 *mmol* dm^{-3} were not determined because of the insufficient accuracy of the analyses owing to appreciable observations of shunts in the devices based on these films (see above). As expected from the above device properties, the Cu_2ZnSnS_4 film derived from the precursor solution with Cu concentration of 17 *mmol* dm^{-3} showed the lowest N_A value. Moreover, the Cu_2ZnSnS_4 film obtained from the precursor solution containing 15 *mmol* dm^{-3} of Cu ions also showed a relatively low N_A value, although a slight increase was observed; the value was still in the range comparable to device-quality $Cu(In,Ga)(S,Se)_2$ and $Cu_2ZnSn(S,Se)_4$ films [46-52]. Conversely, Cu_2ZnSnS_4 films obtained from precursor solutions with relatively high Cu concentrations (21 and 23 *mmol* dm^{-3}) had relatively large N_A values, suggesting that these films were highly doped.

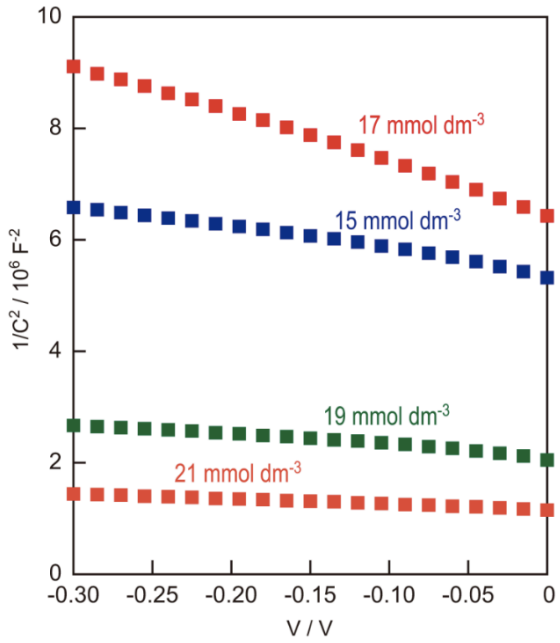

Figure III.6. $1/C^2$ plot of fabricated Cu_2ZnSnS_4 films at different Cu concentrations. Quoted from original manuscript: *T. H. Nguyen et al.*, ChemSusChem, 9 (17) (2016) 2414-2420.

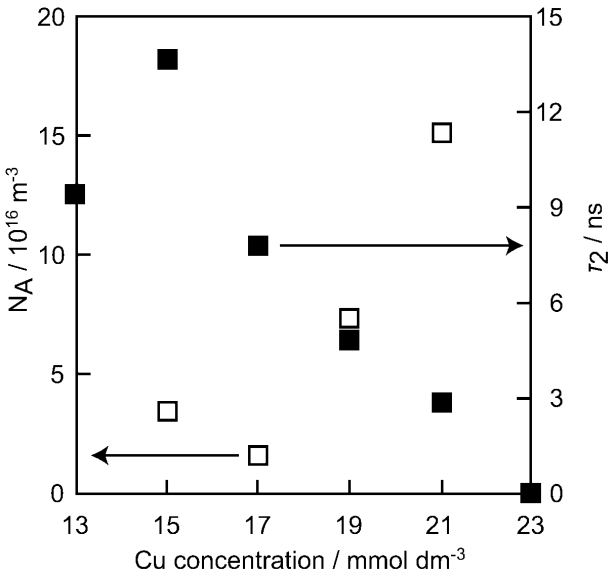

Figure III.7. Acceptor densities (N_As) and carrier lifetime (τ_2) of Cu_2ZnSnS_4 films derived from precursor solutions with different Cu concentrations. Quoted from original manuscript: *T. H. Nguyen et al.*, ChemSusChem, 9 (17) (2016) 2414-2420.

Indeed, when the external quantum efficiency (EQE) spectra of these four devices were compared, appreciable differences were observed at a long wavelength region; the devices with a relatively low N_A showed significant EQE responses in this region, whereas the devices with a relatively high N_A showed an appreciable drop in the EQE response, as shown in Figure III.8. Because an insufficient space charge region was formed in the latter devices owing to high N_A values of their Cu_2ZnSnS_4 films, photons in the long wavelength, which penetrated into a relatively deep part of the photoabsorber layer, were not utilized efficiently. Relatively low J_{SC} values of the devices based on these films (see Figure III.5) are likely owing to this electrostructural failure.

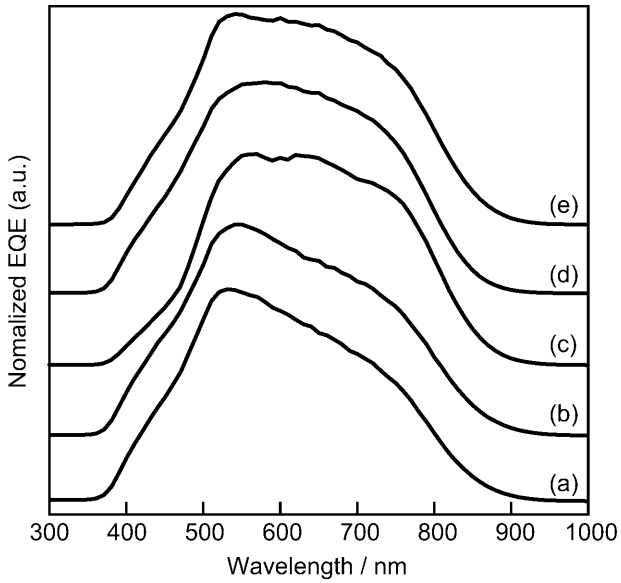

Figure III.8. EQE spectra of solar cells based on Cu_2ZnSnS_4 films derived from precursor solutions with different Cu concentrations: (a) 21 *mmol* dm^{-3}, (b) 19 *mmol* dm^{-3}, (c) 17 *mmol* dm^{-3}, (d) 15 *mmol* dm^{-3}, and (e) 13 *mmol* dm^{-3}. Quoted from original manuscript: *T. H. Nguyen et al*., ChemSusChem, 9 (17) (2016) 2414-2420.

As another parameter to evaluate the characteristics of Cu_2ZnSnS_4 films prepared in this study, the lifetime of the photoexcited carriers in the films was also calculated from room temperature time-resolved photoluminescence (TRPL) spectra of the films (Figure III.9) by applying a double-exponential function. Because the initial decay with a faster time constant (τ_1) would show a fast transient in which the PL signal is dominated by the charge separation owing to the built-in field of the layer, the time constant (τ_2) for the later long tail part was used for the analyses [48, 53]. The results are shown in Figure III.7. For Cu_2ZnSnS_4 films derived from precursor solutions with relatively high Cu contents (i.e., films containing relatively large amounts of Cu), the τ_2 values decreased linearly with the increase in Cu content. This trend is consistent with the increase in N_A in the film. A band-to-impurity channel would be the main part of carrier recombination in these films. Thus, the τ_2 value of the Cu_2ZnSnS_4 film derived from the precursor solution with Cu concentration of 17 *mmol* dm^{-3}, which had the lowest N_A value, was larger than those of the films derived from precursor solutions with Cu concentrations above 19 *mmol* dm^{-3}. However, the τ_2 values of Cu_2ZnSnS_4 films derived from precursor solutions with Cu concentration of 13 and 15 *mmol* dm^{-3} decreased even though the films had a lower film quality, different from the dependence of N_A on Cu content in the Cu_2ZnSnS_4 film.

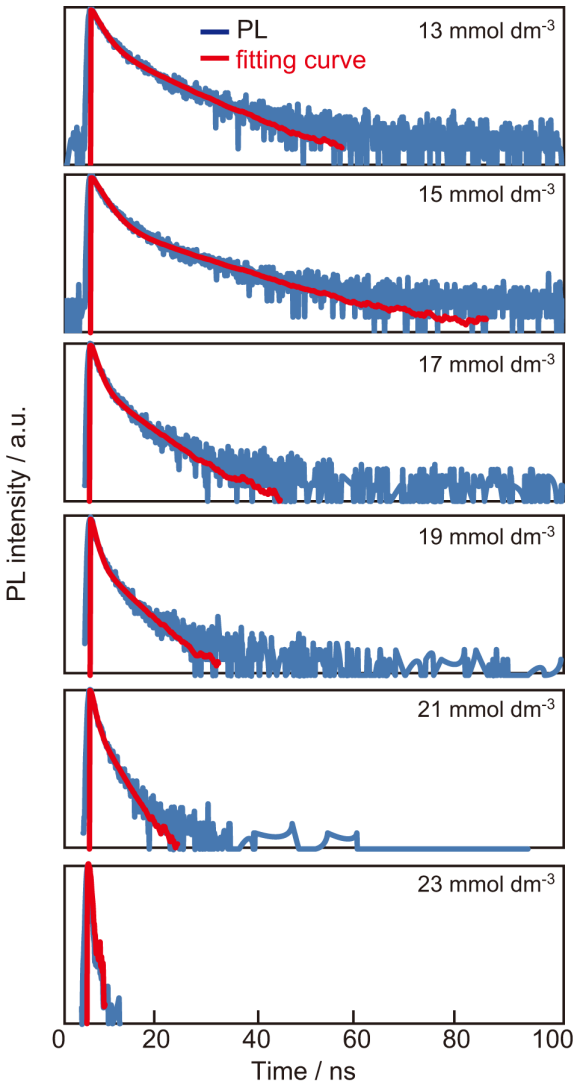

Figure III.9. Time–resolved PL profiles of fabricated Cu_2ZnSnS_4 films at different Cu concentrations. Quoted from original manuscript: *T. H. Nguyen et al.*, ChemSusChem, 9 (17) (2016) 2414-2420.

Theoretical studies reported by Wei et al. predicted that the most probable acceptor defect formed in the Cu_2ZnSnS_4 compound was an anti-site defect of Cu on the Zn site (Cu_{Zn}) because of its low formation energy, although the energy of Cu_{Zn} was deeper than that of the favorable Cu vacancy (V_{Cu}) defect [54]. Hence, when the Cu content was close to the stoichiometric composition, the Cu_{Zn} defect was primarily formed in substantial amounts in

the Cu_2ZnSnS_4 film. The relatively large N_A values of the Cu_2ZnSnS_4 films derived from precursor solutions with Cu concentrations above 19 *mmol* dm^{-3} are attributed to the presence of large amounts of Cu_{Zn}, i.e., the Cu_{Zn} defect is the recombination center for enhancing the band-to-impurity carrier recombination to reduce carrier lifetime (τ_2). The reduction of the Cu content in the Cu_2ZnSnS_4 film would reduce the amount of the Cu_{Zn} defects, leading to a decrease in N_A. Moreover, further reduction of Cu would enhance the formation of the favorable V_{Cu} defect. Hence, the observation of a slight increase in N_A in the Cu_2ZnSnS_4 film de- rived from the precursor solution with a Cu concentration of 15 *mmol* dm^{-3} is attributable to this increment. Regarding the increments of the τ_2 values of the Cu_2ZnSnS_4 films with low Cu content (including SnS_2 and ZnS impurities in the films), a possible explanation is that the shallow V_{Cu} defect mainly formed in these films would not act efficiently as a recombination center, resulting in a reduction of the band-to-impurity carrier recombination. Because of the large band gap energies of SnS_2 (2.2 *eV*) and ZnS (3.6 *eV*) [55-59], these compounds did not provide the Cu_2ZnSnS_4 compound with any interband states. Although the presences of such secondary phases would enhance the interface recombination, they might be silent for the band-to-impurity carrier recombination.

Light and dark J–V characteristics of the best solar cells are presented in Figure III.10. The device was based on a Cu_2ZnSnS_4 film derived from the precursor solution with a Cu concentration of 17 *mmol* dm^{-3}. The light J–V curve indicated that the solar cell with an active area of 0.030 cm^2 has a record efficiency of 8.1% with J_{SC}, V_{OC}, and FF of 20 $mAcm^{-2}$, 670 *mV*, and 0.61, respectively. From the light J–V curve, the series resistance (R_s) and shunt resistance (R_{sh}) were also determined to be 2.1 and 0.22 $k\Omega\ cm^2$, respectively.

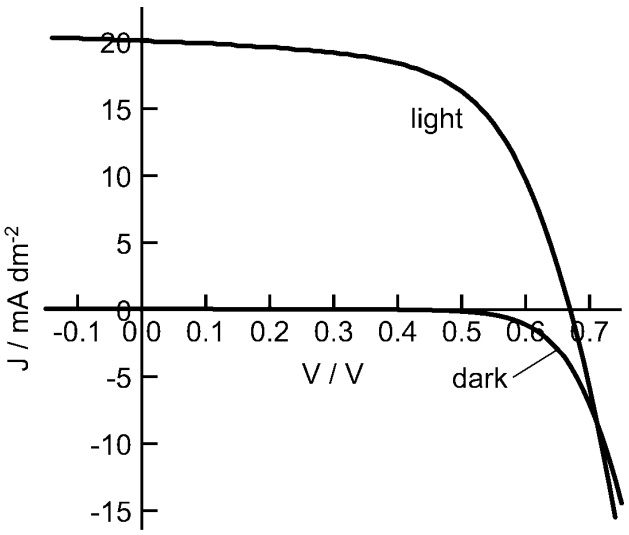

Figure III.10. Light and dark J-V characteristics of the solar cell based on the Cu_2ZnSnS_4 film derived from the precursor solution with Cu concentration of 17 *mmol* dm^{-3}. Quoted from original manuscript: *T. H. Nguyen et al*., ChemSusChem, 9 (17) (2016) 2414-2420.

Compared to the R_s and R_{sh} values of the devices obtained using the other precursor solutions, the best efficiency was attributed to the achievement of relatively low R_s as shown in Table III.2. Furthermore, compared with the device parameters reported for high efficiency cells [6, 7], the J_{SC} value was good, but the V_{OC} and FF values were rather low. Moreover, based on our recent results for Cu_2ZnSnS_4-based devices obtained by electrodeposition, the R_{sh} of the device was not so large, whereas the series resistance (R_s) was in a permissive range [48]. These results suggest the presence of appreciable shunts in the device.

Table III.2. Solar cell parameters of the best devices made from Cu_2ZnSnS_4 films fabricated from precursor solutions with different Cu concentrations. Quoted from original manuscript: *T. H. Nguyen et al*., ChemSusChem, 9 (17) (2016) 2414-2420.

Cu / *mmol dm^{-3}*	13	15	17	19	21	23
J_{SC} / *mA cm^{-2}*	13.2	18.9	20.1	17.0	16.4	0
V_{OC} / *mV*	0.56	0.62	0.67	0.66	0.61	0
FF	0.37	0.51	0.61	0.53	0.50	0
PCE (%)	2.8	5.9	8.1	6.0	5.0	0
R_s / *Ω cm^2*	10.6	6.1	2.1	5.4	7.0	-
R_{sh} / *Ω cm^2*	0.08	0.21	0.22	0.25	0.20	-

For further inspection of device properties, the ideality factor (*n*) and saturation current density (J_s) were also estimated by fitting the dark J–V curves to the standard diode equation [Eq. (1)]:

$$J = J_s\left(e^{\frac{qV}{nKT}} - 1\right) \quad (1)$$

where q, k, and T denote elementary charge, Boltzmann constant, and temperature, respectively. As a result, the *n* and J_s of the present best device were 2.37 and 9.0×10^{-8} *mA cm^{-2}*, respectively. These *n* and J_s values were larger than those of the Cu_2ZnSnS_4-based device obtained by electrodeposition (*n* and J_s of 2.29 and 3.0×10^{-8} *mA cm^{-2}*, respectively). These results imply that strong space charge region (SCR) recombination or

tunneling-enhanced interface recombination are the dominant limiting factors, leading to the observed relatively low V_{OC}. Hence, further improvements of device qualities and interfacial conditions to suppress shunt and recombination are required.

III.4. Conclusion

In this study, we obtained device-quality Cu_2ZnSnS_4 thin films with different Cu content by using a facile spray pyrolysis technique. The metallic composition of the precursor solutions was found to have significant effects on the qualities of the final Cu_2ZnSnS_4 films, such as grain sizes, morphologies, acceptor densities, the nature of the acceptor defects, and carrier lifetimes. A solar cell with an Al/indium tin oxide (ITO)/ZnO/CdS/Cu_2ZnSnS_4/Mo/glass structure derived from the empirically optimal composition of a Cu_2ZnSnS_4 film [Cu/(Zn + Sn) = 0.77 and Zn/Sn=1.05] was shown to have good performance with conversion efficiency of 8.1%. However, there is still a room for improvement because of the relatively low open circuit voltage (V_{OC}) of the device compared to that of the Cu_2ZnSnS_4 devices reported in the literature. Therefore, further studies to improve the V_{OC} by improving the quality of both the Cu_2ZnSnS_4 films and devices are necessary.

References

[1] Y. Qu, G. Zoppi, R. W. Miles and N. S. Beattie, *Materials Research Express*, **2014**, 1, 045040.

[2] W. Wang, M. T. Winkler, O. Gunawan, T. Gokmen, T. K. Todorov, Y. Zhu and D. B. Mitzi, *Adv. Energy Mater.*, **2014**, 4, 1301465.

[3] K. E. Roelofs, Q. Guo, S. Subramoney and J. V. Caspar, *J. Mater. Chem. A*, **2014**, 2, 13464-13470.

[4] T. Schnabel, M. Low and E. Ahlswede, *Solar Energy Materials & Solar Cells*, **2013**, 117, 324-328.

[5] B. Shin, O. Gunawan, Y. Zhu, N. A. Bojarczuk, S. J. Chey and S. Guha, *Prog. Photovolt: Res. Appl*., **2013**, 21, 72-76.

[6] H. Sugimoto, C. Liao, H. Hiroi, N. Sakai and T. Kato, *Proc. IEEE 39th Photovoltaic Specialists Conf. PVSC*, **2013**, 3208-3211. DOI: 10.1109/PVSC.2013.6745135.

[7] S. Tajima, T. Itoh, H. Hazama, K. Ohishi and R. Asahi, *Appl. Phys. Express*, **2015**, 8, 082302.

[8] D. H. Son, D. H. Kim, S. N. Park, K. J. Yang, D. Nam, H. Cheong and J. K. Kang, *Chem. Mater*., **2015**, 27, 5180-5188.

[9] O. Vigil-Galan, M. Espindola-Rodriguez, M. Courel, X. Fontane, D. Sylla, V. Izquierdo-Roca, A. Fairbrother, E. Saucedo and A. Perez-Rodriguez, *Solar Energy Materials & Solar Cells*, **2013**, 117, 246-250.

[10] M. Espindola-Rodriguez, M. Placidi, O. Vigil-Galan, V. Izquierdo-Roca, X. Fontane, A. Fairbrother, D. Sylla, E. Saucedo and A. Perez-Rodriguez, *Thin Solid Films*, **2013**, 535, 67-72.

[11] H. Chen, Q. Ye, X. He, J. Ding, Y. Zhang, J. Han, J. Liu, C. Liao, J. Mei and W. Lau, *Green Chem.,* **2014**, 16, 3841-3845.

[12] M. I. Khalil, R. Bernasconi and L. Magagnin, *Electrochimica Acta*, **2014**, 145, 154-158.

[13] J. Tao, J. Liu, J. He, K. Zhang, J. Jiang, L. Sun, P. Yang and J. Chu, *RSC Adv*., **2014**, 4, 23977-23984.

[14] Q. Tian, X. Xu, L. Han, M. Tang, R. Zou, Z. Chen, M. Yu, J. Yang and J. Hu, *CrystEngComm*, **2012**, 14, 3847-3850.

[15] Z. Zhou, Y. Wang, D. Xu and Y. Zhang, *Solar Energy Materials & Solar Cells*, **2010**, 94, 2042-2045.

[16] J. W. Cho, A. Ismail, S. J. Park, W. Kim, S. Yoon and B. K. Min, *ACS Appl. Mater. Interfaces*, **2013**, 5, 4162-4165.

[17] N. K. Youn, G. L. Agawane, D. Nam, J. Gwak, S. W. Shin, J. H. Kim, J. H. Yun, S. J. Ahn, A. Cho, Y. J. Eo, S. K. Ahn, H. Cheong, D. H. Kim, K. S. Shin and K. H. Yoon, *Int. J. Energy Res*., **2016**, 40, 662-669.

[18] S. M. Bhosale, M. P. Suryawanshi, M. A. Gaikwad, P. N. Bhosale, J. H. Kim and A. V. Moholkar, *Materials Letters*, **2014**, 129, 153-155.

[19] H. Katagiri, K. Jimbo, W. S. Maw, K. Oishi, M. Yamazaki, H. Araki and A. Takeuchi, *Thin Solid Films*, **2009**, 517, 2455-2460.

[20] V. Tunuguntla, W. C. Chen, P. H. Shih, I. Shown, Y. R. Lin, J. S. Hwang, C. H. Lee, L. C. Chen and K. H. Chen, *J. Mater. Chem. A*, **2015**, 3, 15324.

[21] A. Emrani, P. Vasekar and C. R. Westgate, *Solar Energy*, **2013**, 98, 335-340.

[22] S. Kahraman, S. Cetinkaya, M. Podlogar, S. Bernik, H. A. Cetinkara and H. S. Guder, *Ceramics International*, **2013**, 39, 9285-9292.

[23] J. J. Scragg, P. J. Dale and L. M. Peter, *Electrochemistry Communications*, **2008**, 10, 639-642.

[24] S. Khoshmashrab, M. J. Turnbull, D. Vaccarello, Y. Nie, S. Martin, D. A. Love, P. K. Lau, X. Sun and Z. Ding, *Electrochimica Acta*, **2015**, 162, 176-184.

[25] T. K. Todorov, K. B. Reuter and D. B. Mitzi, *Adv. Mater.*, **2010**, 22, E156-E159.

[26] T. J. Huang, X. Yin, C. Tang, G. Qi and H. Gong, *J. Mater. Chem. A*, **2015**, 3, 17788.

[27] J. Tao, J. Liu, L. Chen, H. Cao, X. Meng, Y. Zhang, C. Zhang, L. Sun, P. Yang and J. Chu, *Green Chem*., **2016**, 18, 550.

[28] A. Dalui, A. H. Khan, B. Pradhan, J. Pradhan, B. Satpati and S. Acharya, *RSC Adv.*, **2015**, 5, 97485.

[29] V. Kosyak, M.A. Karmarkar and M. A. Scarpulla, *Appl. Phys. Lett.*, **2012**, 100, 263903.

[30] Z. Su, K. Sun, Z. Han, H. Cui, F. Liu, Y. Lai, J. Li, X. Hao, Y. Liu and M. A. Green, *J. Mater. Chem. A*., **2014**, 2, 500.

[31] J. H. N. Tchognia, Y. Arba, B. Hartiti, K. Dakhsi, J. M. Ndjaka, A. Ridah and P. Thevenin, *J. Mater. Environ. Sci.*, **2015**, 6, 2120-2124.

[32] S. K. Swami, N. Chaturvedi, A. Kumar, N. Chander, V. Dutta, D. K. Kumar, A. Ivaturi, S. Senthilarasu and H. M. Upadhyaya, *Phys. Chem. Chem. Phys.*, **2014**, 16, 23993-23999.

[33] J. Kavalakkatt, X. Lin, K. Kornhuber, P. Kusch, A. Ennaoui, S. Reich and M. C. Lux-Steiner, *Thin Solid Films*, **2013**, 535, 380-383.

[34] S. Thiruvenkadam, D. Jovina and A. L. Rajesh, *Solar Energy*, **2014**, 106, 166-170.

[35] D. Olekseyuk, I. V. Dudchak and L. V. Piskach, *Journal of Alloys and Compounds*, **2004**, 368, 135-143.

[36] F. Hergert and R. Hock, *Thin Solids Films*, **2007**, 515, 5953-5956.

[37] T. Tanaka, A. Yoshida, D. Saiki, K. Saito, Q. Guo, M. Nishio and T. Yamaguchi, *Thin Solid Films*, **2010**, 518, S29-S33.

[38] M. P. Suryawanshi, S. W. Shin, U. V. Ghorpade, K. V. Gurav, C. W. Hong, G. L. Agawane, S. A. Vanalakar, J. H. Moona, J. H. Yun, P. S. Patil, J. H. Kim and A.V. Moholkar, *Electrochim, Acta*, **2014**, 150, 136-145.

[39] R. Klenk, T. Walter, H. W. Schock and D. Cahen. *Adv. Mater.*, **1993**, 5, 114-119.

[40] J. R. Tuttle, M. A. Contreras, M. H. Bode, D. Niles, D. S. Albin, R. Matson, A. M. Gabor, A. Tennant, A. Duda and R. Noufi, *J. Appl. Phys.*, **1995**, 77, 153-161.

[41] R. Schurr, A. Holzing, S. Jost, R. Hock, T. Vob, J. Schulze, A. Kirbs, A. Ennaoui, M. L. Steiner, A. Weber, I. Kotschau and H. W. Schock, *Thin Solid Films*, **2009**, 517, 2465-2468.

[42] A. Weber, R. Mainz and H. W. Shock, *J. Appl. Phys.*, **2010**, 107, 013516.

[43] S. M. Pawar, A. I. Inamdar, K. V. Gurav, S. W. Shin, Y. Jo, J. Kim, H. Im and J. H. Kim, *Vacuum,* **2014**, 104, 57-60.

[44] J. Scragg, J. T. Watjen, M. Edoff, T. Ericson, T. Kubart and C. Platzer-Bjorkman, *J. Am. Chem. Soc.,* **2012**, 134, 19330-19333.

[45] O. Vigil-Galan, M. Courel, M. Espindola-Rodriguez, D. Jimenez-Olarte, M. Aguilar-Frutis and E. Saucedo, *Solar Energy Materials & Solar Cells,* **2015**, 132, 557-562.

[48] W. Septina, M. Kurihara, S. Ikeda, Y. Nakajima, T. Hirano, Y. Kawasaki, T. Harada and M. Matsumura, *ASC Appl. Mater. Interfaces*, **2015**, 7, 6472-6479.

[47] D. Hironiwa, N. Sakai, T. Kato, H. Sugimoto, Z. Tang, J. Chantana and T. Minemoto, *Thin Solid Films,* **2015**, 582, 151-153.

[48] F. Jiang, S. Ikeda, Z. Tang, T. Minemoto, W. Septina, T. Harada and M. Matsumura, *Prog. Photovolt: Res. Appl.* **2015**, 23, 1884-1895.

[49] A. Polizzotti, I. L. Repins, R. Noufi, S. H. Wei and D. B. Mitzi, *Energy Environ. Sci.,* **2013**, 6, 3171.

[50] T. J. Huang, X. Yin, G. Qi and H. Gong, *Phys. Status Solidi RRL*, **2014**, 8, 735-762.

[51] T. P. Dhakal, C. Y. Peng, R. R. Tobias, R. Dasharathy and C. R. Westgate, *Solar Energy*, **2014**, 100, 23-30.

[52] M. Courel, J. A. A. Arvizu, O. V. Galan, *Solid-State Electronics*, **2015**, 111, 243-250.

[53] J. Chantana, T. Watanabe, S. Teraji, K. Kawamura and T. Minemoto, Jpn. J. Appl. Phys., 2014, 53, 05FW03.

[54] S. Chen, J. H. Yang, X. G. Gong, A. Walsh and S. H. Wei, *Physical Review B*, **2010**, 81, 245204.

[55] A. Burton, D. Colombara, R. D. Abellon, F. C. Grozema, L. M. Peter, T. J. Savenije, G. Dennler and A. Walsh, *Chem. Mater.*, **2013**, 25, 4908-4916.

[56] G. Li, R. Su, J. Rao, J. Wu, P. Rudolf, G. R. Blake, R. A. D. Groot, F. Besenbacher and T. T. M. Palstra, *J. Mater. Chem. A*, **2016**, 4, 209.

[57] L. Sun, W. Zhou, Y. Liu, D. Yu, Y. Liang and P. Wu, *RSC Adv.*, **2016**, 6, 3480.

[58] A. Kudo and Y. Miseki, *Chem. Soc. Rev.,* **2009**, 38, 253-278.

[59] M. Kumar, A. Dubey, N. Adhikari, S. Venkatesan and Q. Qiao, *Energy Environ. Sci.*, **2015**, 8, 3134-3159.

Chapter IV

Structural and Solar Cell Properties of an Ag – containing Cu_2ZnSnS_4 Thin Film Derived from Spray Pyrolysis

IV.1. Introduction

In chapter III, the controlling of the Cu, Zn, and Sn compositions in the Cu_2ZnSnS_4 film was found to have significant effects on reduction of secondary phases. At optimal Cu-poor and Zn-rich composition, $Cu_{2-x}S$ or SnS_2 impurities were successfully removed. However, beside secondary phases, the presence of antisite defect is also a challenge need to be solved to improve the quality of films [1-6]. It has been reported that the CZTS thin film tends to include a large number of Cu_{Zn} antisite defects because of its relatively low formation energy compared to that of the favorable Cu vacancy (V_{Cu}) [7-11]. These defects will produce surface and bulk recombination centers, which suppress carrier transportation and limit the device open-circuit voltage. Since Cu and Zn have similar ionic radius, the Cu_{Zn} defects were easily formed when Cu atoms occupy the Zn lattice sites. Therefore, substitution of Cu by another larger ionic radius cations can reduce the formation energy of antisite defects and improve the quality of CZTS thin film.

Recent theoretical results reported by S. Chen et al. predicted that the Ag-based kesterite (i.e., Ag_2ZnSnS_4 (AZTS)) has a low number of Ag_{Zn} antisite defects since significant differences in ionic radiuses between Ag and Zn ions lead to relatively high formation energy of the defect as showed in Table IV.1 [12]. Based on these aspects, a partial replacement of Cu to Ag to obtain $(Cu_{1-x}Ag_x)_2ZnSnS_4$ (ACZTS) films has been attempted in order to reduce the number of the Cu_{Zn} antisite defect; appreciable improvements of solar cell properties were achieved by these ACZTS-based devices have been reported [13-16].

Table IV.1. Calculated defect formation energy of VI and III defects in Cu_2ZnSnS_4 and Ag_2ZnSnS_4 when $\mu_{Cu} = \mu_{Cd} = \mu_{Zn} = \mu_{Ag} = 0$ and the largest value in the achievable chemical potential region. Adapted with permission from Ref. 12.

	Formation energy (eV)			
	$\mu_{Cu} = \mu_{Cd} = \mu_{Zn} = \mu_{Ag} = 0$		Maximum	
Cu_2ZnSnS_4	V_{Cu}	1.14	V_{Cu}	1.14
	Cu_{Zn}	1.41	Cu_{Zn}	0.38
Ag_2ZnSnS_4	V_{Ag}	2.14	V_{Ag}	2.14
	Ag_{Zn}	3.10	Ag_{Zn}	1.80

For the use of the spray pyrolysis deposition, the film composition can easily be controlled by just changing the composition of the used precursor solution. This feature is beneficial to fabricate ACZTS film with different Ag contents. In this study, therefore, the precursor ACZTS films with different amount of Ag were fabricated by varying the molar ration of Ag/(Cu + Zn + Sn) in aqueous precursor solutions for spray pyrolysis deposition. Improvements of solar cell performances achieved by devices based on these ACZTS thin films are reported in relation to structural and electric properties of the ACZTS thin films.

IV.2. Experimental

IV.2.1. Fabrication of ACZTS Thin Film Solar Cells

Three precursor films with different amount of Ag were fabricated by varying the molar ratio of Ag / (Cu + Zn + Zn) in aqueous precursor solutions (Ag / (Cu + Zn + Zn) =0, 0.02, 0.1) Sources of metallic elements were copper nitrate ($Cu(NO_3)_2$), zinc nitrate ($Zn(NO_3)_2$), tin methanesulfonate ($Sn(CH_3SO_3)_2$), and silver nitrate ($AgNO_3$); thiourea ($SC(NH_2)_2$) was

used as the sulfur source. Deposition was carried out by spraying the aqueous solution containing these sources with pH adjusted to 1.5 by adding a few drops of concentrated nitric acid on an Mo-coated glass substrate heated at 380 °*C*. Adjustment of pH is indispensable to avoid formation of precipitates in the solution during the spray deposition [17]. Thus-obtained precursor films were annealed in an evacuated borosilicate glass ampoule containing 20 *mg* of sulfur powder at 600 °*C* for 30 *min* to form CZTS and ACZTS films. In order to complete the solar cell device, a CdS buffer layer was deposited on CZTS and ACZTS films by the chemical bath deposition [17,18]. Then, *i*ZnO and ITO layers were sequentially deposited by radio frequency (RF) magnetron sputtering on CdS-covered CZTS and ACZTS films. Finally, an Al top contact was deposited by thermal evaporation.

IV.2.1. Characterizations

Atomic compositions of CZTS and ACZTS films were determined by inductively coupled plasma (ICP) analysis on a Perkin-Elmer OPTIMA 3000-XL ICP emission spectrometer. For this measurement, the film samples were immersed in aqua regia overnight to dissolve all of the components. The thus-obtained clear solution was then diluted to an appropriate concentration before analysis. Crystallographic structures were analyzed by X-ray diffraction (XRD) analyses using a Rigaku Mini Flex X-ray diffractometer (CuKα, Ni filter) and Raman spectroscopy using a JASCO NRS 3100 Laser Raman Spectrophotometer. The depth profile was analyzed by secondary ion mass spectroscopy (SIMS) using a ATOMIKA SIMS 4100 equipped with O_2^+ source ions (5 *kV*). Photoelectrochemical measurements were performed by using a conventional three-electrode setup. Three electrodes, namely Pt wire, Ag/AgCl and CZTS (or ACZTS)-based films as counter, reference and working electrodes, respectively, were inserted into a three-necked flask with a

flat window containing a 0.2 *M* $Eu(NO_3)_3$ solution with pH 4. Measurements were conducted by a linear sweep voltamonmetric mode with a negative scan direction at the scan rate of 10 $mV\ s^{-1}$ under chopped illumination of simulated sunlight (AM1.5G) using an Asahi Spectra HAL-320 Compact Xenon Light Source. Surface morphologies were examined by using a Hitachi S-5000 FEG field emission scanning electron microscope (SEM) at an acceleration voltage of 20 *kV* and a KEYENCE VK-9700 laser microscope. Current density-voltage (J-V) characteristics and external quantum efficiency (EQE) spectra of solar cell devices under simulated AM1.5G irradiation were determined with a Bunkoh-Keiki CEP-015 photovoltaic measurement system. Capacitance-voltage (C-V) characteristics of solar cell devices were examined by using an HP-HEWLETT PACKED 4284A apparatus. X-ray photoelectron (XP) spectroscopy was performed by using a Shimadzu AXIS ULTRA X-ray photoelectron spectrometer in monochromated Al Kα radiation. For the surface etching, the sample was bombarded by Ar^+ ions accelerated to 3.5 *keV* for appropriate durations.

IV.3. Results and Discussion

As determined by inductively coupled plasma (ICP) analyses, Ag / (Ag + Cu) ratios of thus-obtained CZTS and ACZTS films were 0, 0.016, and 0.104 (These films were labeled CZTS, A(2%)CZTS, and A(10%)CZTS, respectively.). It should be noted that all of the films were confirmed to have group I-poor (i.e., (Ag + Cu) / (Zn + Sn) < 1) and Zn-rich (i.e., Zn / Sn > 1) compositions, which are empirically optimal for CZTS-based solar cells [19]. Figure IV.1a shows XRD patterns of the films. The CZTS film showed several reflections assignable to reflections of the kesterite CZTS structure [20-24]. With increase in the Ag contents of the films, those reflections gradually shifted to lower 2θ angles, as typically shown by magnified images of (112), (200)/(004), and (312)/(116) reflections in Figure

IV.1b. Since the ionic radius of Ag ions is larger than that of Cu ions, the observed shifts of reflections (i.e., increases in lattice constants) are strong indications of the occurrence of gradual replacements of Cu to form mixed kesterite crystals of ACZTS instead of the formation of various separate phases. It should be noted that weak reflections at 2θ of 28.5° and 56.3°, assignable to (111) and (311) reflections of ZnS crystal, appeared for the A(10%)CZTS film. These results indicate presence of a small fraction of ZnS in the present CZTS and ACZTS films (see below). As shown in Figure IV.1c, Raman spectrum of the CZTS film exhibited intense peaks centered at 338 cm^{-1}, which is assigned to the A1-band for kesterite CZTS; three weak peaks centered at 252, 286, and 369 cm^{-1} are also typically observed for kesterite CZTS [13]. Raman spectra of ACZTS films indicated occurrences of slight shifts of A1-bands to lower wavenumber regions though they were not significant (e.g., 336 cm^{-1} for A(10%)CZTS). Since similar results were reported in the literature by several groups [13,16,25], present results were empirical evidences of successful incorporation of Ag components into the kesterite lattice.

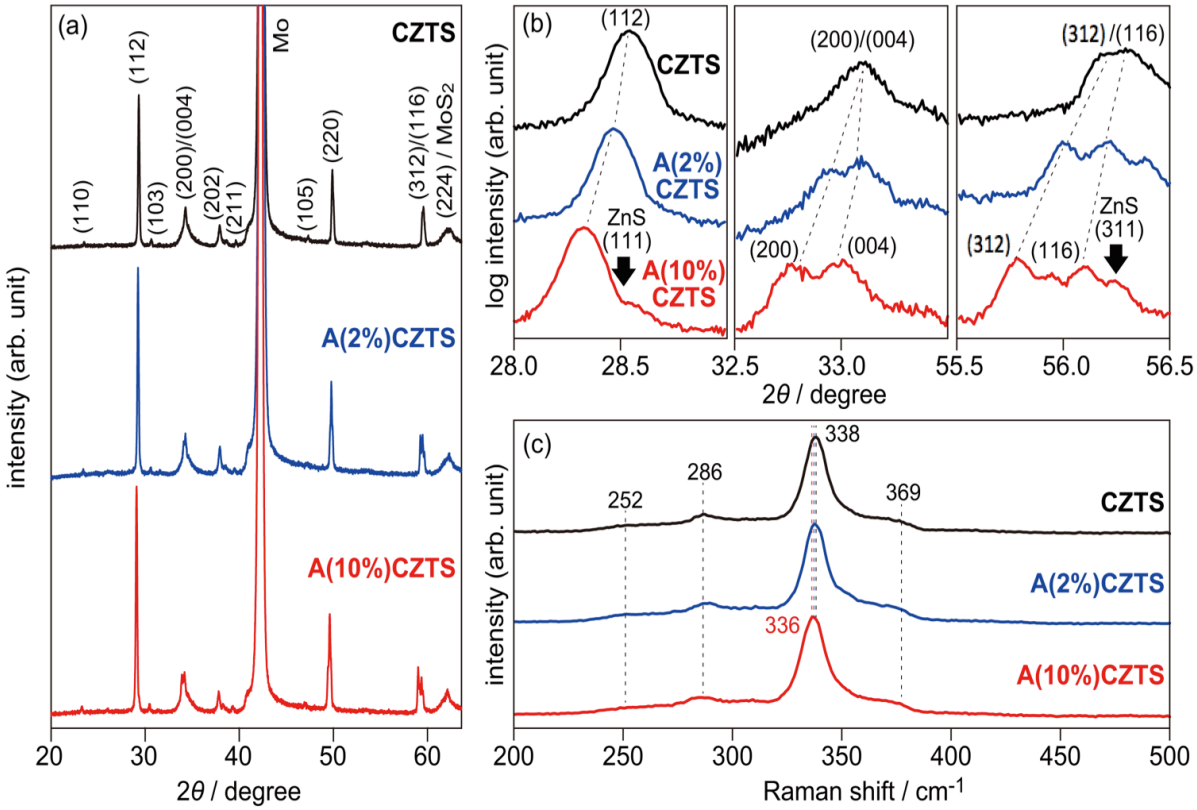

Figure IV.1. (a) XRD patterns of CZTS and ACZTS films, (b) magnified XRD patterns at 2θ ranging from 28° to 30°, and (c) Raman spectra of CZTS and ACZTS films.

Figure IV.2a shows depth profiles of CZTS and ACZTS films obtained by secondary ion mass spectrometry (SIMS). At the surface region, all the film showed appreciable gradients were observed except for the sulfur (S) component. Especially, presences of large contents of Zn components were pronounced for all the films. As discussed above XRD results, these results indicate presences ZnS crystals at the surface of these kesterite films. According to the literature [26,27], such segregations of ZnS at the surface should be due to the evaporation of the Sn component during the high temperature heat treatment. It should also be noted that all the films showed similar depth profiles of constituent elements regardless of presences of Ag components, suggesting compositional idealities among the

CZTS and ACZTS films. Regarding Ag profiles in A(2%)CZTS and A(10%)CZTS films, almost no compositional grading was observed in bulk regions of these kesterite films. Based on results of the structural investigations, we can conclude that different amounts of Ag were incorporated homogeneously in the CZTS films by using the spray pyrolysis deposition method.

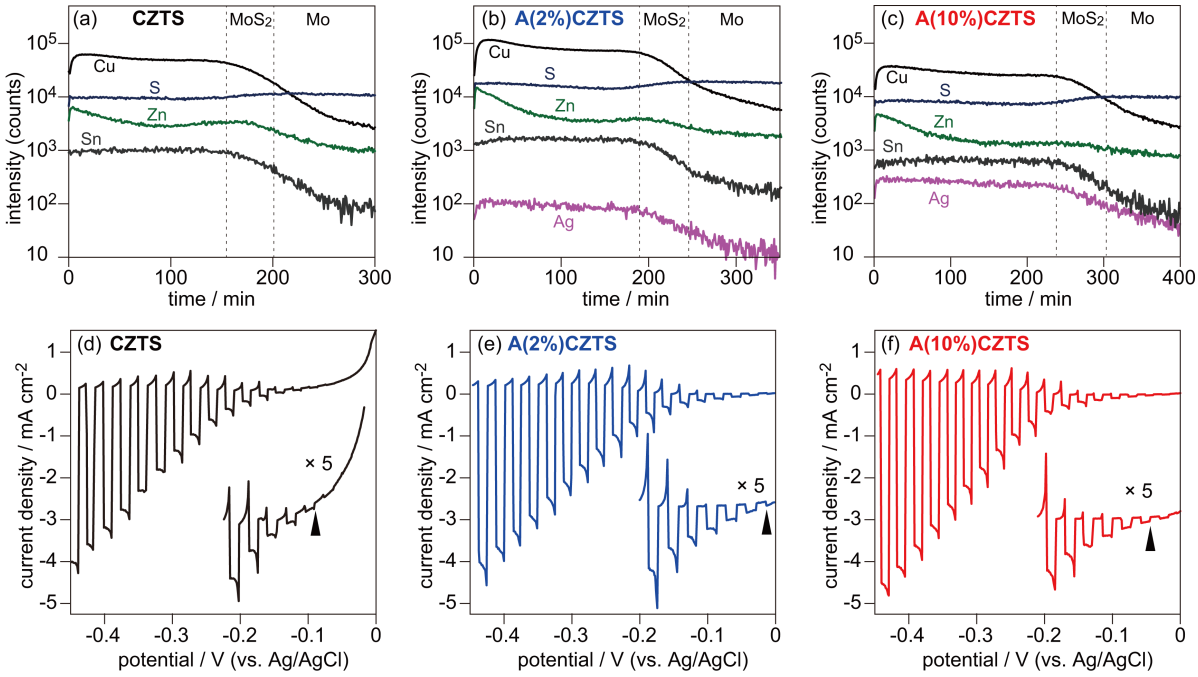

Figure IV.2. (a, b, c) Depth profiles of CZTS and ACZTS films obtained by SIMS analyses (d, e, f) and J-V curves of CZTS and ACZTS films obtained from an aqueous 0.2 *M* $Eu(NO_3)_3$ solution (pH 4) under chopped illumination of simulated sunlight (AM1.5G). Arrows in panels d, e, and f indicate photocurrent onsets, defined as the leading potential showing 0.02 $mA\ cm^{-2}$ of cathodic photocurrent.

Photoelectrochemical measurements of CZTS and ACZTS films were performed in an electrolyte solution containing an Eu^{3+} / Eu^{2+} redox couple at pH 4. Figure IV.2b shows typical photocurrent density-voltage (J-V) plots of these films obtained by using the lock-in

technique. All of the films showed appreciable photocurrents at potentials more negative than ca. -0.1 *V* (vs Ag/AgCl) derived from reduction of Eu^{3+} ions in the solution, indicating p-type characteristics of them. Compared to the CZTS film, slight shifts of photocurrent onsets, defined as the leading potential showing 0.02 $mA\ cm^{-2}$ of cathodic photocurrent, to positive regions were observed for the ACZTS samples, suggesting deepening of their flat band potentials (FBs) induced by Ag incorporation (see below).

Figures IV.3a-3c show top-view SEM images of CZTS and ACZTS films. The CZTS film was composed of densely packed submicron-sized crystal grains. In the CZTS film, appreciable voids were also observed between them, whereas there seemed to be relatively small amounts of voids between the grains in ACZTS films. Moreover, based on the analyses of grain-size distributions obtained by measuring major axes of several tens grains in these films (Figure IV.4), the grains in ACZTS were larger than those in the CZTS film. Formation of relatively large grains in the ACZTS films were also confirmed by their cross-sectional SEM images as shown in Figure IV.5. These results imply that incorporation of Ag is effective for grain growth and suppression of void formation in the present spray pyrolysis deposition system, as was discussed in the previous report for partial replacement of Cu with Ag in the $Cu(In,Ga)S_2$ system [28]. Another point worth noting is that the ACZTS film with a relatively high Ag content (i.e., the A(10%)CZTS film) had many pinholes over the entire surface upon observation of a relatively low magnification using a laser microscope, as shown in Figure IV.3f, whereas no appreciable pinhole was observed in CZTS and A(2%)CZTS films (Figures IV.3d and 3e).

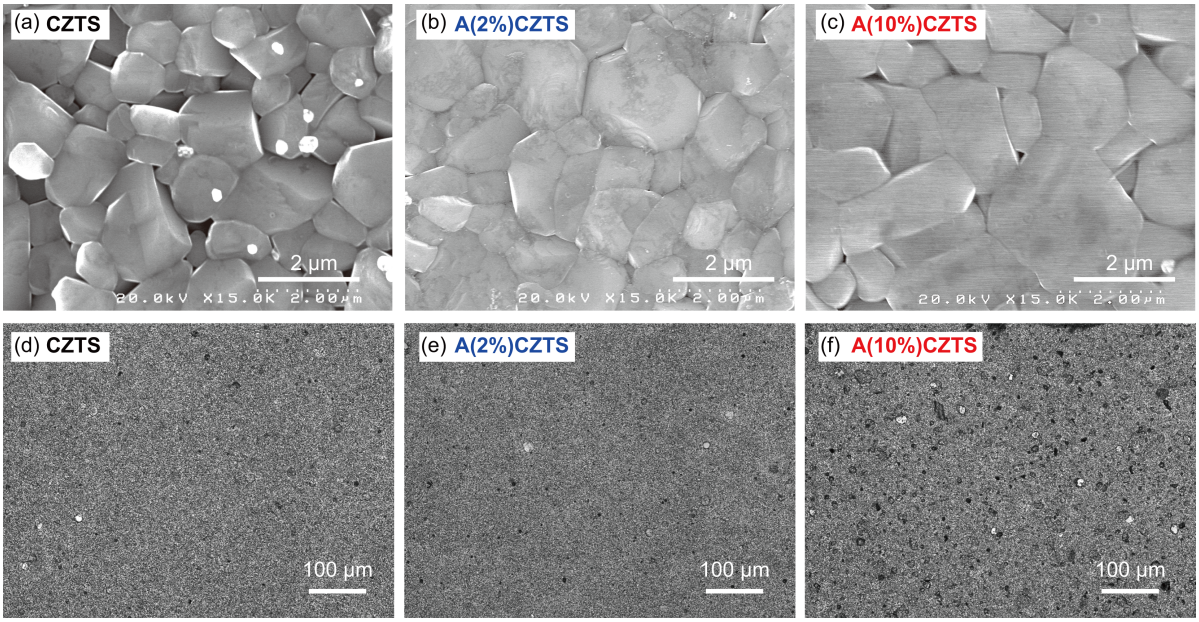

Figure IV.3. (a, b, c) Top-view SEM images of CZTS and ACZTS films and (d, e, f) corresponding laser microscopy images.

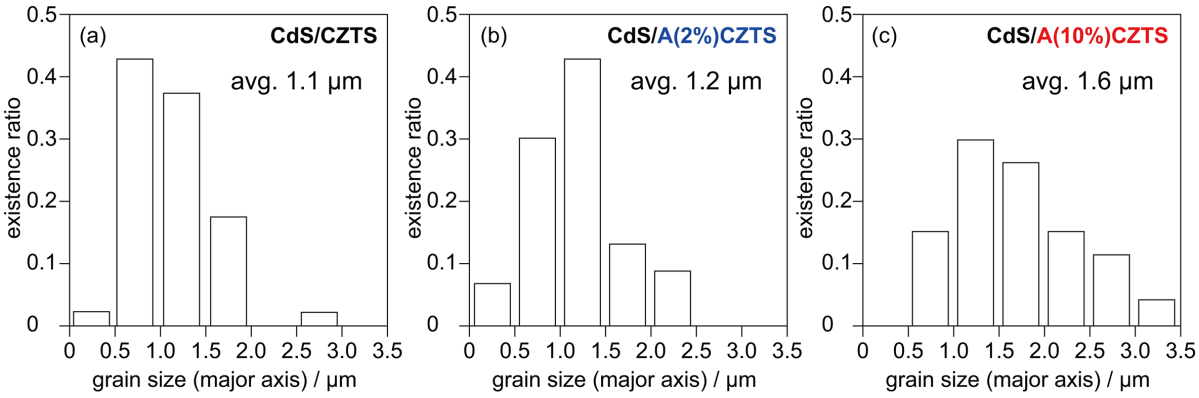

Figure IV.4. Size distributions of grains in (a) CZTS, (b) A(2%)CZTS, and (c) A(10%)CZTS films obtained by measuring major axes of several tens grains in these films.

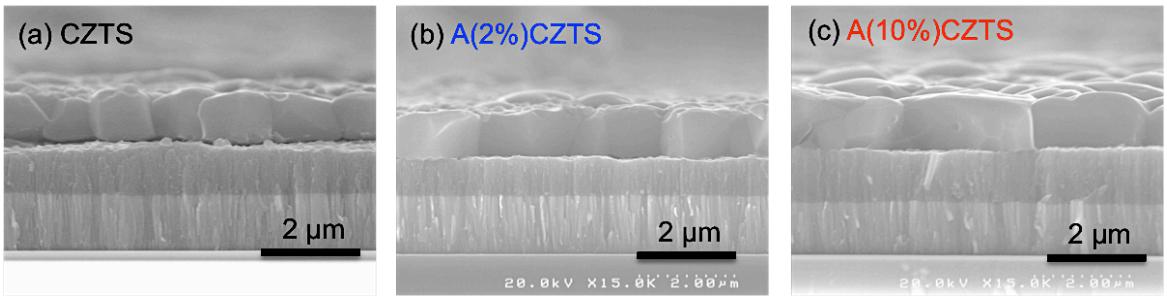

Figure IV.5. Cross-sectional SEM images of (a) CZTS, (b) A(2%)CZTS, and (c) A(10%)CZTS films.

CZTS and ACZTS films were then processed into solar cells with structures of Al/indium tin oxide (ITO)/intrinsic ZnO (*i*-ZnO)/CdS/CZTS (or ACZTS)/Mo/glass. Figures IV.6a-6c shows current J-V curves, Mott-Schottky plots, and external quantum efficiency (EQE) spectra of thus-obtained devices derived from CZTS and ACZTS films. Several parameters extracted from these results are also summarized in Table IV.1. The device made from the CZTS film exhibited power conversion efficiency (PCE) of 4.7%, which is lower than that achieved in our previous study [18]. The appreciably low shunt resistance (R_{sh}) and high series resistance (R_s) resulted in a decrease in PCE of the present device. As shown in Figure 3a, the presence of voids in the CZTS film would be a main factor for shunts. These voids were also likely to have enhanced the formation of the MoS_2 layer due to the ease of diffusion of sulfur vapor during fabrication of the CZTS film, leading to an increase in R_s. The acceptor density (N_A) of the CZTS-based device obtained by capacitance-voltage (C-V) measurement tended to be high. Theoretical study in the literature claimed that formation energy of Cu on Zn antisite defect (Cu_{Zn}) is much lower than other point defects such as Cu vacancy [8]. Therefore, we can expect presences of large amounts of Cu_{Zn} in the present CZTS film compared to the other ones: a probable explanation for the large N_A value

observed for the CZTS-based device is the presence of large amounts of Cu_{Zn} antisite defects [7,11,16]. The large N_A affected the EQE response of the device at a relatively long wavelength region (600-800 *nm*) due to reduction of the width of the space charge layer (SCL). The presence of large amounts of defects should also enhance Shockley-Read-Hall (SRH) recombination at the SCL. These failures are attributed to relatively small short circuit current density (J_{SC}) and relatively small open circuit voltage (V_{OC}).

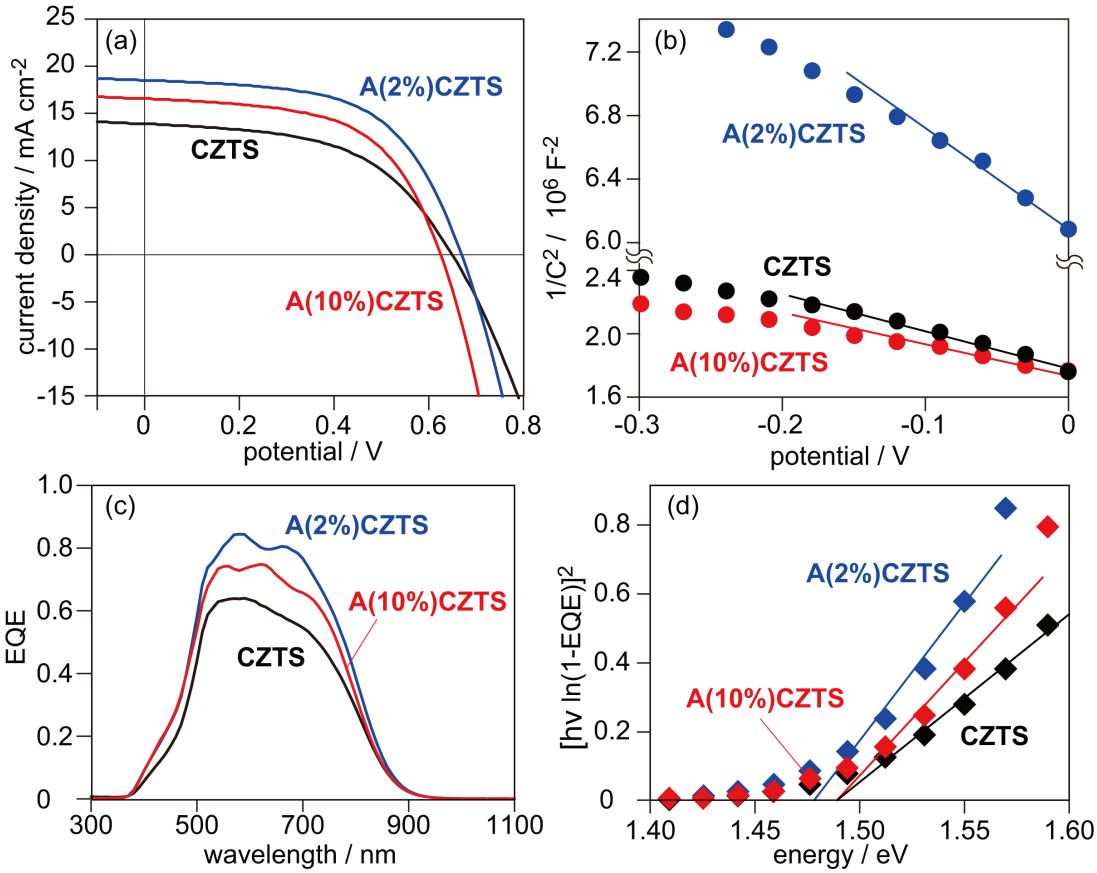

Figure IV.6. (a) J-V curves of CZTS- and ACZTS- based devices under illumination (AM1.5G), (b) C-V characteristics of CZTS- and ACZTS-based devices, (c) EQE spectra of CZTS- and ACZTS-based devices measured in a short circuit condition, and (d) photon energy (hν) vs $(h\nu \times \ln(1\text{-EQE}))^2$ plots of EQE results to determine E_g of CZTS and ACZTS films.

Table IV.1. Solar cell, electric, and optical parameters of CZTS- and ACZTS-based devices.

Absorber layer	CZTS	A(2%)CZTS	A(10%)CZTS
J_{SC} / $mA\ cm^{-2}$	13.9	18.5	16.6
V_{OC} / mV	650	669	625
FF	0.524	0.576	0.571
PCE (%)	4.73	7.14	5.92
R_s / $\Omega\ cm^2$	4.40	2.90	2.00
R_{sh} / $\Omega\ cm^2$	197	240	215
N_A / cm^{-3}	6.02×10^{16}	2.24×10^{16}	7.32×10^{16}
V_{bi} / V	0.803	0.887	0.940
E_g / eV	1.48	1.47	1.48

Significant improvements of device properties were achieved by the use of AZCTS films, especially for the device based on the Ag(2%)CZTS film: the best device achieved PCE of 7.1%. As discussed in the literature [12], the Ag-based kesterite (i.e., Ag_2ZnSnS_4 (AZTS)) was expected to include a small number of Ag_{Zn} antisite defects because significant differences in ionic radiuses between Ag and Zn ions lead to relatively high formation energy of the defect. Hence, Ag incorporation in the present system should contribute the reduction of the Cu_{Zn} defect, leading to reduction of the N_A value. As discussed above, the absence of appreciable voids in the Ag(2%)CZTS film is also beneficial for the solar cell device. It should be noted that the built-in potential (V_{bi}) of the Ag(2%)CZTS-based device was larger than that of the CZTS-based device. Based on the results of above

photoelectrochemical analyses, enlargement of V_{bi} by incorporation of Ag into CZTS caused the positive shift of the FB potential (i.e., valence band maximum (VBM)). Thus, the relatively large V_{OC} achieved by the Ag(2%)CZTS-based device can be explained by differences in the energy structures. However, incorporation of larger amounts of Ag was detrimental in the devices. Since the N_A value of the Ag(10%)CZTS film became larger than that of the Ag(2%)CZTS film, the Ag component would have other unfavorable effects on the film quality though the effects have not been clarified. Another notable failure of the Ag(10%)CZTS-based device is the presence of pinholes in the Ag(10%)CZTS film. Indeed, induction of shunts resulted in significant lowering of V_{OC} in the Ag(10%)CZTS-based device. In addition, we also examined the solar cell performance of the device based on an ACZTS film with a Ag / (Ag + Cu) ratio of 0.055 (i.e., the devices A(5%)CZTS). As a result, the solar cell performance of the device was in the middle between the devices based on A(2%)CZTS and A(10%)CZTS films (Figure IV.7). Thus, the device based on the A(2%)CZTS film is likely to be close to the optimum though further optimizations were not performed at present.

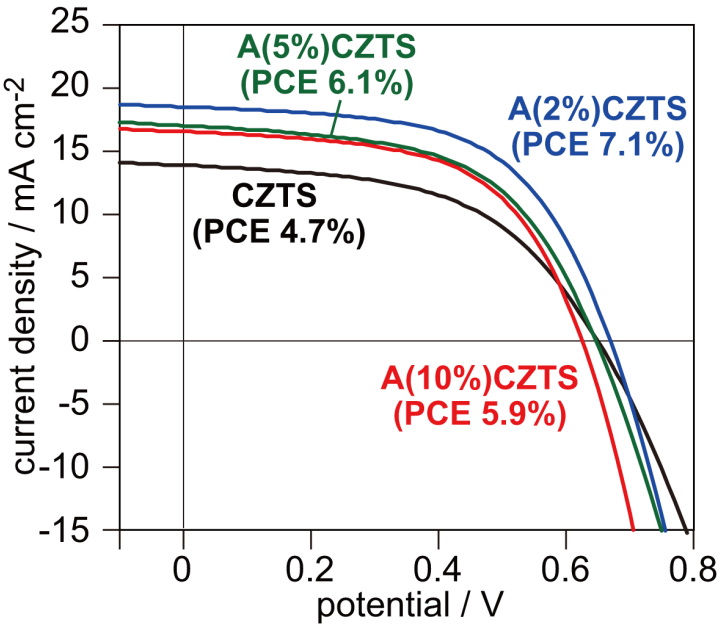

Figure IV.7. J-V curves of CZTS- and ACZTS- based devices under illumination (AM1.5G).

For further evaluation of device properties, electric structures of CdS-CZTS and CdS-ACZTS heterojunctions were evaluated by XP spectroscopy. Figure IV.8 shows XP spectra of CdS/CZTS and CdS/ACZTS films (i.e., CZTS and ACZTS films covered by a CdS layer without processing coverage of Al, ITO, and *i*-ZnO layers) at a shallow binding energy (BE) region (< 25 *eV*). Firstly, all of the samples were bombarded by Ar^+ for 5 min to expose clean CdS surfaces. As a result, all of the samples showed an intense peak derived from the Cd4d core in addition to a broad spectrum at the valence band region. Assuming that onset BEs of valence band spectra were VBM of CdS, we determined energy differences (ΔEs) between the Cd4d core level and VBM of CdS in CdS/CZTS and CdS/ACZTS films After the surfaces of CdS/CZTS and CdS/ACZTS had been bombarded by Ar^+ for ca. 40 *min* to be etched to some extent, Zn3d core level peaks appeared in addition to Cd4d peaks, indicating appearances of CdS/CZTS and CdS/ACZTS heterointerfaces. After deconvolution

of these spectra to separate Cd4d and Zn3d peaks, ΔEs between the Cd4d core and the Zn3d core were estimated. When further Ar^+ ion etching for ca. 80 *min* was carried out, the Cd4d peak disappeared and the XP spectra showed surface structures of CZTS and ACZTS layers. As shown in our previous study, the E_g value of the surface-covered CdS was determined to be 2.44 *eV* [29]. Regarding E_gs of CZTS and ACZTS films, transformation of EQE spectra (Figure IV.6c) into incident photon energy (hν)-vs-(hν×ln(1-EQE))^2 plots was applied. From intersects of linear portions of these plots, E_gs of CZTS, A(2%)CZTS, and A(10%)CZTS films were determined to be 1.48 eV, 1.47, and 1.48 *eV*, respectively: a slight E_g bowing appeared, as expected from our previous study on CZTS and ACZTS powder systems [30].

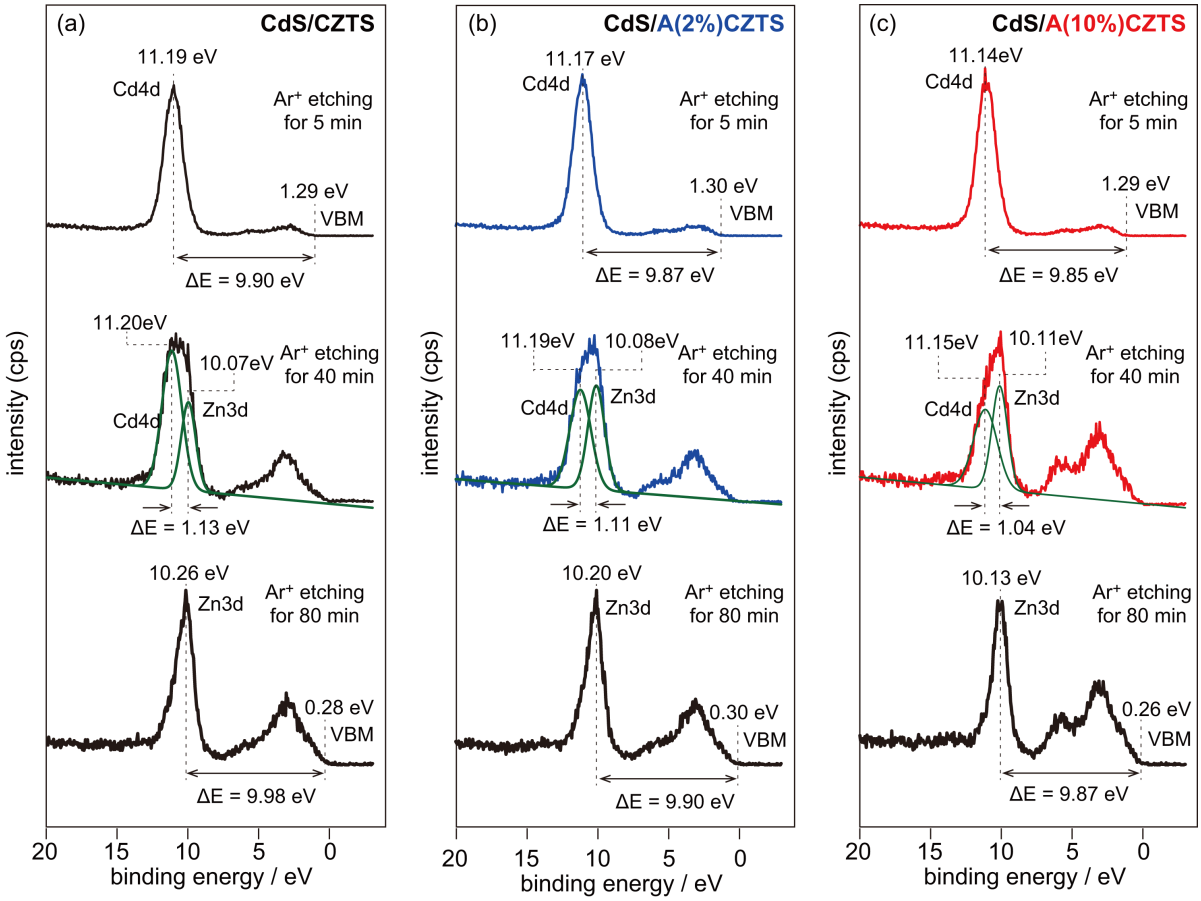

Figure IV.8. XP spectra of (a) CdS/CZTS, (b) CdS/A(2%)CZTS, and (c) CdS/A(10%)CZTS heterostructures obtained after Ar· ion etching for 5 *min* (upper), 39.5 *min* (middle), and 85 *min* (bottom).

Based on these values and parameters, schematic energy diagrams of CdS/CZTS and CdS/ACZTS heterointerfaces were obtained, as shown in Figure IV.9. Significant results of these analyses are differences in the conduction band alignments, i.e., ΔE values between conduction band minimum (CBM) of CdS and those of CZTS (or ACZTS). The ΔE value between CdS and CZTS is largely negative (-0.25 *eV*), indicating cliff-type conduction band alignment (Figure IV.6a), in agreement with many results in the literature [31-34]. Although

cliff-type conduction band alignments were also observed for CdS-ACZTS heterojunctions (Figures IV.9b and 9c), ΔE values became lower than that of the CdS-CZTS heterointerface. As discussed above, these differences in ΔE are likely to originate from positive shifts of FB potentials induced by incorporation of Ag in the CZTS crystalline lattice, leading to increases in V_{bi}s as well as efficient suppression of interface recombination.

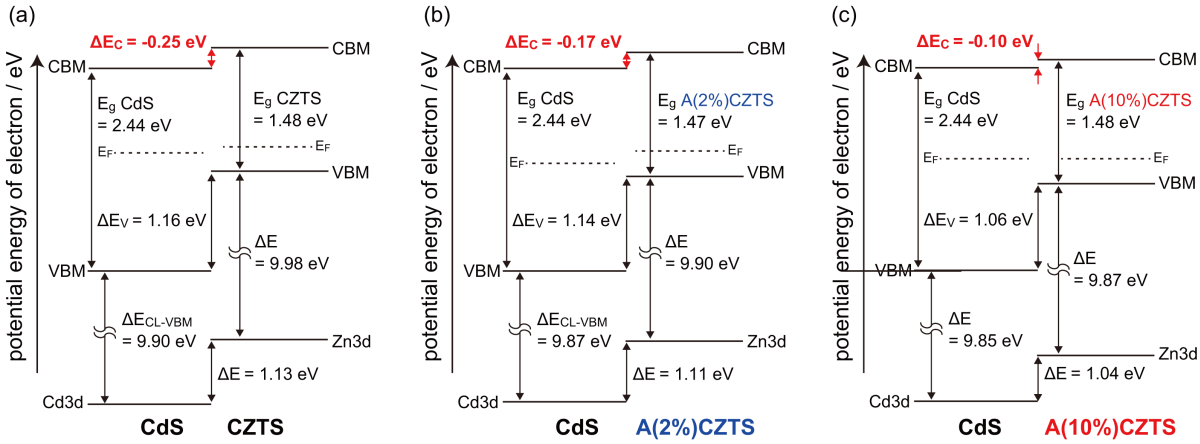

Figure IV.9. Energy diagrams of (a) CdS/CZTS, (b) CdS/A(2%)CZTS, and (c) CdS/A(10%)CZTS heterojunctions estimated from XP spectroscopy and EQE data. The E_g value of the CdS layer was obtained from reference 29.

IV.4. Conclusion

We have demonstrated fabrication of Ag-containing CZTS thin films applicable for photovoltaics: the best PCE achieved in this study was 7.1% using a device based on the Ag(2%)CZTS film. The value is one of the best among the devices based on Ag-incorporated pure sulfide kesterites [16], while much higher PCEs were achieved by using the devices composed of selenide containing kesterites (i.e., Ag-incorporated $Cu_2ZnSn(S,Se)_4$) [14, 15]. Various analyses suggested that PCE values in the present system

depend strongly on film morphologies (e.g., presence of voids and pinholes), defect disparities, and band alignments toward the CdS layer. Since these properties would not have trade-off relations, the strategy for Ag incorporation is promising for further improvements of PCE of CZTS-based solar cells.

References

[1] A. Emrani, P. Vasekar and C. R. Westgate, Solar Energy, 2013, 98, 335-340.

[2] V. Tunuguntla, W. C. Chen, P. H. Shih, I. Shown, Y. R. Lin, J. S. Hwang, C. H. Lee, L. C. Chen and K. H. Chen, J. Mater. Chem. A, 2015, 3, 15324.

[3] J. Tao, J. Liu, L. Chen, H. Cao, X. Meng, Y. Zhang, C. Zhang, L. Sun, P. Yang and J. Chu, Green Chem., 2016, 18, 550.

[4] S. Kahraman, S. Cetinkaya, M. Podlogar, S. Bernik, H. A. Cetinkara and H. S. Guder, Ceramics International, 2013, 39, 9285-9292.

[5] S. Chen, X. G. Gong, A. Walsh and S. H. Wei, MRS Online Proceeding Library Archive, 2011, 1370, 1-12.

[6] T. J. Huang, X. Yin, C. Tang, G. Qi and H. Gong, J. Mater. Chem. *A*, 2015, 3, 17788.

[7] L. Yin, G. Cheng, Y. Feng, Z. Li, C. Yang, X. Xiao, *RSC. Adv.* **2015**, *5*, 40369.

[8] S. Chen, A. Walsh, X. G. Gong, S. H. Wei, *Adv. Mater.* **2013**, *25*, 1522-1539.

[9] M. Grossberg, T. Raadik, J. Raudoja, J. Krustok, *Current Apllied Physics* **2014**, 14, 447-450.

[10] M. Kumar, A. Dubey, N. Adhikari, S. Venkatesan, Q. Qiao, *Energy Environ. Sci.* **2015**, *8*, 3134-3159.

[11] K. J. Yang, J. H. Sim, D. H. Son, D. H. Jeon, D. K. Hwang, D. Nam, H. Cheong, S. Y. Kim, J. H. Kim, D. H. Kim, J. K. Kang, *Journal of Industrial and Engineering Chemistry* **2017**, *45*, 78-84.

[12] Z. K. Yuan, S. Chen, H. Xiang, X. G. Gong, A. Walsh, J. S. Park, I. Repins, S. H. Wei, *Adv. Funct. Mater.* **2015**, *25*, 6733-6743.

[13] C. J. Hages, M. J. Koeper, R. Agrawal, *Solar Energy Materials & Solar Cel* **2016**, *145*, 342-348.

[14] W. Li, X. Liu, H. Cui, S. Huang, X. Hao, *Journal of Alloys and Compounds* **2015**, *625*, 227-283.

[15] T. Gershon, Y. S. Lee, P. Antunez, R. Mankad, S. Singh, D. Bishop, O. Gunawan, M. Hopstaken, R. Haight, *Adv. Energy Mater.* **2016**, *6*, 1502468.

[16] A. Guchhait, Z. Su, Y. F. Tay, S. Shukla, W. Li, S. W. Leow, J. M. R. Tan, S. Lie, O. Gunawan, L. H. Wong, *ACS Energy Lett.* **2016**, *1*, 1256-1261.

[17] T. H. Nguyen, W. Septina, S. Fujikawa, F. Jiang, T. Harada, S. Ikeda, *RSC Adv*. **2015**, *5*, 77565.

[18] T. H. Nguyen, S. Fujikawa, T. Harada, J. Chantana, T. Minemoto, S. Nakanishi, S. Ikeda, *ChemSusChem* **2016**, *9*, 1-8.

[19] H. Katagiri, K. Jimbo, W. S. Maw, K. Oishi, M. Yamazaki, H. Araki, A. Takeuchi, *Thin Solid Films* **2009**, *517*, 2455-2460.

[20] J. J. Scragg, P. J. Dale, L. M. Peter, G. Zoppi, I. Forbes, *Phys. Stat. Solidi B* **2008**, *245*, 1772–1778.

[21] H. Katagiri, K. Jimbo, W. S. Maw, K. Oishi, M. Yamazaki, H. Araki, A. Takeuchi, *Thin Solid Films* **2009**, *517*, 2455-2460.

[22] T. J. Huang, X. Yin, G. Qi, H. Gong, *Phys. Status Solidi RRL*. **2014**, *8*, 735-762.

[23] X. Liu, Y. Feng, H. Cui, F. Liu, X. Hao, G. Conibeer, D. B. Mitzi, M. Green, *Prog. Photovolt: Res. Appl.* **2016**, *24*, 879-898.

[24] D. Tiwari, T. Koehler, X. Lin, R. Harniman, I. Griffiths, L. Wang, D. Cherns, R. Klenk, D. J. Fermin, *Chem. Mater.* **2016**, *28*, 4991-4997.

[25] P. K. Sarswat and M. L. Free, *J. Mater. Sci.* **2015**. *50*, 1613-1623.

[26] C. P. Björkman, J. Scragg, H. Flammersberger, T. Kubart, M. Edoff, *Sol. Energy Mater. Sol. Cells*, **2012**, *98*, 110-117.

[27] A. A. Weber, R. Mainz, H. W. Schock, *J. Appl. Phys.* **2010**, 107, 013516.

[28] W. Septina, M. Sugimoto, D. Chao, Q. Shen, S. Nakatsuka, Y. Nose, T. Harada, S. Ikeda, *Phys. Chem. Chem. Phys.* **2017**, *19*, 12502-12508.

[29] Gunawan, W. Septina, T. Harada, Y. Nose, S. Ikeda, *ACS Appl. Mater. Interfaces*, **2015**, *7*, 16086-16092.

[30] S. Ikeda, T. Nakamura, T. Harada, M. Matsumura, *Phys. Chem. Chem. Phys.* **2010**, *12*, 13943-13949.

[31] A. Polizzotti, I. L. Repins, R. Noufi, S-H. Wei, D. B. Mitzi, *Energy Environ. Sci.* **2013**, *6*, 3171-3182.

[32] K. Sun, C. Yan, F. Liu, J. Huang, F. Zhou, J. A. Stride, M. Green, X. Hao, *Adv. Energy Mater.* **2016**, *6*, 1600046.

[33] M. Bär, B.-A. Schubert, B. Marsen, R. G. Wilks, S. Pookpanratana, M. Blum, S. Krause, T. Unold, W. Yang, L. Weinhardt, C. Heske, H.-W. Schock, *Appl. Phys. Lett.* **2011**, *99*, 222105.

[34] C. Yan, F. Liu, N. Song, B. K. Ng, J. A. Stride, A. Tadich, X. Hao, *Appl. Phys. Lett.* **2014**, *104*, 173901.

Chapter V

Effects of Indium Incorporation on Structural and Photovoltaic Properties of Cu_2ZnSnS_4 Thin Films

V.1. Introduction

In previous chapter, we have proved that a partial replacement of Cu to Ag was found to reduce the Cu_{Zn} antisite defect in CZTS films leading to improvement of solar cell performance. However, in Cu_2ZnSnS_4 (CZTS) material, there are still some other deep defects need to be reduced [1-3].

It was reported that some semiconductor materials contain multivalent elements not just as impurities but also as part of their structural skeleton. These multivalent impurities might transit from one oxidation state to the other by changing the defect charge state, and this transition causes a deep level inside the band gap [4]. For the CZTS compound, it contains of the multivalent element of Sn (i.e., II and IV oxidation state), which deteriorates the electronic properties by forming recombination centers and thus limit the device efficiency [5,6]. Therefore, substitution of Sn by other elements could reduce the recombination and improve performance of CZTS films.

Recently, J. Kim et al. reported enhancement of V_{OC} by applying a double In_2S_3/CdS emitter on CZTSSe absorbers. In_2S_3 was used as a supplier of indium into the CdS/CZTSSe layers during annealing: the diffused indium from the In_2S_3 outer layer into the CZTSSe bottom layer led to increase in carrier densities of the CZTSSe film due to formation of In_{Sn} shallow defects. As a result, CZTSSe solar cells with a V_{OC} deficit of less than 600 mV were obtained [7]. Feng et al. also fabricated a solar cell based on electrodeposited Cu_2ZnSnS_4 with In_2S_3 buffer layer; by applying a post-heat treatment; they found the diffusion of indium to CZTS increased acceptor concentration and induced an extension of external quantum efficiency response of the solar cell to the long wavelength region. The post-heated

In_2S_3/CZTS stack reached appreciably large short circuit current density of more than 20 mA cm^{-2} lead maximum conversion efficiency of 6.9 % [8].

It should be noted that the kesterite was formed by substituting indium and gallium elements in chalcopyrite structure by zinc and tin elements. Therefore, indium can probably be incorporated in the both zinc and tin sites of the CZTS structure. These above reasons motivated us study effects of indium substitution on photovoltaic properties of In-incorporated CZTS (In-CZTS) absorber thin films. In this study, we studied fabrication of In-CZTS films by using a facile spray pyrolysis technique. Effects of indium substitution on structural, morphological and photovoltaic properties of CZTS films were discussed.

V.2. Experimental

V.2.1. Fabrication of In-CZTS Thin Film Solar Cells

An aqueous precursor solution containing copper nitrate ($Cu(NO_3)_2$), zinc nitrate ($Zn(NO_3)_2$), tin methanesulfonate ($Sn(CH_3SO_3)_2$) and thiourea ($SC(NH_2)_2$) was used as a source solution. Excess $SC(NH_2)_2$) with reference to the stoichiometric amount was used to prevent loss of the sulfur component during the spray process and precipitation of a Cu component in the solution. Different amount of $In(NO_3)_3$ was added to the precursor solution with In/(Zn +Sn) ratios of 0, 0.01, 0.02, 0.04, 0.1, 0.2, 0.5 and 0.7. After adjusting pH to 1.5 by adding a few drops of conc. nitric acid, each of the aqueous precursor solutions was sprayed onto an Mo-coated soda-lime glass substrate (Mo/glass) that was preheated at 380 °C using a hot plate. Finally, thus-obtained films were annealed in an evacuated borosilicate glass ampoule together with 20 *mg* sulfur powder at 600 °*C* for 30 *min* to facilitate grain growth.

For fabrication of solar cells, the thus-obtained In-CZTS films were processed to form a device with a structure of Al/ITO/ZnO/CdS/In-CZTS/Mo/glass. On the top of In-CZTS, CdS buffer layer was deposited by chemical bath deposition (CBD). Then, an ITO/ZnO bilayer was deposited by radio frequency (RF) magnetron sputtering and an Al top contact was deposited by thermal evaporation.

V.2.2. Characterizations

Crystalline structures of the films were analyzed by X-ray diffraction (XRD) using a Rigaku Mini Flex X-ray diffractometer (CuKα, Ni filter). Raman spectroscopy using a JASCO NRC 3100 Laser Raman Spectrophotometer (excitation laser having a wavelength of 532 *nm*) was also performed for structural analyses of the films. Morphologies of the films were examined by using a Hitachi S-5000 FEG field emission scanning electron microscope (SEM) at an acceleration voltage of 20 *kV*. Current density-voltage (J-V) characteristics and external quantum efficiency (EQE) spectra of solar cell devices under simulated AM1.5G irradiation (100 $mW\ cm^{-2}$) were determined with a Bunkoukeiki CEP-015 photovoltaic measurement system.

V.3. Results and Discussion

Figure V.1 shows the XRD patterns of In-substituted Cu_2ZnSnS_4 films with different In/(Zn +Sn) ratios. The sample at the In/(Zn+Sn) ratio of 0 (*i.e.*, pure CZTS film) showed the main peaks corresponding to the (101), (112), (200), (202), (220), (312), (224), (008) and (332) planes of reflection assigned to CZTS structure (Figure V.1a) [9-11]. The diffraction peaks of Mo and MoS_2 phases were also observed due to the partial sulfurization of bottom Mo substrates during annealing. With increasing in the In/(Zn+Sn) ratio, main peaks of

CZTS shifted to lower 2θ angles. For the sample at the In/(Zn+Sn) ratio 0.7, main peaks were close to those of the $CuInS_2$ (CIS) compound [12, 13].

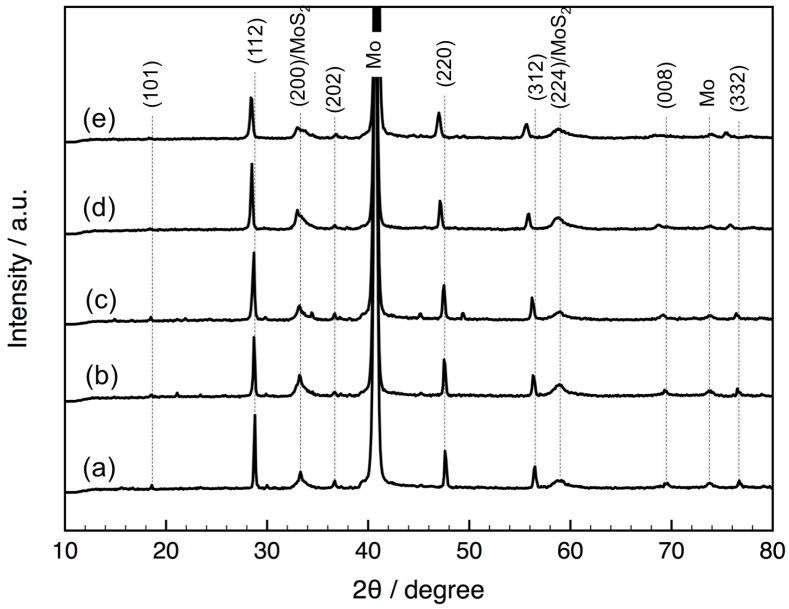

Figure V.1. XRD patterns of In-substituted Cu_2ZnSnS_4 films with different In/(Zn+Sn) ratios: (a) 0, (b) 0.1, (c) 0.2, (d) 0.5 and (e) 0.7. Quoted from original manuscript: *T. H. Nguyen et al*., ECS Transactions, 75 (50) (2017), 15-22.

Raman spectroscopy was also used to investigate presences/absences of possible secondary phases in fabricated films (Figure V.2). The Raman spectrum of the pure CZTS film showed an intense peak centered at 336 cm^{-1} and two weak peaks at 286 and 369 cm^{-1} [14, 15]. With increasing in the In/(Zn+Sn) ratio, these peaks shifted to lower wavenumber regions. For samples with In/(Zn+Sn) ratios of 0.5 and 0.7, additional peak centered at 289 cm^{-1}, which is assignable to the main peak of $CuInS_2$, was appeared [16, 17]. Hence, the In-CZTS films with In/(Zn+Sn) ratios were composed of mixtures of CZTS and CIS compounds. No appreciable impurity compound was confirmed in the films with relatively

low In/(Zn+Sn) ratios (In/(Zn+Sn)≤0.2), we therefore concluded successful formation of pure In-CZTS films with different indium ratios.

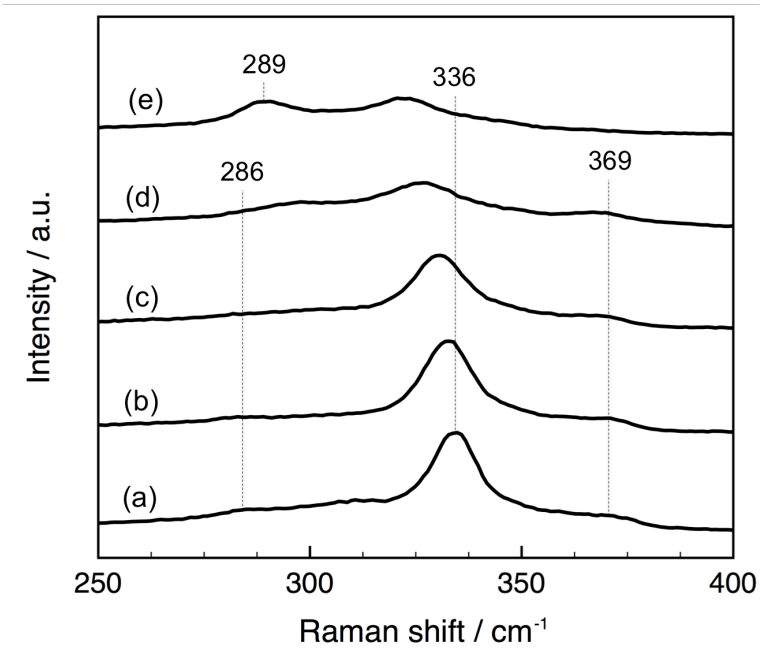

Figure V.2. Raman spectra of In-substituted Cu_2ZnSnS_4 films with different In/(Zn+Sn) ratios: (a) 0, (b) 0.1, (c) 0.2, (d) 0.5 and (e) 0.7. Quoted from original manuscript: *T. H. Nguyen et al*., ECS Transactions, 75 (50) (2017), 15-22.

Morphological properties of fabricated films were investigated by using scanning electron microscope (SEM). Figure V.3 shows surface and cross-sectional SEM images of fabricated In-substituted CZTS films. The pure CZTS film (In/(Zn+Sn) = 0) showed clear micrometer-sized grains in both surface and cross-sectional images (Figures V.3a and b). However, with increasing in the In/(Zn+Sn) ratio, the grain became smaller, and we can easily observe voids in the films, especially for the sample with relatively high In/(Zn+Sn) ratio (In/(Zn+Sn) = 0.5). Flipped parts of film from the Mo substrate were often observed (Figure V.3g and h). Hence, incorporation of indium into the CZTS film showed negatively effects in view of its crystallinity and morphology.

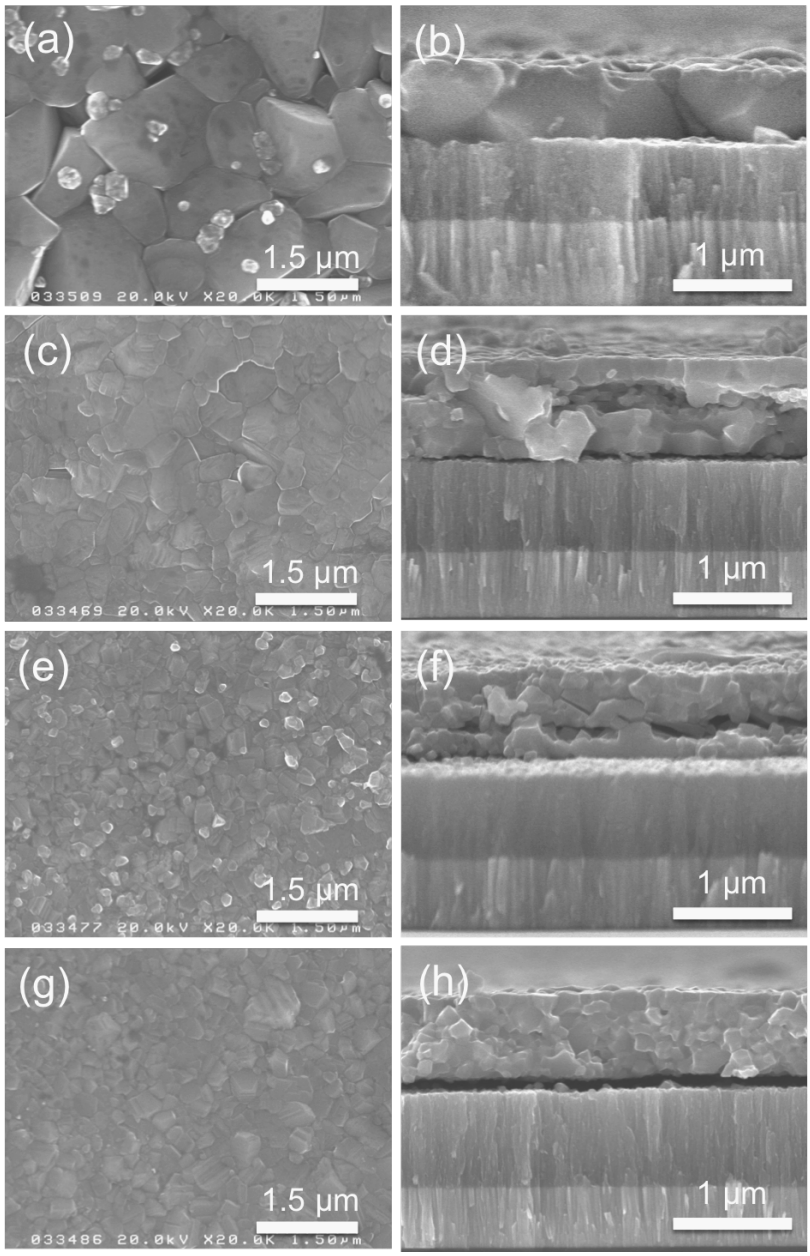

Figure V.3. Top-view (left panels) and cross-sectional (right panels) SEM images of In-substituted Cu_2ZnSnS_4 films with different In/(Zn+Sn) ratios: (a, b) 0, (c, d) 0.1; (e, f) 0.2 and (g, h) 0.5. Quoted from original manuscript: *T. H. Nguyen et al*., ECS Transactions, 75 (50) (2017), 15-22.

Such low quality In-CZTS containing large amounts of indium led to difficulty for fabrication of complete devices. Therefore, we attempted to fabricate the solar cells based on In-CZTS films with In/(Zn+Sn) ratios of 0, 0.01, 0.02 and 0.04. Figure V.4 shows cross-sectional SEM images of fabricated In-substituted CZTS films. It also easy to see the effects of indium substitution to grain growth of films, with increasing of indium content, the grain size become smaller, however all films as a compact layer were successful fabricated on Mo substrates with thickness of 1 μm.

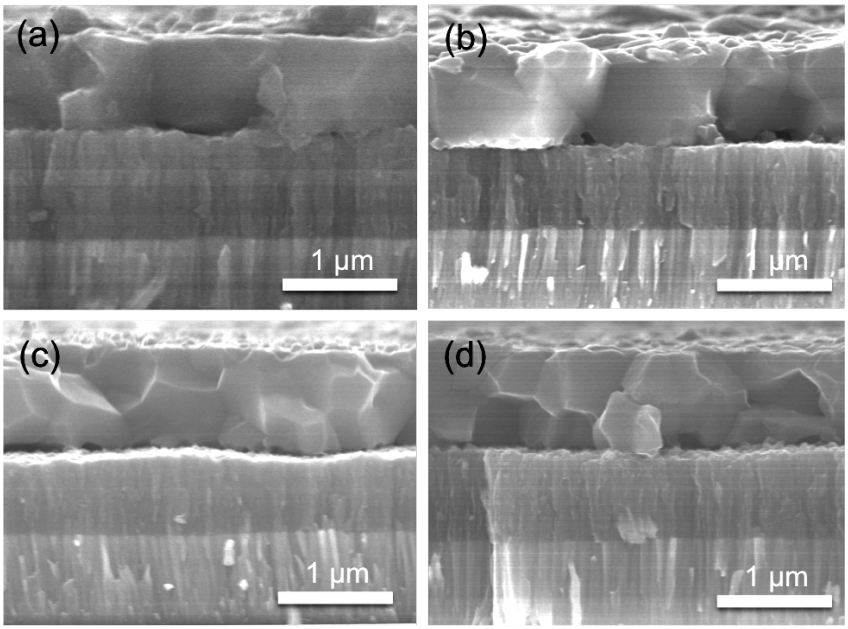

Figure V.4. Cross-sectional SEM images of In-substituted Cu_2ZnSnS_4 films with different In/(Zn + Sn) ratios: (a) 0; (b) 0.01; (c) 0.02 and (d) 0.04.

The fabricated CZTS films were then processed into solar cells with the structure of Al:ZnO/ZnO/CdS/CZTS/Mo/glass. Figure V.5 shows light J-V curves of solar cells derived from the fabricated In-CZTS films with In/(Zn+Sn) ratios of 0, 0.01, 0.02 and 0.04. The cell parameters were summarized in Table V.1. The device made from pure CZTS film exhibited

PCE of 5.6 %. Appreciable improvements of J_{SC} and V_{OC} were observed when the device made based of the In-CZTS film with the In/(Zn+Sn) ratios of 0.01 was used. However, further increase in the In/(Zn+Sn) ratio resulted in a reduction of both J_{SC} and V_{OC}; the PEC value of the device was 4.6 %. Reductions of solar cell parameters were significant in the device based on the In-CZTS film with the In/(Zn+Sn) ratio of 0.04. Based on the fact that the In-CZTS film with the In/(Zn+Sn) ratio of 0.04 had relatively small grain size when compared to that of the pure CZTS (Figure V.4), the decrease in PEC can be explained by the enhancement of charge recombination in the In-CZTS bulk.

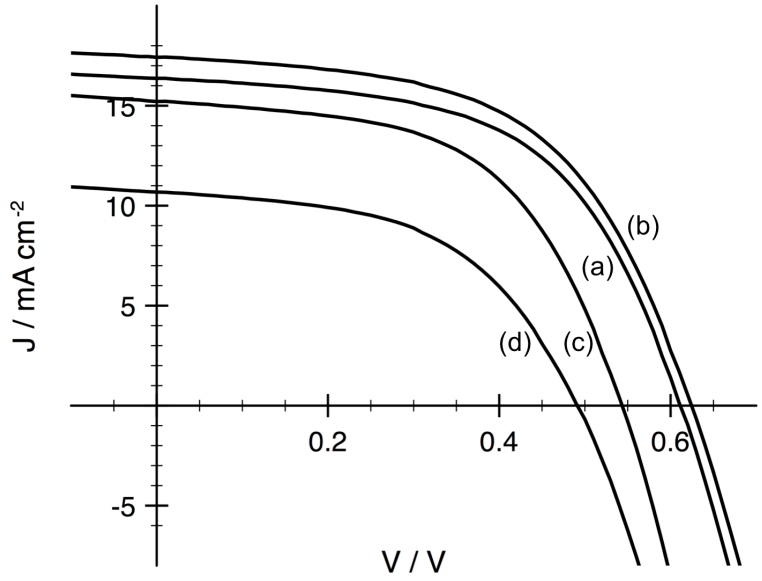

Figure V.5. Light J-V data of In-substituted CZTS-based solar cells derived from fabricated In-substituted CZTS films with different In/(Zn+Sn) ratios: (a) 0, (b) 0.01, (c) 0.02 and (d) 0.04. Quoted from original manuscript: *T. H. Nguyen et al*., ECS Transactions, 75 (50) (2017), 15-22.

Table V.1. Solar cell parameters of solar cells made from fabricated In-CZTS films with different indium content. Quoted from original manuscript: *T. H. Nguyen et al.*, ECS Transactions, 75 (50) (2017), 15-22.

In/(Zn+Sn) ratio	J_{SC} / $mA\ cm^{-2}$	V_{OC} / mV	FF	PCE (%)
0	16.4	611	0.56	5.6
0.01	17.4	629	0.55	6.0
0.02	15.2	543	0.55	4.6
0.04	10.7	491	0.52	2.7

Figure V.6 shows external quantum-efficiency (EQE) spectra of the devices. All the spectra rose at ca. 370 *nm* to ca. 540 *nm* and then gradually degrease to onset wavelength of ca. 900 *nm* corresponding to the band gap of CZTS. Since the low content of indium ratio, there is no significant different on the band gap energy. The devices based on In-CZTS films with indium contents (In/(Zn+Sn) = 0.02 and 0.04) showed appreciable drop in the EQE spectra at relatively long wavelength region (ca. 600-800 *nm*) when compared to those of devices based on the pure CZTS film and the In-CZTS film with the In/(Zn+Sn) ratio of 0.01. Such an EQE loss indicated insufficient carrier collection generated relatively deep region of these In-CZTS films due to their low film quality.

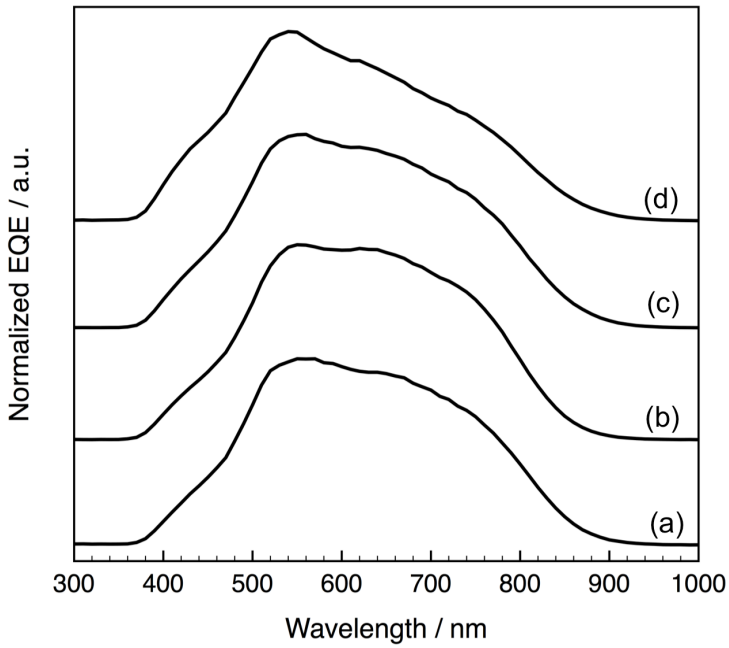

Figure V.6. EQE spectra of In-substituted CZTS-based solar cells derived from fabricated In-substituted CZTS films with different In/(Zn+Sn) ratios: (a) 0, (b) 0.01, (c) 0.02 and (d) 0.04. Quoted from original manuscript: *T. H. Nguyen et al*., ECS Transactions, 75 (50) (2017), 15-22.

IV.4. Conclusion

In this study, we investigated structures of indium-incorporated CZTS films fabricated by using a facile spray pyrolysis technique. The XRD and Raman spectroscopy analyses showed that pure In-CZTS films were successfully fabricated at the In/(Zn+Sn) substitution ratio up to 0.2. From the morphological characterization, the incorporation of indium suppressed grain growth, leading to lowering the film quality. As a result, the solar cell based on the In-CZTS film showed relatively low properties when compared to that of the device based on the pure CZTS film. However, we also observed an appreciable improvement of the device property when the In-CZTS sample with relatively low indium content (In/(Zn+Sn) = 0.01) was employed. Although the main cause(s) of the observed

improvement was not clear at present, the result suggests effectiveness of the indium incorporation with relatively low In/(Zn+Sn) ratio, *i.e.*, the addition of indium to the CZTS film with doping level would be beneficial for improvement of device property. Further studies along this line are necessary.

References

[1] S. Chen, A. Walsh, X. G. Gong, S. H. Wei, *Adv. Mater.,* **2013**, 25, 1522-1539.

[2] M. Kumar, A. Dubey, N. Adhikari, S. Venkatesan and Q. Qiao, Energy Environ. Sci., 2015, 8, 3134.

[3] A. Nagoya and R. Asahi, Physical Review B, 2010, 81, 113202.

[4] K. Biswas, S. Lany and A. Zunger, Appl. Phys. Lett., 2010, 96, 201902.

[5] J. Ge, J. Chu, J. Jiang, Y. Yan and R. Yang, ACS. Appl. Mater. Interfaces, 2014, 6, 21118 – 21130.

[6] X. Liu, Y. Feng, H. Cui, F. Liu, X. Hao, G. Conibeer, D. B. Mitzi and M. Green, Prog. Photovolt: Res. Appl., 2016, 24, 879 – 898.

[7] J. Kim, H. Hiroi, T. K. Todorov, O. Gunawan, M. Kuwahara, T. Gokmen, D. Nair, M. Hopstaken, B. Shin, Y. S. Lee, W. Wang, H. Sugimoto and D. B. Mitzi, *Adv. Mater.*, 2014, **26**, 7427.

[8] F. Jiang, C. Ozaki, Gunawan, T. Harada, Z. Tang, T. Minemoto, Y. Nose and S. Ikeda, *Chem. Mater.*, 2016, **28**, 3283.

[9] K. F. Tai, O. Gunawan, M. Kuwahara, S. Chen, S. G. Mhaisalkar, C. H. A. Huan and D. B. Mitzi, Adv. Energy. Mater., 2016, 6, 1501609.

[10] Z. Su, K. Sun, Z. Han, H. Cui, F. Liu, Y. Lai, J. Li, X. Hao, Y. Liu and M. A. Green, *J. Mater. Chem. A*, 2014, **2**, 500-509.

[11] J. W. Cho, A. Ismail, S. J. Park, W. Kim, S. Yoon and B. K. Min, *Appl. Mater. Interfaces*, 2013, **5**, 4162-4165.

[12] D. Y. Lee and J. Kim, Thin Solid Films, 2010, 518, 6537 – 6541.

[13] R. Guan, X. Wang and Q. Sun, Journal of Nanomaterial, 2015, 579489, 1-8.

[14] J. C. W. Ho, T. Zhang, K. K. Lee, S. K. Batabyal, A. I. Y. Tok and L. H. Wong, ACS Appl. Mater. Interfaces, 2014, 6, 6638-6643.

[15] Z. Li, J. C. W. Ho, K. K. Lee, X. Zeng, T. Zhang, L. H. Wong and Y. M. Lam, *RSC Adv.*, 2014, **4**, 26888-26894.

[16] S. K. Swami, N. Chaturvedi, A. Kumar, N. Chander, V. Dutta, D. K. Kumar, A. Ivaturi, S. Senthilarasu and H. M. Upadhyaya, *Phys. Chem. Chem. Phys.*, 2014, **16**, 23993-23999.

[17] J. A. Garcia, A. P. Rodriguez, A. R. Rodriguez, T. Jawhari, J. R. Morante, R. Scheer and W. Calvet, Thin Solid Films, 2001, 387, 216 – 218.

[18] K. Oishi, W. Shimizu, A. Takeuchi, G. Nishida, M. Yamazaki, M. Nakagawa, N. Aoyagi and H. Katagiri, Phys. Status Solidi B, 2017, 6, 1700112.

Chapter VI

General Conclusions

In this thesis, we demonstrated the successful fabrication of CZTS compound thin films using non-vacuum spray pyrolysis technique for solar cell applications. The optimum annealing condition to obtain homogeneous and pin-hole-less films composed of relatively large grains was clarified by systematic studies for the film deposition. Effects of chemical compositions and elemental substitutions on properties of CZTS films and their device performance were discussed. The summaries throughout this work are described as follows.

In chapter II, CZTS thin films on Mo-coated glass substrate were fabricated by using spray pyrolysis of an aqueous precursor solution containing $Cu(NO_3)_2$, $Zn(NO_3)_2$, $Sn(CH_3SO_3)_2$ and thiourea followed by sulfurization. In order to prepare a stable precursor solution, the mixing order, the appropriate content of thiourea and the adjustment of adequate pH were indispensable to prevent precipitation of SnO_2 induced by the oxidation of Sn^{2+} and Cu^{2+}. Annealing of as-deposited films in sulfur vapor at temperatures ranging from 580 *°C* to 600 *°C* resulted in successful formation of homogeneous films composed of CZTS crystallites. Although the composition of the obtained CZTS films were not an empirical optimum (i.e., a Cu-poor and a Zn-rich compositions) reported in literature, an Sn-rich composition compared to its stoichiometric amount was found to be essential for efficient grain growth of the resulting CZTS films. As a result, a compact CZTS film with relatively large grain sizes was successfully obtained by employing the Sn-rich precursor solution with applying an adequate post annealing at a high temperature (600 *°C*) for a sufficient duration (30 *min*). A solar cell with a structure of glass/Mo/CZTS/CdS/ZnO/ITO/Al based on CZTS film obtained by an optimum annealing condition exhibited maximum conversion efficiency

of 5.8%.

Since an optimal chemical composition was not achieved for the CZTS films used in chapter II, in chapter III we attempted to adjust the Cu, Zn, Sn compositions in the CZTS film by controlling the concentrations of the corresponding metallic ions in the precursor solutions. When a precursor solution containing a stoichiometric composition of Cu, Zn, and Sn as 2:1:1 ratio was used, the resulting CZTS thin film contained a $Cu_{2-x}S$ impurity phase due to the evaporation of Sn components during the annealing process. The $Cu_{2-x}S$ impurity in the CZTS film was successfully removed by reduction in the concentration of Cu in the precursor solution to some extent. However, further reduction of Cu concentration induced formation of SnS_2 secondary phase owing to the shortage of Cu. The CZTS films obtained from the precursor solution containing adequate concentrations of Cu had a compact layer with relatively large grain sizes without presence of secondary phases, whereas the other CZTS films obtained from precursor solutions including different concentrations of Cu were composed of relatively small grains having significant voids. Therefore, the presence of these secondary phases was likely to suppress the grain growth of CZTS films. When the Cu content was close to the stoichiometric composition, the Cu_{Zn} defect was primarily formed in substantial amounts in the CZTS films; it should act as a recombination center for enhancing the band to impurity carrier recombination to reduce carrier lifetime. The reduction of the Cu content in CZTS films would reduce the amount of the Cu_{Zn} defects, leading to a decrease in carrier density and an improvement of carrier life time. Hence, metallic compositions of the precursor solutions were found to have significant effects on the qualities of CZTS films such as grain sizes, morphologies, acceptor densities, the nature of the acceptor defects and carrier lifetimes. A solar cell based on the CZTS film with an empirically optimal composition showed conversion efficiency of 8.1%. The value achieved was one of the best

efficiencies of Cu_2ZnSnS_4-based solar cells derived from a non-vacuum process.

In chapter IV, we attempted to reduce Cu_{Zn} antisite defects, which is the dominant defect in CZTS films because of its low formation energy, by replacement of Cu to Ag to obtain $(Cu_{1-x}Ag_x)_2ZnSnS_4$ (ACZTS). The precursor films with different amount of Ag were fabricated by varying the molar ratio of Ag/(Cu + Zn + Sn) in the aqueous precursor solutions used. The structural analyses by XRD indicated the successful fabrication of Ag-incorporated CZTS thin films instead of formation of various separate phases and other compounds. Ag content was found to be effective for grain growth since Ag-CZTS films had larger crystal grains than those of the CZTS film. The sample with a relatively low Ag content (Ag/(Ag+Cu) of ca. 0.02) had a compact morphology without appreciable voids and pinholes. However, an increase in the Ag content in the CZTS film (Ag/(Ag+Cu) ca. 0.10) induced formation of a large number of pinholes. All fabricated films were processed into solar cells for characterizations. From electrostructural analyses of the devices, the acceptor density of bare CZTS-based device tended to be high; but it was decreased for the CZTS films with Ag/(Ag + Cu) of ca. 0.02, suggesting the reduction in the amounts of unfavorable Cu_{Zn} antisite defects in the Ag-CZTS film in comparison with those in the bare CZTS film. The use of the Ag-CZTS film also improved band alignment at the p-n junction, leading to increase in the built-in potential V_{bi}s as well as efficient suppression of the interface recombination. As can be expected from these results and discussion, the solar cell based on the film with Ag/(Ag+Cu) of ca. 0.02 achieved the best conversion efficiency of 7.1%.

In chapter V, we investigated effects of In incorporation on structural and photovoltaic properties of CZTS thin films. In-incorporated CZTS films were fabricated from precursor solutions containing precursor solutions with several In/(Zn + Sn) ratios (0, 0.01, 0.02, 0.04, 0.1, 0.2, 0.5 and 0.7). From structural analyses, pure In-CZTS films were successful

fabricated at the In/(Zn+Sn) ratio was lower than 0.2. However, incorporation of In into the CZTS lattice was found to suppress the grain growth, leading to poor quality especially for the films with high In contents. The very low In content with In/(Zn+Sn) ratio of 0.01 had beneficial for improvement of solar cell performance. As a result, the maximum conversion efficiency of 6.0% was achieved.

In summary, the feasibility of non-vacuum spray pyrolysis technique to deposit CZTS thin films for the use of photovoltaic applications was investigated. The as-deposited film was composed of densely packed small granule particles with a thickness of 1μm, indicating successful deposition of a homogeneous film. The annealing treatment at relatively high temperatures for a sufficient duration was necessary to improve the crystalline of CZTS films. Although, CZTS film as a compact layer with large grain size was obtained, the presence of secondary phases and antisites defects are main challenges for high quality films. By controlling chemical composition for optimal Cu-poor and Zn-rich composition, the secondary phases were reduced with the decrease of carrier density and the increase of carrier lifetime. Silver incorporation to CZTS films helped to reduce the antisite Cu_{Zn} defect and improve the band alignment at the p-n junction. In incorporation was also found to have beneficial for conversion efficiency of solar cell. Hence, substitution by other elements to CZTS films was shown to improve the quality of the film. As a result, promising solar cell efficiencies were achieved, although some faults such as the formation of thick MoS_2 layer and cliff-type conduction band alignment of CZTS and CdS layers, caused the recombination at the interface; further improvement of the solar cell performance could be expected by optimizations other doping elements, annealing conditions (i.e., pressure, vapor) and different buffer layers. Since CdS was used as buffer layer in our solar cell structure, it is a toxic material and low transparency in the blue wavelength region. The CdS buffer layer

can be replaced by other suitable materials, which are non-toxic and have higher band gap energies such as In_2S_3, ZnO or ZnS. These buffer layers can be fabricated by spray pyrolysis technique.

As mentioned, the current highest power conversion efficiency of CZTS-based thin film solar cells of 9.2 % was obtained by using vacuum sputtering method. In this study, by using non-vacuum spray pyrolysis method to fabricate CZTS film, the achieved conversion efficiency of 8.1% approaches to that of vacuum method. This shows a capability of spray pyrolysis method for fabricating high quality CZTS thin film absorbers. Since this method is versatile, simple and easy to handling in fabrication process, it also can realize a fast deposition rate and the equipment for large-scale production is similar to that used for conventional spray coating in various industrial processes. Therefore, spray pyrolysis method is one of the most suitable techniques to achieve low-cost, environmental friendly production of photovoltaic thin films. In addition, CZTS material has many advantages because of optimum band gap energy, high absorption coefficient and less-toxic, earth-abundant constituent elements. Fabrication of CZTS-based thin film solar cell using spray pyrolysis method showed promising perspective for practical photovoltaic applications.

List of publications

Peer-reviewed publications included in the present thesis:

1. "*Cu_2ZnSnS_4 thin film solar cells with 5.8% conversion efficiency obtained by a facile spray pyrolysis technique*"
   T. H. Nguyen, W. Septina, S. Fujikawa, F. Jiang, T. Harada, and S. Ikeda
   RSC Advances, **5** (95), 77565-77571 (2015).

2. "*Impact of Precursor Compositions on the Structural and Photovoltaic Properties of Spray-Deposited Cu_2ZnSnS_4 Thin Films*"
   T. H. Nguyen, S. Fujikawa, T. Harada, J. Chantana, T. Minemoto, S. Nakanishi, and S. Ikeda
   ChemSusChem, **9** (17), 2414-2420 (2016).

3. *"Effects of Indium Incorporation on Structural and Photovoltaic Properties of Cu_2ZnSnS_4 Thin Films*"
   T. H. Nguyen, T. Harada, S. Fujikawa, S. Nakanishi, and S. Ikeda
   ECS Transactions, **75 (**50**)**, 15-22 (2017).

4. "*Structural and Solar Cell Properties of Ag-containing Cu_2ZnSnS_4 Thin Film Derived from Spray Pyrolysis*"
   T. H. Nguyen, T. Kawaguchi, J. Chantana, T. Minemoto, T. Harada, S. Nakanishi, and S. Ikeda
   ACS Applied Materials & Interfaces, Accepted.

Conferences Presentations:

1. "*Cu_2ZnSnS_4–based Thin Film Solar Cells with More Than 8% Conversion Efficiency Obtained by Using A Spray Pyrolysis Technique*"

   T. H Nguyen, T. Harada, S. Nakanishi and S. Ikeda

   43rd IEEE Photovoltaic Specialists Conference, June 5-10, 2016, Portland, Oregon, America.

2. "*Enhancement of Carrier Lifetime of Cu_2ZnSnS_4/CdS junction via Ag-Doping for Solar Cell Application*"

   T. H. Nguyen, T. Harada, S. Nakanishi and S. Ikeda,

   2017 International Workshop on Electrified Interfaces for Energy Conversions, May 18-21, 2017, Kanagawa, Japan.

3. "*Open Circuit Voltage Improvement of Spray-Pyrolyzed Cu_2ZnSnS_4 Thin Film Solar Cells by Silver Doping*"

   T. H. Nguyen, T. Harada, J. Chantana, T. Minemoto, S. Nakanishi and S. Ikeda

   27th International Photovoltaic Science and Engineering Conference, Nov 12-17, 2017, Otsu, Japan.

Acknowledgements

The works in this thesis have been conducted at Research Center for Solar Energy Chemistry, Osaka University. I gratefully acknowledge Ministry of Education, Culture, Sports, Science and Technology (MEXT) Japan for providing the scholarship for my study.

First and foremost, I am deeply grateful to my supervisors Prof. Shigeru Ikeda and Prof. Shuji Nakanishi for their guidance, support and encouragement throughout my study. Thank them very much for giving me a pleasure-working environment with many useful discussions and meetings; this is a great experience for me on doing research.

I could not forget to thank Prof. Michio Matsumura who encouraged and helped me to make my dream came true. His encouragement made me feel heartwarming, thank him very much for giving me an opportunity to become his student in Osaka University. I also would like to express my appreciation to Dr. Takashi Harada for always ready to help me whenever I need his support on technical problems or many other things. I am thankful to Ms. Kyoko Sekiya and Ms. Emiko Tasaka for their kind support on the paperwork. Many thanks to my senior Dr Wilman Septina, my friend Dr. Hasyiya Adli and other members of Matsumura laboratory and Nakanishi laboratory. They were very kind and friendly. Thank them for helping, sharing their experiences and accompanying me.

I am grateful to Prof. Nguyen Quang Liem, Dr. Ung Thi Dieu Thuy, Dr. Tran Thi Kim Chi and other people in Institute of Materials Science (IMS), Vietnam Academy of Science and Technology (VAST) for teaching and helping me during the time I studied in Laboratory of Optoelectronic Materials. I would like to thank Dr. Dinh Nhu Thao for his motivation and encouragement to help me continue my study.

I also would like to send my thanks to all of my friends in Japan for the time spent together, I will not forget these memories. Special thanks to my sister Van Trang for always being with me and helping me. I am very fortunate to have her during my hard times. Thanks to my friend Huy Nguyen, My Bui, Huong Pham for being patient beside me and listen to me when I need them. They are my very special friends.

Finally, I am deeply indebted to my parents Nguyen Chuyet and Le Thi Tuyet for their love and uncounted things they have done for me. They always support and encourage me whenever I feel down, a big thanks to them for being my motivation to make me stronger. I also would like to thank my younger sisters Thu Hoai and Tam Hieu for their encouragement and their talks to help me forget my stressful things.

There are many other people, who helped me and contributed to this thesis but I cannot list here. Thank them very much for their contributions to my study and for being a part of my life.

Osaka, March 2018

Nguyen Thi Hiep